# LENS EPITHELIAL CELL MIGRATIONAL MODEL: UNDERSTANDING

# MOTILE BEHAVIOUR DURING POSTERIOR CAPSULE OPACIFICATION

# ON NATUARAL AND SYNTHETIC SUBSTRATES

By MEGHAN MARSHALL (B. A. Sc.)

A Thesis

Submitted to the School of Graduate Studies

in Partial Fulfillment of the Requirements

for the Degree

Master of Applied Science

McMaster University

DESCRIPTION

MASTER OF APPLIED SCIENCE (2008)                    McMaster University

(Chemical Engineering)                                     Hamilton,

Ontario

TITLE: Lens Epithelial Cell Migrational Model: Understanding Motile Behaviour During

Posterior Capsule Opacification on Natural and Synthetic Substrates

AUTHOR: Meghan Marshall, B.A.Sc. (Queens University)

SUPERVISOR: Dr. H. Sheardown

NUMBER OF PAGES: x, 120

## ACKNOWLEDGEMENTS

I am immensely thankful to Dr. Heather Sheardown for her sage and scholarly leadership as well as the enduring patience and support she brought to her work as my Supervisor for graduate studies. I want to express deep gratitude to my parents, to Duncan, my brother, and to Rachael, my sister, and to my extended family as well for their faith in me and for their love and support throughout my graduate studies.

There are many more people to thank. Thank you to Carolyn Cerny for being a most understanding and wonderful undergraduate summer student, and for her work in creating my surfaces and running all the subsequent surface characterization techniques and cell studies. Thank you to Diana Morarescu for her expert guidance in the lab and for sharing her insights with me as my thesis progressed. Thank you to Renita D'Souza for working with me on the ATR-FTIR samples and results and for her support. Thank you to Laura Wells for giving me that extra little push in thinking and in being there for my model breakthrough. Thank you to Steve Kornic for his timely assistance in running the ATR-FTIR results and to Rana Sodhi for very kindly running the XPS results. Thank you to Geetha Mahadevan for her dedication of time and care in thoughtfully editing this manuscript.

Finally, I am grateful to the Sheardown laboratory group for being such genuine, kind, supportive and amazing people. Having a great laboratory group and a supportive professor makes a world of difference to one's overall graduate education experience. I have gone through challenging times during this graduate study, including a change of

thesis approach from a laboratory-based to theoretical research project. People's extra

help and time was deeply appreciated and I could not have done it without the support of

the extraordinary community at McMaster University.

# ABSTRACT

Cataract surgery is currently the most common surgical procedure done in the world. However, within 5 years, approximately half of these patients will develop posterior capsule opacification (PCO). In cataract surgery, the biological lens is replaced with an intraocular lens (IOL). PCO is caused by migration and transformation of residual lens epithelial cells (LEC) that remain in the capsule following the surgery. LECs which have migrated to the posterior capsule within the first month of surgery are thought to be the major contributors to PCO since after this time, the capsule completely seals.

A mathematical model has been developed in order to better understand the process of LEC migration during PCO. The model addresses the impact of substrate and substrate modification as well as the presence and absence of the growth factors transforming growth factor beta (TGFβ) and fibroblast growth factor (FGF2). It was developed from a first order rate of decay model taken from process control.

$$cell\ speed = (\beta_o + \beta_{GF}) \left[ 1 - e^{-\frac{x - x_o}{\tau_o}} \right] + 1 - e^{\frac{x - x_{oo}}{\tau_{oo}}}$$

If the cell speed is divided by the distance travelled by the cell up to the point of posterior capsule breach, the time for the LECs to breach the capsule posterior can be calculated. The model was tested with literature data and was able to predict the effects of cell speed on the presence of various extracellular matrix components and growth factors. It was determined that potentially modification with fibronectin may be useful for the prevention of PCO

Preliminary experimental validation of the model was performed by modifying silicone substrates with various extracellular matrix derived peptides. Results demonstrate that peptide modified surfaces may be more resistant to EMT by increasing cell adhesion and decreasing cell migration. Therefore, this LEC migrational model will be a useful tool in the development of superior IOLs and materials.

# TABLE OF CONTENTS

# LIST OF FIGURES

## LIST OF TABLES

# LIST OF ABREVIATIONS

α-SMA: α-smooth muscle actin
CN: Collagen
ECM: Extracellular matrix
EMT: Epithelial to mesenchymal transition
Fg: Fibrinogen
FGF: Fibroblast growth factor
FN: Fibronectin
GRDNP: Gly-Arg-Asp-Asn-Pro
GRGDSP: Gly-Arg-Gly-Asp-Ser-Pro
IOL: Intraocular lens
LEC: Lens epithelial cell
LN: Laminin
 Nd:YAG: neodymium-doped yttrium aluminum garnet laser
PCO: Posterior capsule opacification
PMMA: Poly (methyl methacrylate)
RGD: Arg-Gly-Asp
RGDS: Arg-Gly-Asp-Ser
RGDSPASSKP: Arg-Asp-Asn-Pro-Ala-Ser-Ser-Lys-Pro
TGF: Transforming growth factor
VN: Viminin
YGRGD: Tyr-Gly-Arg-Gly-Asp
YIGSR: Tyr-Ile-Gly-Ser-Arg

# CHAPTER 1: INTRODUCTION

## 1.0 LITERATURE REVIEW

Cataract formation, an opacification of the crystalline lens, is the number one

cause of world blindness, (WHO 1998, WHO 2000) affecting over 20 million people

worldwide (Mansfield *et al.* 2004). Treatment involves removal of the opacified lens and

replacement with an intraocular lens (IOL), which restores quality of vision. This

procedure is performed more than 2 million times annually in the United States (US)

alone. (Werblin 2006) However, a secondary opacification of the implanted lens can

occur. Known as posterior capsule opacification (PCO), this wound healing response

occurs in approximately half the patients who have undergone cataract surgery within the

first 5 years post-surgery. (Bullimore *et al.* 1993, Sponer *et al.* 2005) Currently, PCO is

treated with a neodymium-doped yttrium aluminum garnet (Nd:YAG) laser capsulotomy;

however there are risks for the patient including cystoid macular edema, retinal

detachment, new onset of glaucoma, and worsened preexisting glaucoma as well as a

financial burden to the health care system associated with this procedure. (Apple *et

al.*1992, Pandey *et al.* 2004) In 1996, the cost of Nd:YAG laser capsulotomy for the

treatment of PCO was US $500 million. (Steinert *et al.* 1991, Werblin 2006) Clearly,

there are therapeutic and financial incentives for preventing the occurrence of PCO.

## 1.1 Lens anatomy

The lens is a transparent biconvex structure, whose main function is accommodation and refraction. (Lens *et al.* 2008) It is enveloped by the capsule, an elastic membrane composed primarily of collagen (CN). (Lens *et al.* 2008) The anterior side of the capsule is bathed in the aqueous humor, while the posterior side is bathed in the vitreous humor. The watery fluids, which have a composition similar to that of blood plasma are thought to regulate many functions of the lens. (Lens *et al.* 2008) Upon wounding or disruption such as occurs in cataract surgery, lens epithelial cells (LEC)s may become displaced and adhere to the capsule rather than to the lens. (Jong-Hesse *et al.* 2004)

In addition to lens epithelial cells (LECs), which are located directly under the capsule, and the lens also contains cortical fiber cells, which are located in the center of the lens directly beneath the lens epithelium. (Apple *et al.* 1992, Hawse *et al.* 2005) A single row of cuboidal epithelial cells form the outer most layer of the lens (Apple *et al.* 1992, Hawse *et al.* 2005) and form two biological zones: the anterior LEC zone in which there exists minimal mitotic activity and the equatorial LEC zone where the cells are highly mitotic. (Apple *et al.* 1992, Pandey *et al.* 2004)

In the natural process of development and aging, the anterior lens epithelium migrates towards equatorial lens region. (Lens *et al.* 2008) Growth factors including

transforming growth factor betas (TGFβ)s and fibroblast growth factors (FGF)s present in

the ocular media are responsible for the growth, maintenance and differentiation of the

lens. (Saika *et al.* 2004, Shirai *et al.* 2006, Wormstone *et al.* 2002a)  As the lens ages or

following trauma or injury, LECs at the equatorial zone are stimulated by a gradient of

growth factors in the surrounding ocular media to exit the cell cycle and terminally

differentiate into myofibroblasts through a process called epithelial to mesenchymal

transition (EMT). (Hawse *et al.* 2005, Kalluri *et al.* 2003)  In EMT, organized epithelial

cell structures are disintegrated to enable cell movement and morphogenesis into

fibroblastoid cells. (Kalluri *et al.* 2003)   The cytoplasmic processes of LEC gradually

elongate and, as new layers of cortical fiber cells form, old cells are directed toward the

cell nucleus and the nuclei and internal organelles of the older fiber cells eventually

disappear. (Apple *et al.* 1992, Bassnett 1992, Hawse *et al.* 2005, Lens 2008)  The

resulting myofibroblasts exhibit a "spindle-shaped" morphology.  LEC differentiation is a

process which occurs gradually over a lifetime but which slows in later years, causing the

lens to slowly increase in weight and size. (Apple *et al.* 1992, Hawse *et al.*  2005)


## 1.2 Posterior capsule opacification

During cataract surgery, the removal of the native opacified lens and its

replacement with an intraocular lens (IOL) triggers an increase in the level of such

cytokines as TGFβs and FGFs in the aqueous humor.  A breach in the blood aqueous

barrier or autocrine induction by LECs occurs which regulates changes in cell phenotype. (Jong-Hesse *et al.* 2004, Lee *et al.* 1999, Saika *et al.* 2004, Wallentin *et al.* 1998) PCO arises when residual LECs, remaining in the lens capsule post-cataract surgery, are stimulated to undergo a wound healing response and attempt to regenerate the lens cortex. (Pandey *et al.* 2004)

Post-operatively, residual LECs remain attached to the anterior portion of the capsule. It is these residual LECs which are responsible for PCO. (Marcantonio *et al.* 2000). These cells proliferate, migrate and establish a monolayer on the anterior and posterior capsular surface, which continues to line the capsule many years after surgery. (Marcantonio *et al.* 2000, Saika *et al.* 2001a, Wormstone *et al.* 1997) A study done by Liu and colleagues demonstrates that the cells grow from the equator radially inward on the anterior capsule. (Liu 1996) In the equatorial region cells grow in multiple layers between the IOL and the capsule, contributing to the formation of a "donut-shaped" lesion known as Sommering's ring. However LECs in the equatorial region can also breach the posterior capsule at which point, they will also grow radially inward. (Liu 1996) (Liu 1996, Nishi *et al.* 2007, Nixson 2004) It is not the monolayer of translucent epithelial cells which contribute to PCO, but rather their opacification.

Opacification usually holds two morphological forms, fibrous metaplasia, the more common type, and Hirschberg-Elschnig pearl (or simply pearl) formation. (Apple 1992, Pandey 2004) The fibrous type of PCO is thought to originate mainly from LECs present on the anterior capsule although it can also be generated from the equatorial

epithelial cells. (Pandey *et al.* 2004)  These cells proliferate and form fibrous tissues by undergoing fibrous metaplasia. (Findl *et al.* 2005, Ishibashi *et al.* 1994, Pandey *et al.* 2004, Wormstone *et al.* 1997)  During this process, LECs can migrate from the anterior to the posterior capsule.  Pearl formation, though to originate from the equatorial zone, occurs when residual LECs become displaced, circulate through the aqueous, and land on the posterior capsule forming clusters of LEC/protein aggregates which resemble pearls. (Apple *et al.* 1992)  Remnants of Sommering's ring, the buildup of fibrous cells and tissues in the equatorial region, can also break off to form pearls. (Apple *et al.* 1992, Jong-Hesse *et al.* 2004)

In both cases, cells can express the myofibroblastoid cell phenotype highlighted by expression of markers such as α-smooth muscle actin (α-SMA). (Bloemendal 1979, Liu 1996, Marcantonio *et al.* 2000)  In addition, the cells secrete increased amounts of extracellular matrix (ECM) proteins including CN I and III, fibronectin (FN), and tenascin with down regulation of CN IV production. (Jong-Hesse *et al.* 2004, Ishibashi *et al.* 1994, Linnola *et al.* 2000, Linnola *et al.,* Marcantonio *et al.* 2000, Olivero *et al.*1993) The myofibroblasts stimulate capsular contraction which results in capsular wrinkling and light scatter in the line of the visual axis. (Mansfeild 2004, Wormstone *et al.* 2004) Additionally, ECM deposition and Elschnig's pearls contribute to light distortion. (Liu 1996) *In vivo*, the PCO response is known to cause the onset of visual impairment from 3 months to 4 years post surgery. (Apple *et al.* 1992)

## 1.3 PCO prevention

Apple and colleagues proposed five factors for minimizing PCO: capsular fixation, creation of a small continuous circular capsulorhexis smaller than the diameter of the IOL such that the capsulorhexis edge is on the IOL surface, IOL biocompatibility, IOL design which induces maximal IOL optic-posterior capsule contact and maximal barrier effect. (Apple 1992) Additionally, pharmacological and immunologic inhibitors have also been used to minimize PCO. (Apple *et al.* 1992, Fine 1992) Of these factors, the square edged IOL design leading to maximum barrier effect has proven to be an extremely effective method of PCO reduction. (Findl *et al.* 2005, Nishi *et al.* 2004, Nixson 2004) However, the complication has not been eradicated by design changes and it has been suggested that further exploration of IOL biocompatibility may be key to its prevention. (Kayatama *et al.* 2007)

## 1.4 Barrier effect and formation of the capsular bend

The effectiveness of IOL design on minimizing PCO has been suggested to stem from two mechanical effects on the remaining lens epithelial cells. The capsular bend theory proposed by Nishi and colleagues suggests that the sharp bend which the IOL makes in the posterior capsule as the two are pressed against each other inhibits cellular migration through contact inhibition. (Nishi *et al.* 2000, Nishi *et al.* 2002, Nishi *et al.* 2007) Alternatively, the contact pressure theory proposed by Nagamoto suggests that pressure created by the force of the capsule on the posterior of the IOL acts mechanically

as a barrier to cell migration. (Nagamoto *et al.* 2003) It has been demonstrated that cellular migration from the anterior to posterior occurs within one week of IOL implantation. (Kayatama *et al.* 2007) However, it is unlikely in this critical period that the barrier effect is sufficient to inhibit PCO as a human lens is 10 times more volumous than the IOL. (Nishi *et al.* 2007) Additionally, compression is thought to occur within two months with the development of Sommering's ring leading to pressure on the IOL. (Nishi *et al.* 2007, Nixon 2004). Therefore, the capsular bend theory seems more plausible and will be the focus of the current discussion.

The sharp-edged IOL design induces a sharp bend in the capsule. (Katayama 2007) The cells on the anterior lens migrate until they arrive at this barrier where they are thought to be inhibited a phenomenon thought to occur independently of the lens material. (Nishi *et al.* 2004, Findl *et al.* 2005) Nishi and colleagues discovered that with sharp edge IOLs, as cells reach this barrier, they have the myofibroblast phenotype and stained negative for Ki-67, a nuclear protein which stains positive for all stages of growth except the Go phase suggesting that cell migration is the primary factor in PCO. (Nishi *et al.* 2007) Moreover, once these cells reach the edge they do not proliferate. In contrast, round edged IOLs stained positive from the anterior to the posterior regions. Thus it is suggested that contact inhibition of the LECs is induced by the capsular bend.

LECs are known to migrate to the posterior capsule within 7 to 11 days following implantation. (Hayashi *et al.* 2002, Nishi *et al.* 2002, Wormstone *et al.* 1997) The anterior capsule is first to contact the IOL followed by the posterior capsule. (Nishi *et al.*

2003) The bend seals much like a zipper from the haptic up to the IOL. Clinically and experimentally the capsular bend is complete within 2 to 4 weeks for 360° around the anterior and posterior capsule edges. (Hayashi *et al.* 2002, Nishi *et al.* 2002, Sacu *et al.* 2005) at which point, the cells experience a "damming" effect and can no longer travel from the anterior to the posterior capsule. (Nishi *et al.* 2007) Cells begin to migrate and gather at the equatorial edge in a layered fashion. Fibrosis occurs along the equatorial position and over a period of approximately two years, the biological response to the IOL is complete. (Nixon 2004) Vyas and colleagues and Nixon both demonstrated that the barrier effect can remain for 2 years post-operation. (Nixon 2003, Vyas *et al.* 2007) In the case of round edged IOLs however, a 360° capsular bend never fully developed and LECs continued to migrate to the posterior. (Nixon 2003) As a result, in sharp edged IOLs, less PCO is present 1 year, 3 years, and 5 years post surgery, compared to the round edged IOL, although complete PCO prevention did not occur during this period. (Findl *et al.* 2005)

Due to the previous findings, it is thought that migration of LECs to the posterior prior to sealing of the capsular bend is key to the progression of PCO. Once the barrier is formed, contact inhibition of the cells will be induced. (Nishi *et al.* 2007) This implies that LECs which are on the posterior have accumulated prior to the capsular bend seal or from where the capsular bend has failed to seal. Moreover, PCO is thought to be dependent on the properties of the cells which have migrated, particularly their mitotic capacity which is a function of the patient age. (Liu 1996, Nishi *et al.* 2007, Wormstone

*et al.* 1997)

### 1.5.0 Extracellular matrix (ECM)

The healthy capsule is comprised of mainly collagen (CN) fibrils (Saika *et al.*

1998) and includes ECM proteins such as CN IV, laminin (LN) and FN. (Oharazawa *et*

*al.* 1999, Olivero *et al.*1993, Parmigiani *et al.* 1991)  The ECM provides mechanical

strength, structure and elasticity to support the lens.  The basement membrane is a 50 –

100 nm layer of specialized ECM, mainly CN IV and LN, located basolateral to the LEC

sheet. (LeBleu *et al.* 2007, Saika *et al.* 1998, Saika *et al.* 2001a)  The ECM plays a

significant role during PCO, as it has been shown to influence cell proliferation and

migration as well as to modulate cell phenotype and myodifferentiation of the LECs. (de

Jonne-Hesse 2004, Oharazawa *et al.* 1999, Olivero *et al.* 1993, Saika *et al.* 2004)  Under

normal conditions, CN IV is present; however under pathologic conditions, CN I and III

and FN are also expressed.  During PCO, excessive amounts of ECM proteins including

CN types  I, III, IV, V and VI, vitronectin (VN), FN (Linnola *et al.* 2000, Linnola  *et al.*

2003, Saika *et al.* 2001a, Saika *et al.* 2003, Saika *et al.* 2004)  as well as proteoglycans

(Ishibashi *et al.* 1994, Saika *et al.* 1998, Saika *et al.* 2003) are deposited by LECs in

random fibrous structures instead of in an orderly layer of basement membrane.

(Ishibashi *et al.* 1994, Saika *et al.* 2003)  Of the ECM proteins, CNs I, III, and IV, FN,

LN, and VN are the most widely studied and, with the exception of CN IV, are markers

of PCO. (Ishibashi *et al.* 1994, Linnola *et al.* 2000a, Linnola *et al.* 2000b, Linnola *et al.*

2003, Olivero *et al.* 1993, Prockop *et al.*1995)  Many of these ECM components contain

the cell adhesion peptide Arg-Gly-Asp (RGD) which is recognized by cell surface

integrins and which promotes a variety of cell functions including adhesion and

migration. (Oharazawa *et al.* 1999, Boateng 2004)  Oharazawa and colleagues studied

human LEC migration on ECM coated dishes in serum free medium and demonstrated

that on CN IV, LN, and FN surfaces, cell proliferation was not enhanced; however cell

adhesion and migration were enhanced on all surfaces. (Oharazawa *et al.* 1999)


**1.5.1 Laminin**

LN, a member of the glycoprotein family, is an adhesive ECM component known

to promote cell migration and basement membrane production. (Boateng *et al.* 2004,

Melinda *et al.* 1996, Paez *et al.* 2007, Terranova 1986)  It is the most abundant

noncollagenous protein in the basement membrane. (LeBleu *et al.* 2007, Terranova 1986)

LN is a heterotrimeric molecule composed of polypeptide units alpha, beta and gamma

(α, β and γ) chains. (LeBleu *et al.* 2007, Paez *et al.* 2007)  The α is the predominant chain

is and associated with integrin binding and cellular interactions. (Boateng *et al.* 2004,

Paez *et al.* 2007, Terranova 1986, Tzu *et al.* 2008) (Tarone *et al.* 2000, Tzu *et al.* 2008)

RGD, located within the α-chain, in addition to the peptide sequence Tyr-Ile-Gly-Ser-Arg

(YIGSR) located within the β1-chain, are the dominating adhesion peptides of the LN

molecule concerned with cell attachment activity. (Boateng *et al.* 2004, Melinda *et al.*

1996, Runyan 1988)

**1.5.2 Collagen**

CN is triple helical protein molecule which either gives structural support and rigidity to the ECM or provides a basement membrane to which the LECs can attach. (LeBleu *et al.* 2007) CN I is the most abundant protein in the body while CN IV is the most abundant basement membrane protein. (LeBleu *et al.* 2007) CN IV belongs to the class of network-forming CNs which form basement membranes (de Jonne-Hess 2004) while CNs I and III are from the class of fibril-forming CNs that form connective tissues. (LeBleu *et al.* 2007, Prockop *et al.* 1995) The major cell-binding domain of collagen is RGD although the protein is capable of binding other ECM proteins (Linnola *et al.* 2000a, Linnola *et al.* 2000b, Linnola *et al.* 2003, Oharazawa *et al.* 1999)

**1.5.3 Fibronectin in wound healing: The adhesion and migration protein**

FN, the most studied ECM protein is known to promote cell adhesion and migration (Aota *et al.* 1995), and is unique in comparison to connective ECM proteins in that it is active during wound healing. (Clark *et al.* 2003) FN is a dimeric molecule composed of three types of homologous repeating units: types I, II, and III. FN III, which comprises the central binding domain, includes adhesion the RGD adhesion sequence. (Clark *et al.* 2003) Each of the dimers contain one RGD recognition moiety and a nearby synergy site. (Koo *et al.* 2002) The cell binding domain within the FN molecule is determined to a large extent by the RGD sequence. In the healthy human eye, FN is minimally expressed and is localized to the outer surface of the lens capsule (Oharazawa

11

*et al.*1999, Parmigiani *et al.* 1991)  However, in PCO, FN is present in the aqueous humor and is found on and within the lens capsule. (Linnola *et al.* 2000, Linnola *et al.* 2003, Olivero *et al.* 1993)  LECs on FN surfaces have been shown to elongate and cluster, exhibiting the myofibroblast morphology. (Oharazawa *et al.* 1999)  Therefore it is thought that FN may be one of the key components responsible for inducing EMT and therefore leading to PCO.  (Oharazawa *et al.*1999, Parmigiani *et al.* 1991)

**1.6 Adhesion peptides**

Adhesion peptides are small synthetically derived sequences of amino acids derived from the adhesion domains within ECM proteins.  The process of integrin adhesion to adhesion peptides occurs in four partly-overlapping steps: cell anchoring, cell spreading, organization of the actin cytoskeleton, and finally, formation of focal adhesions. (Hersel *et al.* 2003)  The RGD containing peptide Gly-Arg-Gly-Asp-Ser-Pro (GRGDSP) termed as Peptide IV was first isolated in 1981 in the fourth β-turn of the FN III. (Pierschbacher *et al.* 1981)  Pierschbacher and colleagues demonstrated that the minimum effective sequence of binding activity was RGDS, and that the Ser- residue is not always needed for binding activity. (Pierschbacher *et al.* 1981)  In general, it has been found that the presence of RGD on a synthetic surface increases cell spreading, migration, differentiation, cell survival, focal contact formation, and in some cases proliferation and that the number of cells attached to a surface is dependent on the RGD surface density.  However, a critical minimum density is required for a cellular response.

12

(Hersel *et al.* 2003)  The capacity of RGD to address numerous growth factors, its influence on cell adhesion, and in general, its impact on cell behaviour, make it an attractive candidate for use in biomaterials or as pharmacological inhibitors. (Hersel *et al.* 2003)  As a result, RGDS is by far the most employed and most effective peptide for enhancing cell interactions with biomaterials. (Hersel *et al.* 2003)  RGD has a lower binding affinity than FN because RGD interacts with the $\beta$ I/A domain of the integrin, while FN contains both the $\beta$ I/A of the integrin and the synergistic sites within the FN III domain, which interact with the propeller domain and the $\beta$ I/A domain of the integrin. Interaction of both sites is thought to be necessary for the strong binding of $\alpha_5\beta_1$ to FN. (Garcia *et al.* 2002)  Regardless, modification of biomaterials with RGD has been widely used to promote cell adhesion to biomaterials.

An appropriate RGD peptide can be chosen for an application based on the selectivity of a certain integrin type which may elicit a specific cell behaviour. Migrational behaviour can be influenced by targeting a certain integrin type.  In the case of PCO, it may be of interest to reduce the speed of cell migration speed.  A reduction in migration is best achieved at a high RGD density. (Hersel *et al.* 2003, Koo *et al.* 2002) Alternatively, peptides which have specificity for certain integrins can be selected.  For example, by targeting the $\beta 1$ integrin which has been speculated by Hersel and colleagues to act as the "brakeman" of the cell may limit cell migration. (Hersel *et al.* 2003) Therefore selecting an RGD peptide such as GRGDS, which is known to have increased $\beta 1$ integrin activity and specifically $\alpha_5\beta_1$ may promote cell adhesion. (Hersel *et al.* 2003)

It has been previously demonstrated using vascular smooth muscle cells that low densities of immobilized adhesion peptides encourage cells to synthesize and deposit matrix molecules, whereas high peptide densities do not. (Mann *et al.* 2002) Therefore, it may be of interest to examine the effects of peptide density on LEC migration in order to minimize fibrous deposition. In addition, it has been shown that endothelial cells differentiate maximally at intermediate RGD densities (Ingber *et al.* 1989) Furthermore, it is thought that transdifferentiation of LECs *in vivo* can be prevented by inhibiting the attachment and migrations of LECs onto FN deposited during the wound healing process. Thus selecting an appropriate RGD density may suppress EMT and contain the LEC phenotype. (Oharazawa *et al.* 2005)

## 1.6 Integrins

The integrins, a superfamily of transmembrane glycoproteins found on the cell surface mediate cell-cell and cell ECM interactions. (Hynes 2002, Oharazawa *et al.* 1999) Integrins consist of α and β subunits which are noncovalently associated. (Oharazawa *et al.* 1999) Their large extracellular domains and smaller intracellular cytoplasmic tails serve as transmembrane mechanical links from the extracellular contacts to the cytoskeleton within the cell. (Hynes 2002)

Significant differences in integrin distribution exist within the lens environment of a diseased capsule which has undergone PCO and an intact and healthy lens. While the

non-specific integrin subunit $\beta1$, a receptor for CN, RGD and LN, is present in the lens of

both the healthy adult and one affected by PCO, (Beck *et al.* 2001, Marcantonio *et al.*

2004, Nishi *et al.* 1997a) $\alpha_5\beta_1$, known as the mesenchymal integrin (Zavadil *et al.* 2005)

Although many integrins can bind to FN, $\alpha_5\beta_1$ binds solely to the RGD domain of FN and

is thought to be the main receptor for this ligand. (Marcantonio *et al.* 2004)  Since FN is

also upregulated during wound healing, both are thought to influence the advancement of

PCO.  (Aota *et al.* 1995, Marcantonio *et al.* 2004)

It is important for cells to regulate adhesion and migration in a spatial and

temporal manner. (Lauffenburger 1996) Different integrins can be expressed concurrently

or at different times on the cell surface. (Hersel *et al.* 2003)  Additionally, integrin

expression and activation can be upregulated or downregulated, depending on the

environmental conditions. While one integrin will have only weak bonding strength,

many integrins together will form a strong bond. (DiMilla *et al.* 1991)  The reversibility

of processes aids in cell motility or adhesivity, (Hynes 2002) enabling the cell to explore

its environment without necessarily becoming bound to a surface.

Cell migration is largely influenced by environmental substrate conditions and the

bonds which the integrins make with their surface.  This in turn influenced by the affinity

of the integrin receptor for the surface, the number of integrin ligand bonds formed and

the availability of ligands. (DiMilla *et al.* 1996)  Focal adhesions, created by bundling a

group of integrins, act as anchorage points between the ECM and the cytoskeleton.  It is

within these focal contacts that signaling networks occur. (Marcantonio *et al.* 2004)

Integrins must also coordinate signals from adhesion receptors with those of other signaling receptors such as growth factor receptors, in a process known as integrin crosstalk. (Schwartz 2002) Within the cell, integrins and growth factors share many common biological pathways. It is therefore possible for integrins to modulate growth factor signals or vice versa and in many cases, integrins enable growth factor signaling. Moreover, integrin signaling cannot occur without integrin attachment to the ECM or to another cell. (Schwartz 2002) The actual outcome of signal transduction with integrin crosstalk is dependent on the external environment of the cell. (Schwartz 2002) Relevant to PCO, the integrins $\alpha_v\beta_6$ and $\alpha_5\beta_1$ are influenced and regulated by the TGF $\beta$ family. (Marcantonio *et al.* 2004, Yoshino *et al.* 2001) Moreover, FN and its receptor $\alpha_5\beta_1$ are key factors in transdifferentiation of LECs into myofibroblasts which is one the major causes of PCO. (Marcantonio *et al.* 2004, Yoshino *et al.* 2001)

## 1.8 Biomaterials Effects on PCO

The biocompatibility of an IOL can be separated into two components, namely the mechanical compatibility against surrounding organs and biological compatibility of the material. (Saika *et al.* 2004) Mechanical biocompatibility is determined by the fit of the haptic loop to the capsular bag and the influence of IOL shape on the migration of LECs through the equatorial region onto the posterior. (Saika *et al.* 2004) It is well

known that the square edge optic is the most mechanically biocompatible design. (Nishi *et al.* 2000, Nishi *et al.* 2004)  It is also well known that maintaining the LEC phenotype is the major influence on PCO. (Apple *et al.* 1992, Saika *et al.* 2004)  Although the mechanical properties of the material influence cell phenotype, once the barrier created by the optic against the capsule is created cell phenotype is less relevant.  Still, the influence of the IOL material on cell phenotype prior to capsular bend formation is of considerable importance. (Nishi *et al.* 2007)

Maintaining the LEC phenotype is among the most important determinants of IOL biocompatibility.  LEC adhesiveness to the anterior IOL affects the extent of capsular opacification. (Oshika 1998, Kayatama *et al.* 2007)  As more the cells adhere to the surface, there is less possibility of the cells undergoing EMT, migrating to the posterior capsule and impeding the visual axes. (Saika *et al.* 2004)  Furthermore, maintaining the LEC phenotype will produce a more ordered layer of ECM; cells which undergo EMT deposit excessive amounts of disordered ECM which will further encourage the myofibroblastic phenotype. (Boukamp *et al.* 1993)

The ECM protein responsible for a desired bioactive bond is FN in a process known as the sandwich theory proposed by Linnola. (Linnola 1997)  Briefly, it is thought that the anterior surface of the capsule will bond to the bioactive surface of the IOL directly or as a result of the formation of a tight adhesive bond which inhibits LEC proliferation.  The anterior capsule will thus remain clear.  Inside the bag, LECs can

proliferate and migrate behind the IOL at the equator. The square edged optic is thought

to direct the proliferating LECs to form a monolayer between the posterior and anterior

capsules resulting in the formation of a "sandwich" between cells and the posterior

capsule comprised of capsule, FN, cells, FN, IOL, which prevents further migration.

(Linnola *et al.* 2000)

The three main types of materials currently used for IOLs include silicone, poly

(methyl methacrylate) (PMMA) and acrylic. (Abela-Formanek *et al.* 2002, Saika *et al.*

2004) Rates of PCO in acrylic and silicone optics are similar at both year one and year

three post implantation (Findl *et al.*2005, Hayashi *et al.* 2002, Sacu *et al.* 2005) while

PMMA generally has a higher incidence of PCO. (Wormstone *et al.* 2002a) The speed of

capsular bend formation is initially faster in acrylic IOLs but is similar to that observed

with silicone after 4 weeks of implantation. The rate of capsular bend formation and thus

contact of the IOL to the capsule in PMMA is significantly slower at all stages and this

may be one reason for the lack of success of this material compared to the other

materials. (Saika *et al.* 2002) Therefore, acrylic and silicone materials will thus be the

focus of this work. Clinically both of these materials perform well *in vivo* with

differences in IOL performance being attributed by and large to design related rather than

to material related differences.

Despite the knowledge of what happens at a biological level with cells and ECM

proteins, the reason for their response to a biomaterial is still largely misunderstood.

(Saika *et al.* 2004) Although factors such as hydrophilicity and surface topography have

been explored as possible explanations for different cell behaviours, with PCO, surface

properties have been shown to be very influential. (Kayatama *et al.* 2007, Linnola 1997,

Nagata *et al.* 1998, Oshika 1998, Saika *et al.* 2004, Yuen *et al.* 2006) Acrylic lenses lead

to increased rates of ECM production rendering these materials more adhesive than

silicone and PMMA lenses (Ohika *et al.* 1998, Saika *et al.* 2004) It was demonstrated

that the adhesive force created between a CN sheet and acrylic was over three times that

of PMMA, moreover, silicone surfaces showed no adhesion. Scores for adhesion in

rabbit eyes showed a similar tendency. (Oshika 1998) Therefore it seems reasonable to

suggest that changes in cell adhesion to the surfaces may be used to alter cell adhesion,

cell migration and cell phenotype.

It is thought that rapid adhesion of the optic to the posterior capsular surface may

contribute to the suppression of LEC invasion. (Saika *et al.* 2004) This was demonstrated

by Kayatama and colleagues who tested acrylic surfaces for cell migration on a CN

membrane at low (group A), medium (group B) and high (group C) surface

adhesivenesses. The migrational area of LECs was 5.65% of the original area in group

A, 2.83% in group B and 1.41% in group C, indicating less migration as adhesiveness

increases. This corresponded with PCO rates in rabbit eyes of 19% in group A, 17.5% in

group B and 5.5% in group C. It has been demonstrated with a high resolution digitized

retroillumination images that at day 90, 180, 1 and 2 years that the presence of LECs on

the posterior capsule was significantly less in acrylic lenses compared to silicone and

PMMA presumably due to this higher adhesivity with these materials. (Hollik *et al.* 1998) The formation of a bioactive bond formed due to the adhesive nature of the acrylic was the postulated theory as to why PCO was minimized. (Hollik *et al.* 1998) Oshika and colleagues also observed lower PCO rates of these three different IOL materials in rabbit eyes. (Oshika 1998)

Creating a material such as an adhesion peptide-modified surface which may form bioactive bonds with the surrounding environment therefore seems to have promise for minimizing or even eliminating PCO. *In vivo*, the cells will be sandwiched in between the IOL and the capsule and are originally attached to the capsule. It can be assumed that FN will be the ECM component which governs the speed of migration on the capsule. Work of Goodman and colleagues on myoblast cell migration across LN, FN and combined LN and FN surfaces revealed that migration occurred much more rapidly on LN than on FN. Interestingly, on the combined surfaces, a major reduction in cell speed which closely resembled that of pure FN was seen. (Goodman *et al.* 1989) As LN and FN are the main basement membrane components of the capsule over which residual cells migrate, these results, albeit with a different cell type, suggest that FN can be assumed to govern cell speed and that modification with FN or a FN based cell adhesion peptide may lead to decreased migration.

Furthermore, it seems reasonable to suggest that an IOL material of lower "compatibility" which is less attractive to the cells would also limit cell speed. However,

in this case, it seems likely that the cells will prefer to be attached to the native capsule

which presents many integrin binding sites.  In this case, the speed of cell migration will

likely be more influenced by the cell capsule.  Therefore, it is reasonable to suggest that a

balance will exist which will result in optimal cell adhesion and migration.  By

developing IOL materials which promote cell adhesion to such an extent as to limit cell

movement, migration of the cells to the posterior capsule and therefore PCO would be

limited.  Based on current understanding of the effects of cell adhesion proteins and

peptides on cells, it seems that modification with a fibronectin based peptide such as

RGD may improve the efficacy of IOL materials.  However the influence of RGD-

modified IOL's on lens cell interactions has yet to be demonstrated.  Furthermore, an

understanding of the effect of such parameters as ligand density is necessary in order to

optimize the surface properties of the IOL materials.


## 1.9 Growth Factors

While not the focus of the current work, the role of growth factors on the

properties of the migrating lens epithelial cell layer cannot be overlooked and must be

included in any model which describes lens epithelial cell migration.  Growth factors

promote lens cell proliferation, migration, differentiation and survival, which all

contribute to PCO. (Saika *et al*. 2004, Shirai *et al*. 2006, Wormstone *et al*. 2002a,

Wormstone *et al*. 2002b)  Although there are many growth factors which are upregulated

in the injured lens, TGFβ2 and FGF are the most important and are known to play major roles in the regulation of LEC behaviour. (Saika *et al.* 2004, Shirai *et al.* 2006, Wormstone *et al.* 2002b) TGFβ2 is responsible for the fibrogenic transdifferentiation of LECs to myofibroblasts while FGF is responsible for proliferation and survival of these two cell species. (Shirai *et al.* 2006) *In vivo*, co-regulation of these growth factors ultimately facilitates the process of PCO. (Saika *et al.* 2004, Shirai *et al.* 2006, Tanaka *et al.* 2004)

TGFβ2 is the major TGFβ isoform found in the eye. Concentrations on the order of 1 ng/mL are present in the aqueous humor, but this growth factor is found largely in its latent form in the uninjured lens. (Saika *et al.* 2000, Wormston *et al.* e 2006) It has also been suggested that the ECM can act as a reservoir for TGFβ and that it is through ECM-bound growth factors that LECs are continuously regulated. (Saika *et al.* 2000) Increased production and activation of TGFβ2 occurs following injury or surgical trauma. (Saika *et al.* 2000, Wormstone *et al.* 2006) In order for intracellular signaling to occur, the TGFβ must bind with the TGFβ receptors I and II (and in some cases III), all of which have been found to be expressed in proliferating LECs. (Saika *et al.* 2000)

Many previous studies support an important role of TGFβ2 in the development of PCO. (Lois *et al.* 2005, Saika *et al.* 2000, Tanaka *et al.* 2004, Wormstone *et al.* 2004, Wormstone *et al.* 2006) It has been demonstrated that TGFβ induces epithelial to mesenchymal transition as evidenced by positive markers such as α-SMA, intracellular

FN staining and formation of spindle-shaped cells, production of excessive and un-

orderly fibrotic ECM such as CN types I and III, and FN, as well as capsular contraction,

wrinkling and in general opacification. (Lois *et al.* 2005, Saika *et al.* 2000, Tanaka *et al.*

2004, Wormstone *et al.* 2004, Wormstone *et al.* 2006). Paradoxically, TGFβ also induces

cell apoptosis. (Maruno *et al.* 2002) which leads to the death of most cells in TGFβ

treated epithelial lens explants during culture. (Maruno *et al.* 2002) *In vivo* however, the

presence of TGFβ and FGF is thought to overcome and counteract TGFβ2-induced cell

loss. (Tanaka *et al.* 2004)

Fibroblast growth factor (FGF), which is also upregulated and activated during

injury, is known to be the main growth factor associated with proliferation and long-term

cell survival of lens epithelial cells. (Tanaka *et al.* 2004, Wormstone *et al.* 1997)  A

capsular break caused a 10 fold increase in FGF2 accumulation in the rat lens 14 hours

after injury. (Tanaka *et al.* 2004) Furthermore, it was demonstrated that FGF2 had a

marked increase on cell proliferation in the absence and presence of TGFβ2 post-injury.

FGF2 is known to be a potent mitogen for both LECs and myofibroblasts; thus, FGF2

may promote cellular proliferation over the entire progression of PCO. (Mansfield *et al.*

2004) Tholozan and colleagues have demonstrated that the capsule acts as a reservoir for

FGF, and through ECM proteolysis executed by matrix metalloproteinases also

stimulated by the injury, biologically significant concentrations of soluble FGF are

known to be present in the capsule. (Tholozan *et al.* 2007)

It has been proposed by Wormstone and colleagues that there exists two stages of growth factor function throughout PCO. The first occurs during the first 2 to 3 months post surgery, when, due to the inflammatory response, the concentration of growth factors in the ocular media is well above basal levels. This leads to significant changes to the capsular bag, although most cases of PCO at this point do not cause compete visual impairment. After a few months, protein levels return to basal level at which point PCO is thought to progress through either paracrine regulation by basal levels of growth factors in the ocular media or autocrine signaling by residual LECs. (Wormstone *et al.* 2002a) As the LECs breach the posterior before the capsule has fully sealed which is known to occur within the first month, we are most concerned with this first of the two stages. Based on the molecular biology of process is clear that both TGFβ and FGF2 play key roles during the first critical month before the capsular bend has sealed and therefore will be considered in this work.

## 1.10 Models of Cell Migration

There exist three key elements which influence cell migration, namely, migrating cells adhere dynamically to their underlying substrata, generate contractive forces required for cytoskeletal elements and morphologically polarized to have a front and rear. (DiMilla *et al.*1991, DiMilla *et al.* 1993)

Models suggest that cell migration is governed primarily through adhesion.

24

(DiMilla *et al.* 1991, DiMilla *et al.* 1993, Maheshwari *et al.* 2000) which in many cell systems is known to be mediated by integrins. (DiMilla *et al.* 1991) Integrins on the cell surface are responsible for both adhesion to the underlying substrata, and transmission of the contractile force responsible for locomotion from the internal cytoskeleton to the external substrata and vice versa. (Lauffenburger 1996) Cell adhesion has been shown to be influenced by such factors as substrata surface density, integrin expression level, and integrin binding affinity (Maheshwari *et al.* 2000).

In many cases, cell speed and substrata protein concentration or adhesiveness has a biphasic relationship. (DiMilla *et al.* 1991, Hersel *et al.* 2003) At low levels of protein or on a "slippery surface", the cell does not have sufficient ligands presented to the cell integrins and therefore lacks the traction to migrate. (DiMilla *et al.* 1991, DiMilla *et al.*1993, Palecek *et al.* 1997, Zelenka. 2004, Zelenka *et al.* 2007) The cell remains stationary as there is not enough contractile force for the cell cytoskeleton to overcome the focal adhesions which are attaching the immotile cell to the surface. However, if the protein density is increased or a cell is presented with a more "tacky" surface, the cell is able to attach to the surrounding ECM and overcome the local adhesive forces, thus propelling the cell forward. (Zelenka. 2004, Zelenka *et al.* 2007) As the adhesion of the surface is further increased, integrin expression will become upregulated and migration of the cells is thus increased. It has been demonstrated that maximum rates of cell migration occur at intermediate protein densities. (DiMilla *et al.* 1991, DiMilla *et al.* 1993, Palecek *et al.* 1997) At high protein densities, the cells attach themselves to the surrounding

ECM so strongly that they are unable to overcome the adhesive force and the cell remains stationary. (DiMilla *et al.*1993) The process of cell migration and the effect of substratum adhesiveness has been described well in a model created by DiMilla and colleagues. (DiMilla *et al.* 1993)

Horowitz and colleagues explored the effects of ligand binding activity of integrins by imposing different mutations within the integrin. (Horowitz 1996) It was determined that ligand affinity also had dramatic effects on cell migration. Mutations which locked an integrin receptor into a high affinity state or antibody activation resulted in significant migrational inhibition. Similarly, increasing focal adhesion and cytoskeletal organization decreased the cell migration rate. Conversely, increases in random migration were seen in integrins which had a mutation in the cytoplasmic domain of the beta integrin which reduces cytoskeletal linkages. (Horowitz 1996)

Subtle changes in peptide structure can have significant effects on the resulting migration. For example, GRGDS has been shown to have a biphasic relationship with cell speed whereas the lower affinity ligand GRGD found to exhibit a monophasic relationship. (Hersel *et al.* 2003, Maheshwari *et al.* 2000) Furthermore, ligand clustering can also affect cell interactions. (Maheshwari *et al.* 2000, Koo *et al.* 2002)

## 1.11 Rationale and Scope of Work

Clearly the problem of PCO is endemic. LECs which escape to the posterior

capsule before the capsular bend has formed are thought to be the key factor in its

pathology. (Kayatama 2007) However, the migration process and the effects of the

surrounding environment, including the lens material, remain relatively poorly

understood. It is known for example that square edged IOLs perform better than rounded

IOLs but the impact of IOL surface properties and the potential for modification of these

materials has not been fully explored. In order to better understand the effect of substrate

properties on the motile behaviour of lens epithelial cells, a model of cell migration was

developed. Parameters for the model were determined using literature data for cells other

than lens epithelial cells based on the assumption that cell type was a less important

factor than for example the nature of the integrins present on the surface. However,

ultimately, determination of the model parameters using lens epithelial cells would be

necessary in order to validate the model's ability to predict and to use the model to

optimize IOL surfaces.

In parallel silicone, as a model lens material, was modified with cell adhesion

peptides GYRGDS and YIGSR based on the hypothesis that increasing cell adhesion to

the IOL would alter lens cell migration, and minimize changes in cell phenotype, thereby

ultimately minimizing PCO. Presumably, discouraging EMT would lead to greater cell

adhesion allowing for capsular bend formation prior to posterior migration of the cells.

Preliminary in vitro studies using human lens epithelial cells were performed with these modified surfaces. Ultimately, it is thought that a combination of experimental studies and modeling will enable the development of superior IOL materials.

## CHAPTER 2: LENS EPITHELIAL CELL MIGRATION MODEL DEVELOPMENT

### 2.0 RATIONALE FOR THE MIGRATION MODEL

In order to better understand parameters which may affect the motile behaviour of LEC, a migration model was developed Model parameters were determined using data from the literature. The model explores the effects of different substrata, the growth factors TGFβ2 and FGF2 as well as integrin expression, affinity and activity on cell speed and using data from the model, the time it would take the LEC to breech the IOL posterior as a function of material properties and their densities was predicted. Due to the limited data available, parameter values in many cases were poorly defined, demonstrating the need for validation using in vitro data from lens epithelial cells. However, it is thought that ultimately, using a model such as this would enable prediction of material parameters which would reduce lens epithelial migration, known to be a major contributing factor in PCO.

Existing models of cell migration such as that proposed by DiMilla *et al.* 1991 examine the more microscopic aspects of cell migration. In the current work, the model was developed to predict macroscopic effects - distance traveled per unit time based on microscopic surface properties. While data used to obtain model parameters were from cells other than lens epithelial cells, the overall properties of the system are captured and ultimately cell specific properties can be incorporated with the generation of additional

data. Notwithstanding the above, it is reasonable to suggest that data from other epithelial or mesenchymal cells may provide some insight into the properties of lens epithelial cells as migration is governed by both external factors such as substratum properties which are independent of cell type and internal factors such as integrin expression. While the latter factor is cell specific, the nature of integrins does not differ significantly between different cell types and ultimately these parameters could be incorporated to generate a more generic model of cell migration.

Cell speed and the time it takes the cell to breech the posterior have an inverse relationship as seen in Figure 1. Thus, throughout the discussion, for simplicity, cell speed will be discussed as it is this parameter that is widely used in the literature. (DiMilla *et al.* 1993, Goodman *et al.* 1989, Palecek *et al.* 1997)
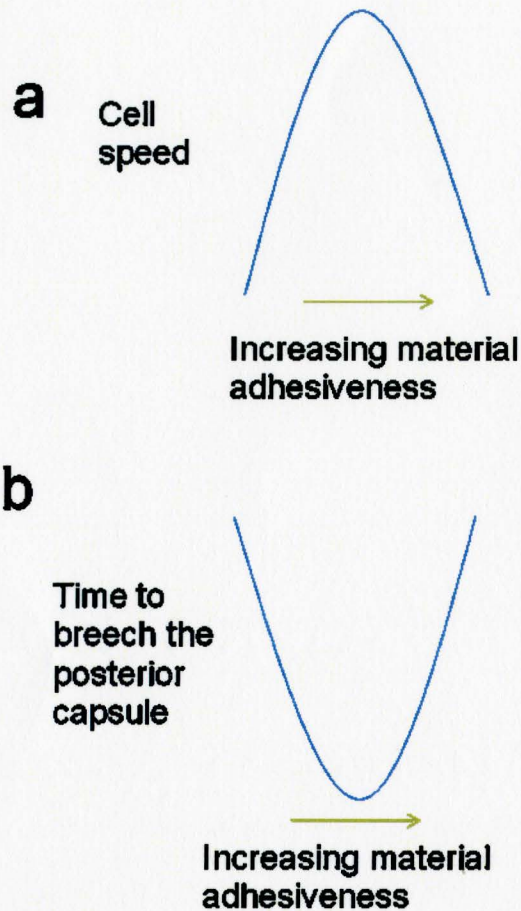
Figure 1: a; Cell speed has a biphasic relationship with cellular adhesion. If the distance the cell travels from the posterior to the anterior is divided by the cell speed, the time it takes the cell to breach the posterior can easily be determined and will have an inverse relationship with cell speed as seen in b.

## 2.1 Model Assumptions

This model was developed to describe the time taken by a single cell assumed to be located three quarters of the distance from the anterior surface of the IOL to the lens equator where it is considered to have breached the posterior. These positions were selected because *in vivo*, the majority of residual cells are known to be found in the

equatorial zone of the lens. Thus using a location closer to the edge of the IOL provides

a more realistic measurement of the time to breach the posterior than using a more

anterior location. (Davidson *et al.* 2000) A schematic view of this movement can be seen

in Figure 2.
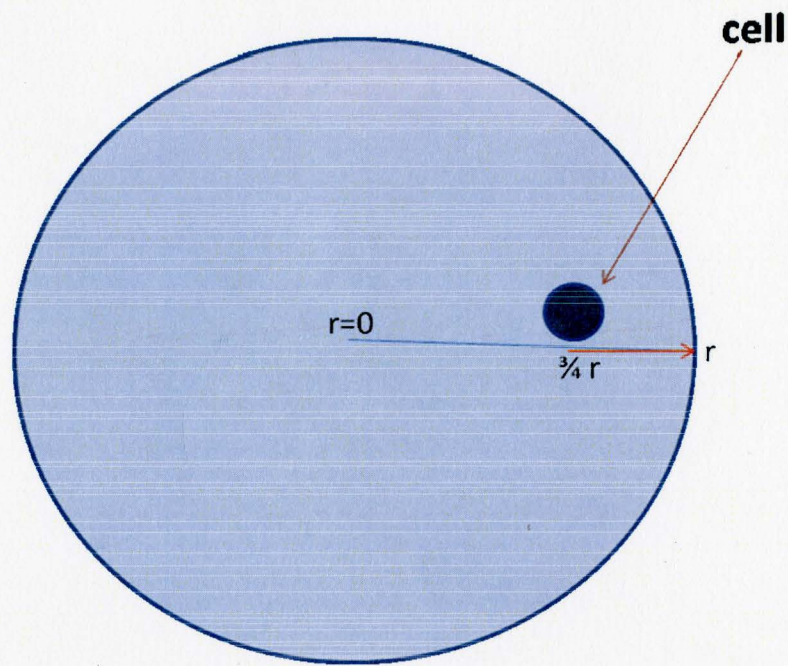


Figure 2:  Movement of a single cell along the IOL from 3/4r to r.

In this model, a simplified two-dimensional circular IOL is assumed with a

midpoint of r=0.  Moreover, since the natural lens is spherical, in this model, the effects

of curvature are ignored.  This model assumes that direction of travel is one-dimensional

and in the direction of r.  The cell will therefore travel from 3/4r to r, the perimeter of the

circle. This model does not account for cell mitosis and assumes that the cells are

migrating only. It is assumed that the IOL has a diameter of 12 mm. For simplicity, and

to allow for the use of literature data to determine the migration speeds, it was assumed

that cells of different types move with similar speeds under the influence of similar

factors. This allowed for the fitting of data from various cell types in the literature to be

used to obtain model parameters. This is a reasonable assumption as evidenced by the

work of Hirano *et al.* who examined cell attachment activities on different RGD surfaces.

Cell lines used included ovary CHO-K1 cells originating in the Chinese hamster, kidney

NRK cells originating in the rat, epidermoid carcinoma A431 originating in the human,

cervix HeLa.S3 cells origination in the human, and liver RLC-16 cells from rats. There

were no differences in cell binding activity using different tetrapeptides with the different

cell lines. This implies that cell adhesion and migration depends more on the type of

integrin presented to the adhesion peptide than the specific cell type as different cells

contain the same integrin subunits. (Hirano *et al.* 1993) Furthermore, Palecek and

colleagues discovered that both the $\alpha_{iib}\beta_3$ and $\alpha_5\beta_1$ integrins promoted maximum cell

speed at a detachment force of $2\text{-}4 \times 10^8$ N which implies that different integrins with

different ligand recognition motifs can transmit similar intracellular forces. (Palecek *et al.*

1997) Thus, it seems reasonable, particularly in a first pass, to model both different cell

types and in some cases different integrins similarly. This model will focus on the

mesenchymal integrin, $\alpha_5\beta_1$ which is known to promote lens cell migration and thus

influence PCO. Hersel and colleagues determined that with the addition of a growth

factor, cells become less adherent and more motile thus increasing the range of cellular

migration speeds. (Hersel *et al.*2003). This phenomenon is accounted for in the model. However, for modeling purposes, similar cellular behaviour was assumed for the two growth factors; that is, while the magnitude of the specific parameter, a generic function can be used to describe cellular response.

## 2.2 Model Development

As shown in Equation 1, the cell speed is assumed to be a function cell adhesion which is a function of surface properties such protein density or the presence of cell adhesion motifs, cell properties, specifically the density, affinity and activity of cell surface integrins and solution properties such as the presence of soluble factors specifically TGFβ2 and FGF2 and integrin expression, affinity and activity.

*Cell speed= F(surface) +F (soluble factors)+F(integrins)*          (Equation 1)

A "mechanistic" model was developed based on trends observed in the literature. (DiMilla *et al.* 1991, DiMilla *et al.* 1993, Maheshwari *et al.* 2000, Palecek *et al.* 1997). The model equations used were developed to allow for flexibility and ability to predict the wide variety of migrational behaviours. It should be noted that biphasic behaviours are typically observed with natural ECM components including FN and CN IV. (Maheshawari 2000, Palecek *et al.* 1997, DiMilla *et al.* 1991, DiMilla *et al.* 2003) Triphasic behaviours are the result of several different factors as illustrated by the

DiMilla model. (DiMilla *et al.* 1991) including asymmetry of adhesion within the cell

and other factors. Under these conditions, the maximum cell speed is exhibited over a

more wide range of cell substratum adhesiveness.

To best capture the widest variety of shapes seen in the literature, equations

typically observed in process control were selected. Equations typically used to describe

a first order step input into a well mixed continuous stirred tank reactor was selected for

the first part of the model as seen in Equation 2. (Marlin 2000) While in process control,

the parameters of this model have specific meanings for a step change, (Marlin 2000), in

the current work, the parameters can be translated and enable measurement of specific

factors related to cell migration. In process control, $\beta_o$ is the height of the step input.

However, in the current work, this parameter represents the maximum cell speed of the

function. Note that this may not be the maximum which the first part of the function

could achieve on its own as in process control. Moreover, the second part of the function

can dominate and the cell speed curve will start to descend before the first part of the

function has a chance to reach its maximum value. Thus, $\beta_o$ is a theoretical maximum as

it is not always achieved in the actual function. In process control, $\tau$, known as the time

constant, is essentially the volume of the reactor divided by the volumetric flow rate.

(Marlin 2000) $\tau_o$ represents the 63.2% of the final change in the steady state output.

(Marlin 2000) In this model $\tau_o$ is the surface adhesiveness value at which the LEC will

reach 63.2% of $\beta_o$ and as such may serve as a universal gage with which to compare

different surface sensitivities and cell speeds.

$$cell\ speed = \beta_o\left[1 - e^{-\frac{x}{\tau_o}}\right]$$          (Equation 2)

In the model, described by Equation 2, cell immotility is associated with a

substrate density of zero based on an x intercept of zero. *In vivo*, this will occur at a non-

zero value because in order for cellular attachment to occur in the first place, the substrate

will have a certain non zero density of cell adhesion ligands. To account for this, the

function must be shifted $x_o$ to the right as seen in Equation 3.

$$cell\ speed = \beta_o\left[1 - e^{-\frac{x-x_o}{\tau_o}}\right]$$          (Equation 3)

This model thus far represents monophasic cell migration behaviour which is

appropriate in some specific circumstances such as in the work of Maheshwari and

colleagues who used low affinity RGD clusters. (Maheshwari *et al.* 2000) To capture the

more relevant bi- or triphasic relationships which have been shown to exist in other

systems, (DiMilla *et al.* 1991, DiMilla *et al.* 1993) an exponential term was added to the

model. In this case, $x_{oo}$ represents the point at which the exponential function will

become dominant as described in Equation 4. The $x_{oo}$ must be selected to allow for a

short lag period as the exponential function will begin with small values and will not start

to decrease at significant rates in the first part of the function. In biphasic functions, $x_{oo}$

36

can be selected such that there exists one $\beta_o$ value after which point the function will start

to descend. In triphasic functions, the cell is at a maximum speed for a variety of cell

substratum adhesiveness values. $x_{oo}$ can be selected such that it allows the first part of

the function to plateau for a range of surface adhesiveness values and then the second

part of the function dominates after the plateau period. Thus, this model can capture

monophasic, biphasic and triphasic functions

Finally, the rate of cellular acceleration on the low end of substrate adhesiveness

may not be the rate of deceleration at higher levels of substrate adhesiveness as evidenced

by results from DiMilla and colleagues with CHO cells migrating over FN and CN IV

substrata. (DiMilla $et\ al.$ 1993) To account for this, $\tau_o$ and $\tau_{oo}$ are assigned to the first and

second part of the model respectively seen in Equations 3 and 4.

$$cell\ speed = \beta_o \left[ 1 - e^{-\frac{x-x_o}{\tau_o}} \right] + 1 - e^{\frac{x-x_{oo}}{\tau_{oo}}} \qquad \text{(Equation 4)}$$

Equation 4 and its components are shown in Figure 3.

**Cell speed**

$$\beta_o\left[1-e^{-\frac{x-x_o}{\tau_o}}\right] \qquad 1-e^{-\frac{x-x_{oo}}{\tau_{oo}}}$$

$0.632\beta_o$

$\beta_o$

$x_o \quad \tau_o \quad x_{oo} \quad \tau_{oo}$

**Increasing material adhesiveness (or protein density)**
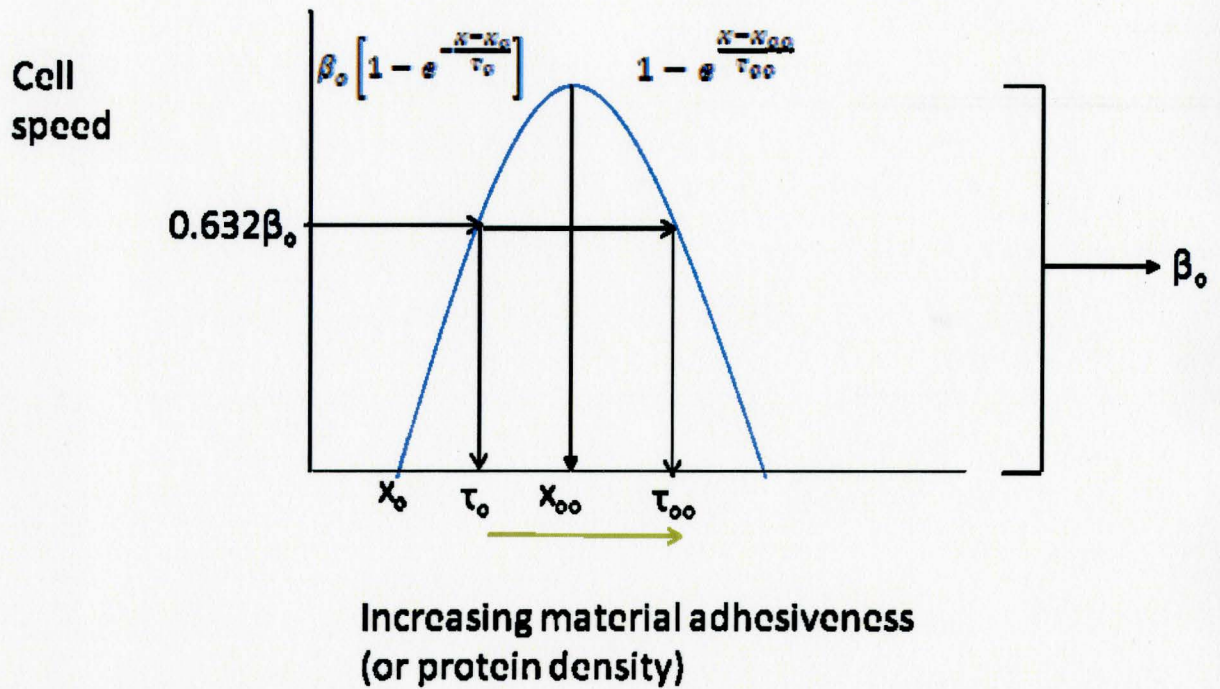
Figure 3:  Model of cell speed versus substratum adhesiveness where $x_o$ is the x intercept at which point the model is initiated and the cell remains immotile, $x_{oo}$ value that the second exponential part of the model prevails.  The ascending part of the graph represents a step input of a first order rate of decay model with a height of $\beta_o$ and the descending section is an exponential function.  Note that in this case, as the graph is symmetric about the center of the function and will have equivalent $\tau$ values.

The model to this point contains 5 separate parameters and provides information

on the effects of the surface and cell expression of integrins.  However, since it has been

shown that the addition of growth factors will affect cellular migration (Maheshwari *et al.*

2000) additional parameters are needed.  In this work it was found that the shape of the

curve did not change but the maximum cell speed was found to be altered by the presence

of the growth factor, specifically EGF in this case.  To account for this, in the final

model, the parameter $\beta_o$ was changed by the factor $\beta_{GF}$.  Of note, the value of this factor

38

may be positive or negative to account for the presence of growth factors which stimulate

or inhibit migration. The final equation used to describe the data is shown in Equation 5

is depicted in Figure 4. In keeping with the desire to maintain a more macroscopic view

of the system, the model does not distinguish between the effect of different growth

factors but rather considers the combined effect. In this way, the model could include

TGFβ2, FGF2 or the combined effect of both.

$$cell\ speed = (\beta_o + \beta_{GF})\left[1 - e^{-\frac{x-x_o}{\tau_o}}\right] + 1 - e^{\frac{x-x_{oo}}{\tau_{oo}}} \qquad \text{(Equation 5)}$$
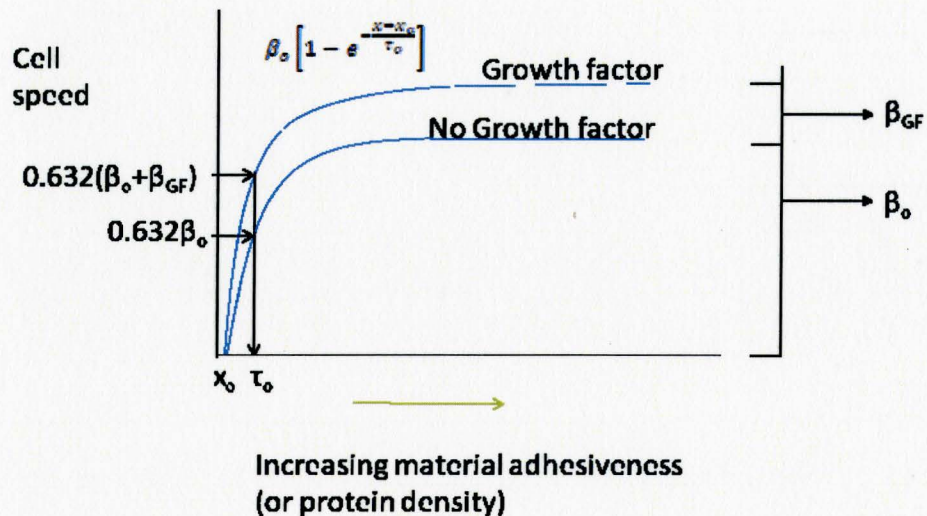


Figure 4: An increase in the maximum cell speed of $\beta_{GF}$ due to the addition of a growth
factor into the environment. Figure adapted from Hersel *et al.* 2003.

Figure 4 depicts a monophasic model. In this case, $\tau_{oo}$ would be infinite.

Inserting this value into Equation 5, makes the second exponential fraction equivalent to zero and the overall exponential function equivalent to 1. As a result, the second part of the equation is cancelled to obtain the original monophasic first order rate of decay.

$$cell\ speed = (\beta_o + \beta_{GF})\left[1 - e^{-\frac{x-x_0}{\tau_0}}\right] + 1 - e^{\frac{x-x_{00}}{\infty}} \quad \text{(Equation 6)}$$

$$cell\ speed = (\beta_o + \beta_{GF})\left[1 - e^{-\frac{x-x_0}{\tau_0}}\right] + 1 - e^{0} \quad \text{(Equation 7)}$$

$$cell\ speed = (\beta_o + \beta_{GF})\left[1 - e^{-\frac{x-x_0}{\tau_0}}\right] \quad \text{(Equation 8)}$$

Ultimately, it would also be of interest to incorporate the effect of integrin expression, affinity and activity was explored. Palecek and colleagues investigated the effect of increasing the expression of $\alpha_5$ integrin; this integrin is known to be associated with migration on FN substrata. They also explored the effects of $\alpha_{iib}\beta_3$ and higher affinity mutant of $\alpha_{iib}\beta_3(\beta_{1-2})$ in inactive versus activated states on fibronectin substrata. It was determined that a shift to the left and a narrowing of the parabolic graph shape in CHO speed versus FN concentration was achieved with increasing $\alpha_5$ expression, upon integrin activation and upon shifting from a lower to a higher affinity integrin. (Palecek et al. 1997) Hersel and colleagues showed similar results. (Hersel et al. 2003) Interestingly, the maximum speed remains unchanged when varying the integrin expression, activation or affinity. This is thought to be the result of saturation of the integrins. If the expression, affinity or activation of the integrin is increased, this

saturation point is reached more quickly. (Palecek*et al.* 1997)  A similar observation was

made by DiMilla. (DiMilla *et al.* 1991)  For the purposes of this work, it can therefore be

inferred that cell speed is minimized at both low and high levels of ligand or receptor

occupancy. Since it is of interest to select surfaces with high adhesiveness or protein

concentrations, a lower level of cellular integrin expression may occur.  As seen in the

curves, small changes in integrin expression affinity or activity can lead to comparatively

large changes in cell speed. (Palecek *et al.* 1997)

In this model, increased integrin expression, affinity or activation is expected to

lead to a shift left in the graph at $x_{oo}$ of $x_{ooi}$, as well as a shift at $x_o$ of $x_{oi}$. The function

also narrows as the integrins are now more sensitive to changes in substrate density. $\tau$

values thus become smaller and are now written as $\tau_o$-$\tau_{oi}$ and $\tau_{oo}$-$\tau_{ooi}$ . This is seen in

Equation 9 which does not distinguish between integrin expression, affinity or activation;

therefore, one of these effects or any combination of these effects may be explored.  The

shift in the cell speed versus cell substratum adhesiveness is a result of different integrin

influences and can be seen in Figure 5.

$$cell\ speed = (\beta_o + \beta_{GF}) \left[ 1 - e^{-\frac{x-x_o-x_{oi}}{\tau_o-\tau_{oi}}} \right] + 1 - e^{\frac{x-x_{oo}-x_{ooi}}{\tau_{oo}-\tau_{ooi}}} \quad \text{(Equation 9)}$$
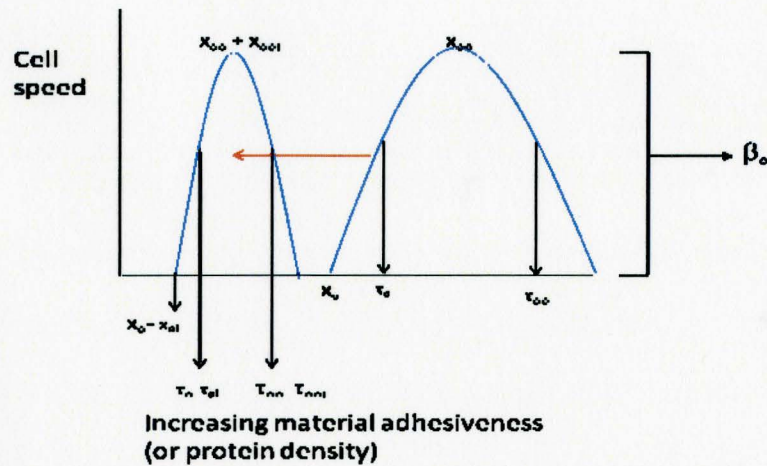
Figure 5: Effect of integrin increase in concentration, increase in affinity or activation by a shift of $x_{oi}$ and $x_{ooi}$ left along the x axis and a change in the $\tau$ values of $\tau_o$-$\tau_{oi}$ and $\tau_{oo}$-$\tau_{ooi}$. Figure adapted from: Hersel *et al.* 2003.

Dividing the distance the cell has to travel by the speed determined from Equation 9 will compute the time it takes for the LECs to breach the capsule posterior seen in Equation 10. A model constant of 1500μm is assumed based on the assumed initial position of the cell ¾ the distance along a 6mm IOL.

$$time\ to\ breach\ = d/\{(\beta_o + \beta_{GF})\left[1 - e^{-\frac{x-x_o-x_{oi}}{\tau_o-\tau_{oi}}}\right] + 1 - e^{\frac{x-x_{oo}-x_{ooi}}{\tau_{oo}-\tau_{ooi}}} \}\quad \text{(Equation 10)}$$

## CHAPTER 3: MODEL CALCULATIONS

### 3.1 Acrylic surface calculations for cell speed

Kayatama and colleagues performed migration assays using human SRA01/04 LECs. (Kayatama 2007) Using CN I coated membranes and three different acrylic IOLs (low, medium and high tackinesses), cell migration measurements were made. Data from this work were converted to cell speed using methods presented in Appendix A.

### 3.1 Estimation of the capsular cut-off density

As noted, there exists a competition between the lens capsule and the IOL and this will in turn determine which substrate will govern cell speed. It is hypothesized that in cases where the substrate is less conducive to cell adhesion, the LEC speed will be governed by the capsule. As such, a theoretical capsular cut-off density was established to reflect the critical value of substrate adhesiveness based on for example cell adhesion peptide density, where below this value, the cells will prefer to adhere to the capsule and this will govern cell migration not the IOL. Based on this hypothesis, materials below this critical density are thought to be unsuitable as IOL materials. The critical density was determined based on data from Cammerata and colleagues who studied the composition of the healthy bovine lens (Cammarata 1986). Assuming that the bovine lens and the human lens will have a similar distribution and density of proteins, CN, LN, FN, entasin, and heparin sulphate proteoglycans (HSPG)s were determined to be at the densities

43

shown in Table 1. While not likely true, it was assumed that all of the proteins behave

similarly and can therefore be lumped together to get a generic overall density. The

capsule take-over cutoff density of 300 molecules $/\mu m^2$ is the sum of all of the protein

densities listed multiplied by 1.5 and rounded to give a conservative estimate.

Table 1: Substrate densities in the healthy bovine lens. Data taken with permission from
Cammarata 1986, Table 1.

| Substrate | Density (molecules/$\mu m^2$) |
|---|---|
| CN | 65 |
| LN | 33 |
| FN | 27 |
| Entacin | 45 |
| HSPG | 35 |

### 3.1 Graphing and Statistics

SigmaPlot 9.0 was used for all statistical analyses. The SigmaPlot curve fitter uses the

Marquardt-Levenburg algorithm, a non-linear regression equation, to determine the

parameters of the independent variable which gives the best fit between the data and the

equation. This method seeks parameters which minimize the sum of squared differences

between predicted and observed values of the dependent variable as shown in Equation

11.

$$SS = \sum_{i=1}^{n} w_i (y_i - \hat{y}_i)^2 \qquad \text{(Equation 11)}$$

Equation 11 was used to fit the model to the literature data. Three assumptions are made

in non-linear regression (Montgomery 2003):

1  The population is normally distributed about the regression

2  The variance of the dependent variable within this population is constant

   regardless of the value of the independent variable

3  Residuals are independent of each other

To test these assumptions and to assess the efficacy of the non-linear regression, three

test statistics were used; normality, constant variance and the Durbin-Watson statistic.

SigmaPlot utilizes the Kolmogorov-Smirnov test to check for a normally distributed

population. Constant variance is computed by using the Spearman rank correlation

between the absolute values of the residuals and observed value of the dependent

variable. The Durbin-Watson statistic is a measure of serial correlation between

residuals and typically can happen if time is a factor in one of the variables.

## CHAPTER 4: MODEL RESULTS AND DISCUSSION

45

## 4.1 MODEL RESULTS

In order to test the model, all of its components including protein or surface adhesivity, the presence of a growth factor and integrin concentration, affinity, and activity were evaluated as shown in Figures 7 through 15. In addition, a large range of cell speed versus surface adhesivity graph functions was examined including monophasic, biphasic, and triphasic. A summary of the type of surface, range of densities at which they occur, and cell types used can be found in Table 2. A summary of all the parameters and statistics used in Figures 7 through 15 can be found in Table 3. All data proved to be normally distributed while the majority of the data failed both the constant variance and the Durbin-Watson tests presumably due to the large number of parameters to be fitted, even in the simplest cases and the relative lack of data points available for fitting.

Table 2:  Substrates, their range of densities and cell type used for the migration tests

| Substrate | Lowest surface density tested (molecules/$\mu$m$^2$) | Highest surface density tested (molecules/$\mu$m$^2$) | Cell type | Author | Figure |
|---|---|---|---|---|---|
| LN | 120 | 300 | MM14dy Myoblasts | Goodman 1989 | Figures 7, 13 |
| FN | 4000 | 60000 | Murine NR6 fibroblasts | Maheshwari 2000 | Figure 6, 13 |
| FN | 400 | 1250 | Human smooth muscle cells | DiMilla 1993 | Figure 8, 14 |
| CN IV | 400 | 14000 | Human smooth muscle cells | DiMilla 1993 | Figure 8, 14 |
| GYRGD (exploring the effect of growth factors with EGF) | 1000 | 50000 | Murine NR6 fibroblasts | Maheshwari 2000 | Figure 9 |
| FN (exploring cellular integrin concentration) | 1$\mu$g/mL (concentration) | 100$\mu$g/mL (concentration) | B2 Chineses hamster ovary cells transfected with human $\alpha$5 Cadna | Palecek 1997 | Figure 10 |
| Fibrinogen (FG) (exploring cellular integrin activation and affinity) | 1$\mu$g/mL (concentration) | 100$\mu$g/mL (concentration) | B2 Chineses hamster ovary cells expressing human $\alpha$IIb$\beta$3 and $\alpha$IIb$\beta$3($\beta$1-2) | Palecek 1997 | Figure 11 |
| acrylic | 24gf | 63gf | Human LECs SRA01/04 | Kayatama 2007 | Figure 12, 15 |

Table 3a: Summary of all parameters used in Figures 6 through 15.

| | $\beta_o$ ($\mu$m/hr) | $x_o$ (*mol/$\mu$m$^2$) | $\tau_o$ (*mol/$\mu$m$^2$) | $x_{oo}$ (*mol/$\mu$m$^2$) | $\tau_{oo}$ (*mol/$\mu$m$^2$) | $x_{oi}$ (*mol/$\mu$m$^2$) | $\tau_{oi}$ (*mol/$\mu$m$^2$) | $\beta_{GF}$ ($\mu$m/hr) | $x_{ooi}$ (*mol/$\mu$m$^2$) | $\tau_{ooi}$ |
|---|---|---|---|---|---|---|---|---|---|---|
| Fig 6 | 42.9 | 2600 | 4414.1 | 32000.0 | 9944.9 | - | - | - | - | - |
| Fig 7 | 76.8 | 34.2 | 160.1 | 302.7 | 76.0 | - | - | - | - | - |
| Fig 8 | FN 2708 | FN 268 | FN 165445 | FN 720 | FN 191 | FN - | FN - | FN - | FN - | FN - |
| | CNIV 25 | CNIV 376 | CNIV 4320 | CNIV 8701 | CNIV 2493 | CNIV - | CNIV - | CNIV - | CNIV - | CNIV - |
| Fig 9** | No EGF 14.8 | No EGF 803.9 | No EGF 896.6 | No EGF - | No EGF $\infty$ | No EGF - | No EGF - | No EGF - | No EGF - | No EGF - |
| | EGF 14.8 | EGF 824.0 | EGF 896.6 | EGF - | EGF $\infty$ | EGF - | EGF - | EGF 11.9 | EGF - | EGF - |
| Fig 10*** | 17 | 0.7 | 3.4 | 9.9 | 3.7 | 0.17X -1.8 | 0.17X -28.3 | | 0.17X -75.8 | 0.17X 1.8 |
| | | | | | | 0.47X 0.6 | 0.47X -8.6 | - | 0.47X 13.1 | 0.47X 20.5 |
| | | | | | | 1.0X - | 1.0X - | | 1.0X - | 1.0X - |
| Fig 11a**** | 19 | 0.02 | 0.03 | -0.8 | 0.7 | LAR -0.15 | LAR -1.73 | | LAR -5.38 | LAR 0.48 |
| | | | | | | HAR -0.047 | HAR 0.014 | - | HAR 19.94 | HAR -8.37 |
| | | | | | | LAA -0.047 | LAA -0.031 | | LAA 3.70 | LAA -2.17 |
| | | | | | | HAA - | HAA - | | HAA - | HAA - |
| Fig 11b**** | 19 | 0.3 | 0.1 | 0.7 | 0.8 | HAR 0.3 | HAR 0.25 | - | HAR 2.2 | HAR -0.7 |
| | | | | | | LAA - | LAA - | | LAA - | LAA - |
| Fig 12 | 6.0 | 17.8 | 7.2 | - | - | - | - | - | - | - |
| Fig 13 | FN 42.9 | FN 2600 | FN 4414.1 | FN 32000.0 | FN 9944.9 | - | - | - | - | - |
| | LN 76.8 | LN 34.2 | LN 160.1 | LN 32000.0 | LN 76.0 | | | | | |
| Fig 14 | 6.0 | 17.8 | 7.2 | - | - | - | - | - | - | - |
| Fig 15 | FN 42.9 | FN 2600 | FN 4414.1 | FN 32000.0 | FN 9944.9 | - | - | - | - | - |
| | LN 76.8 | LN 34.2 | LN 160.1 | LN 32000.0 | LN 76.0 | | | | | |

*mol/$\mu$m$^2$ is equivalent to molecules/$\mu$m$^2$

** $\beta_o$, $\tau_o$, and $x_o$ values are the same in the presence and absence of EGF

***$x_{oi}$, $\tau_{oi}$, $x_{ooi}$, $\tau_{ooi}$ values are taken with respect to the 1.0X $\alpha$5 integrin concentration

**** $x_{oi}$, $\tau_{oi}$, $x_{ooi}$, $\tau_{ooi}$ values are taken with respect to the resting low affinity integrin state

Table 3b: Test statistics to assess the appropriateness of using non linear regression to solve the model addressing Figures 6 through 15. Note that where R$^2$ = 1, not enough data was available to fit to the number of parameters given in the cell speed equation.

| | Normality | Constant variance | Durbin–Watson statistic | R$^2$ |
|---|---|---|---|---|
| Figure 6 | passed | failed | failed | 1.0 |
| Figure 7 | passed | failed | failed | 1.0 |
| Figure 8 FN | passed | passed | failed | 1.0 |
| CNIV | passed | passed | failed | 1.0 |
| Figure 9* EGF | passed | failed | passed | 0.96 |
| No EGF | passed | failed | failed | 1.0 |
| Figure 10** 0.17X | passed | passed | failed | 0.80 |
| 0.47X | passed | failed | failed | 0.90 |
| 1.0X | passed | passed | failed | 0.88 |
| Figure 11a*** LAR | passed | passed | failed | 0.81 |
| HAR | passed | passed | failed | 0.32 |
| LAA | passed | passed | failed | 0.80 |
| HAA | passed | passed | failed | 0.82 |
| Figure 11b*** HAR | - | - | - | - |
| Figure 11b*** LAA | - | - | - | - |
| Figure 12 | failed | failed | failed | 1.0 |
| Figure 13 FN | passed | failed | failed | 1.0 |
| LN | passed | failed | failed | 1.0 |
| Figure 14 | failed | Failed | failed | 1.0 |
| Figure 15 | failed | failed | failed | 1.0 |

Figure 6, which shows fibroblast migrational data from Maheshwari *et al* (2000)

demonstrates the triphasic relationship which exists between cell speed and FN density.

At a density of between 900 to 20000 molecules/$\mu m^2$, cells accelerate from immotile to

their maximum speed. Cells reach a maximum speed of 42.9$\mu m$/hr ($\beta_o$) at a density of

approximately 20000 molecules/$\mu m^2$. From approximately 20000 to 40000

molecules/$\mu m^2$, cells travel at this plateau velocity, at which point they start to decelerate.

$\tau_o$ (4414.1 molecules/$\mu m^2$) is much smaller than $\tau_{oo}$ (9944.9 molecules/$\mu m^2$) which is

reflected in the rapid acceleration and much slower deceleration. Based on the data, an $x_o$

value where theoretically the cells are immobile occurs at a FN density of 2600

molecules/$\mu m^2$. In reality this is not the case and the lens material will compete with the

capsule in terms of which substrate will govern cell motility. The concentration at which

the second exponential part of the model dominates ($x_{oo}$) occurs at a FN density of 32000

molecules/$\mu m^2$.

As noted in Table 2, the model fits the data with perfect accuracy as reflected in

the $R^2$ value of 1.0. However, in this case, as in most cases in this work, the lack of data

and the relatively large number of parameters fitted limited the fitting potential.

Therefore, the $R^2$ must be used with caution and there is clearly a need to test the model

and determine the parameters using additional data. The data are normally distributed as

they passed the normality test. The data however failed the constant variance test and the

Durbin-Watson test indicating that the model may not be picking up all of the trends in

the data and the residuals may be correlated.
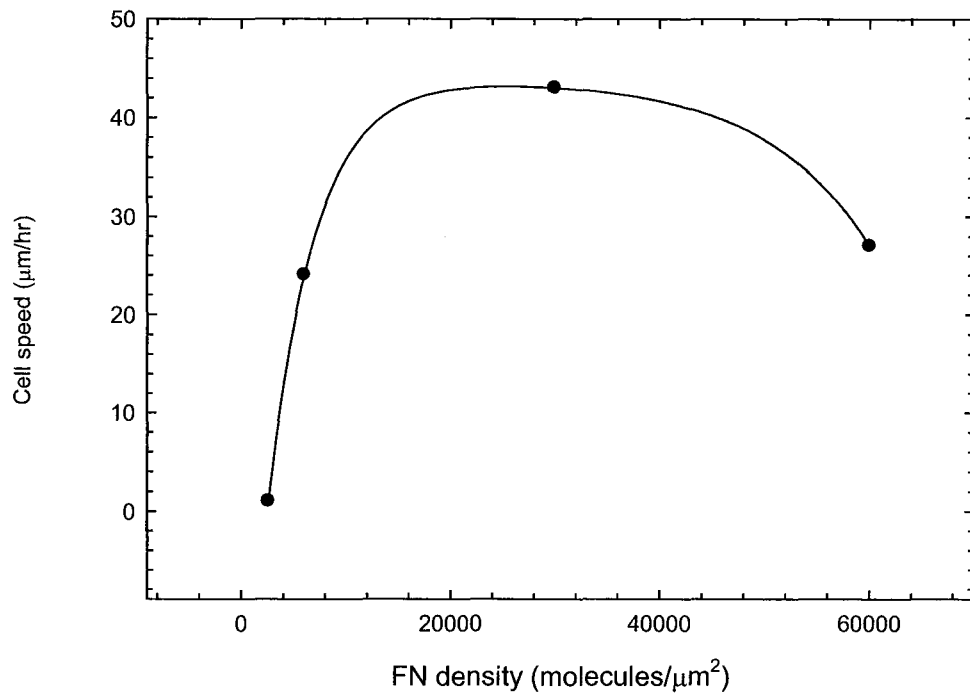
Figure 6: Cell speed on different FN surface densities. The filled circles represent the data and the solid line represents the model. Data taken with permission from Maheshwari *et al.*, 2000, Figure 3a.

Figure 7 depicts the movement of myoblast cells over a LN surface. The function is biphasic and quite similar to that of FN however it is more of a parabolic shape and does not have a plateau. Thus, on the lower end of surface density, cells accelerate until approximately 400 molecules/$\mu m^2$ at a speed of 76.8 $\mu m/hr$ ($\beta_o$) after which point they begin to decelerate. The range of densities at which cells are motile on this surface are two orders of magnitude smaller than that of FN and spans over a much smaller distance. Again however, additional data are necessary to capture the real effects.

51
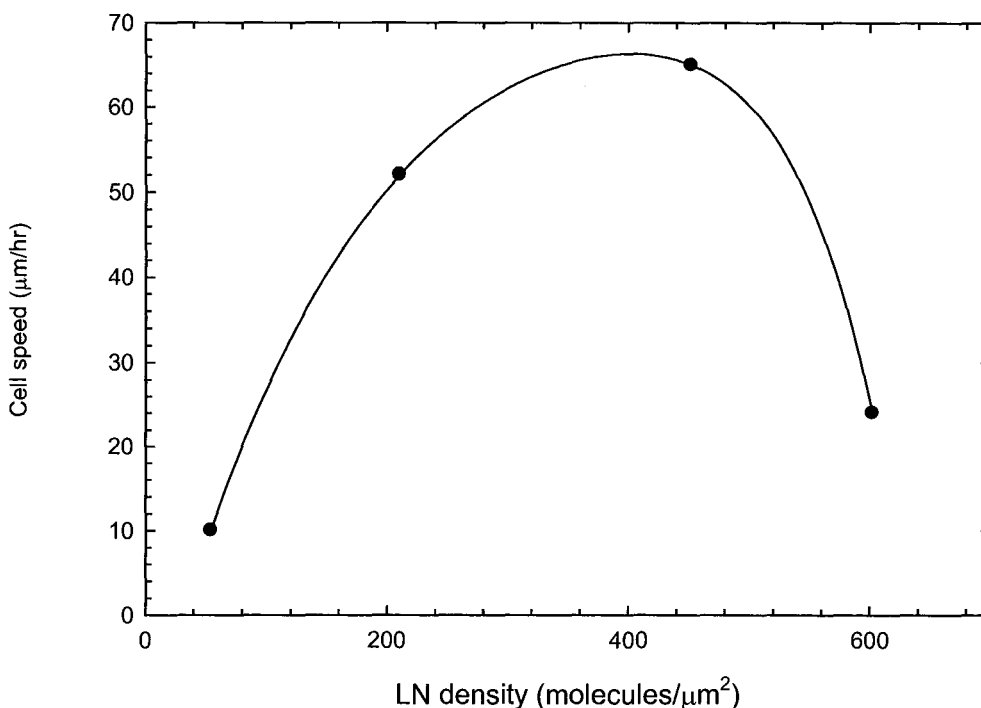
Figure 7: Myoblast cell speed on different LN surface densities. The filled circles represent the data and the solid line represents the model. Data taken with permission from: Goodman 1989 *et al.*, Figure 5a.

Figure 8 depicts smooth muscle cell migration on both FN and CN IV surfaces. Both proteins exhibit the characteristic biphasic relationship. FN is shows a triphasic trend different from the biphasic trend seen in Figure 6 presumably because different cell types were used which will express different integrins and therefore possess different migrational behaviours. The range of surface densities at which the FN cell speed curve takes place in Figure 8 compared to Figure 6 is over an order of magnitude lower; again, likely due to the expression of different integrin types. Thus different adhesivity and

different cell speeds will be achieved. This contradicts the assumption that different cell types behave similarly and will be further addressed in the discussion.
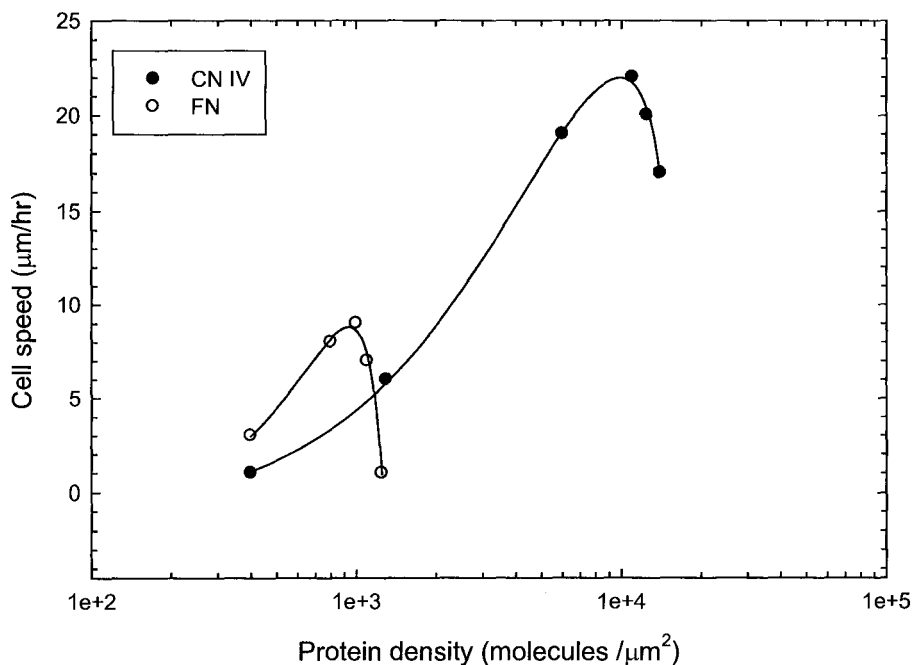


Figure 8: Cell speed at different FN and CN IV surface densities. The filled circles represent the data and the solid line represents the model. Data taken with permission from DiMilla *et al.* 1993 Figure 3b.

Figure 9 depicts murine fibroblast migration on a low affinity GYRGD surface in the presence and absence of EGF. A monophasic relationship between cell speed and surface density exists in this case. It can be seen that the EGF has the effect of increasing the maximum cell speed from 14.8µm/hr to ($\beta_o$) 26.7 µm/hr, an increase of 11.9 µm/hr ($\beta_{GF}$). In this case, the $\tau_o$ values, indicating the rate of cellular acceleration with

increasing surfaces density are equivalent in the presence and absence of EGF, but the

overall speed of travel is altered. In this model, $\tau_{oo}$ is equivalent to $\infty$, which causes the

second portion of the model to cancel leaving the monophasic exponential decay which

plateaus at a height of $\beta_o$ in the absence of EGF or $\beta_o + \beta_{GF}$ in its presence.
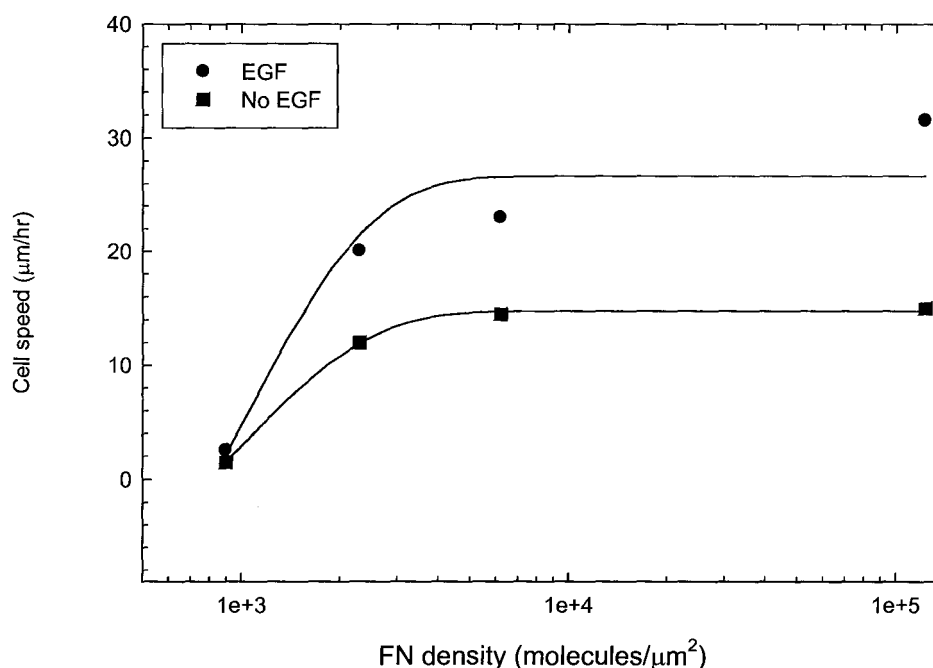


Figure 9: Cell speed on different GYRGD (low affinity peptide) surface densities in the
presence (filled circles) and in the absence (filled squares) of EGF. The solid lines
represent the model. Parameters were determined from SigmaPlot for the No EGF
model, subsequently, $\tau_o$ was turned into constants and $\beta_o$ and $x_o$ were parameter. $\beta_{GF}$ was
determined by subtracting $\beta_o$ ( EGF model) from $\beta_o$ (No EGF model) Data taken with
permission from Maheshwari 2000, Figure 3 a and b, 1RGD/star.

Figure 10 depicts the relationship between cell speed and FN density when cells

express different $\alpha_5$ integrin concentrations.  It can be seen that with increasing concentrations of the integrin, the range of FN densities over which cell motility occurs narrows and the curve shifts to the left. However the $\beta_o$ values do not change. Additionally, the range of FN density over which high cell speeds occur is narrowed.  In this case however, not all data tested reach the specified $\beta_o$ value before the cells begin to decelerate.  Moreover, concentrations of 1.0X, 0.47X and 0.17X (where X indicates relative $\alpha_5$ expression) reach maximum cell speeds of approximately 17μm/hr, 12.5μm/hr and 16μm/hr.  Since it has been demonstrated that the hight of the graph should not change when the cell speed curve is shifted left or right (Hersel 2003) and in Figure 10, there is a lot of difference, this is presumably attributed to the large amount of error associated with the data.  As the cell speed curve narrows, the second part of the model will dominate at an earlier time point.  This results in a lower maximum cell speed as might be expected based on the fact that the cells are unable to bind as efficiently. Furthermore, the values of $x_{oi}$ and $x_{ooi}$ become larger, which leads to a shift in the graph to the left with increasing concentration.  $\tau_{oi}$ and $\tau_{ooi}$ values become smaller which causes the cellular migration curve to have increased sensitivity to changes in substratum adhesivness.  Morover, the acceleration and deceleration are increased.  The only case where this trend is not seen is in the $\tau_{oi}$ value of the 0.47X of -8.62 molecules/μm$^2$ making the overall $\tau$ value ($\tau_o$-$\tau_{oi}$) larger and the response slower. With this model, the Marquardt-Levenburg algorithm is much more accurate.  The relationship between cell speed and ?? are wider in range.  Acceptable fitting was evidenced by the R$^2$ of 0.88 and

0.90 for 1X and 0.47X respectively.
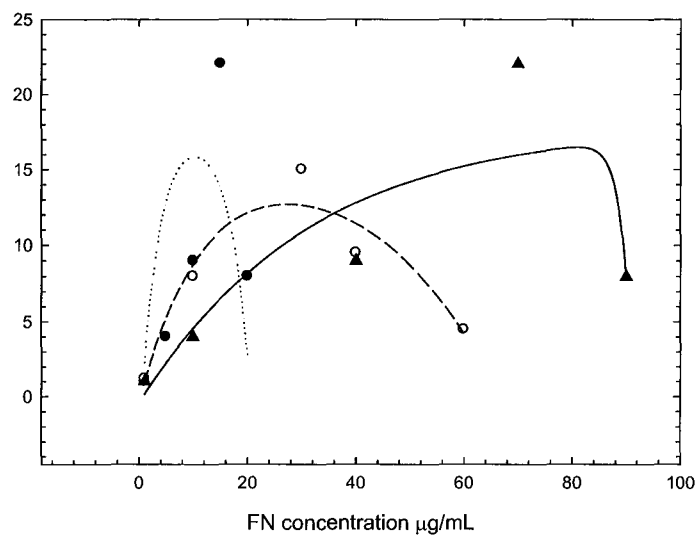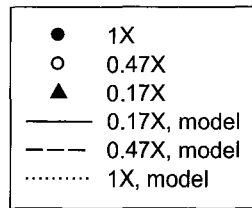


Figure 10: Cell speed on different FN surface densities where cells populations express different relative $\alpha_5$ concentrations of 0.17X (filled triangles), 0.47X (open circles) and 1.0X (filled circles) where X indicates relative $\alpha_5$ expression. The solid line represents the model for 0.17X, Te dashed line represents the model for 0.47X and the dotted line represents the model for 1.0X. $\beta_0$ was set as a constant of 17 for all integrin concentrations. This was a guess between the highest values of each integrin concentration data point. All other values were determined from SigmaPlot. Shifts in the graph of $x_{oi}$, $x_{ooi}$, $\tau_{oi}$, $\tau_{ooi}$ were then determined with respect to the 1.0X integrin concentration. Figure taken with permission from Palecek 1997, Figure 1a.

Figures 11a and 11b depict the range of cell speeds over fibrinogen (FG)

substrates with cells expressing a low integrin affinity in resting (LAR) and activated

states (LAA) and a high affinity integrin in resting (HAR) and activated states (HAA). The $x_{oi}$ and $x_{ooi}$ values decreased when increasing integrin, activity or affinity, narrowing the curve and shifting it to the left. $\tau_{oi}$ values essentially follow the same trend as in Figure 10 with only minor differences between HAR and LAA values. $\tau_{ooi}$ values however did not follow any trend; this can likely be attributed to errors in the data or to the lack of available data leading to errors in the model prediction. In this model, a $\beta_o$ of 19 µm/hr was specified however, similarly to Figure 10, with the exception of the LAR, none of the graphs reached this maximum value before beginning to decelerate. Maximum cell speeds reached were approximately 14 µm/hr for HAR, 10 µm/hr for LAA and 15.5 µm/hr for HAA.

In Figure 11a, using the Marquardt-Levenburg algorithm, wider cell speed curves show a better fit as evidenced by the increasing $R^2$ value with narrowing from 0.97 for LAR decreasing to 0.32 for HAR. LAA and HAA values were 0.80 and 0.82, respectively which are still quite low. Clearly, the HAR value is not an acceptable fit to the data. Thus for the HAR and LAA graphs the data were replotted in Figure 11b with hand selected parameters to demonstrate that the model has the ability to fit more narrow and irregular shapes. Additionally, the data for HAR and LAA are not a bi- or triphasic functions but seem to have a tetraphasic or "S" shaped trend which is not specifically captured by the model.
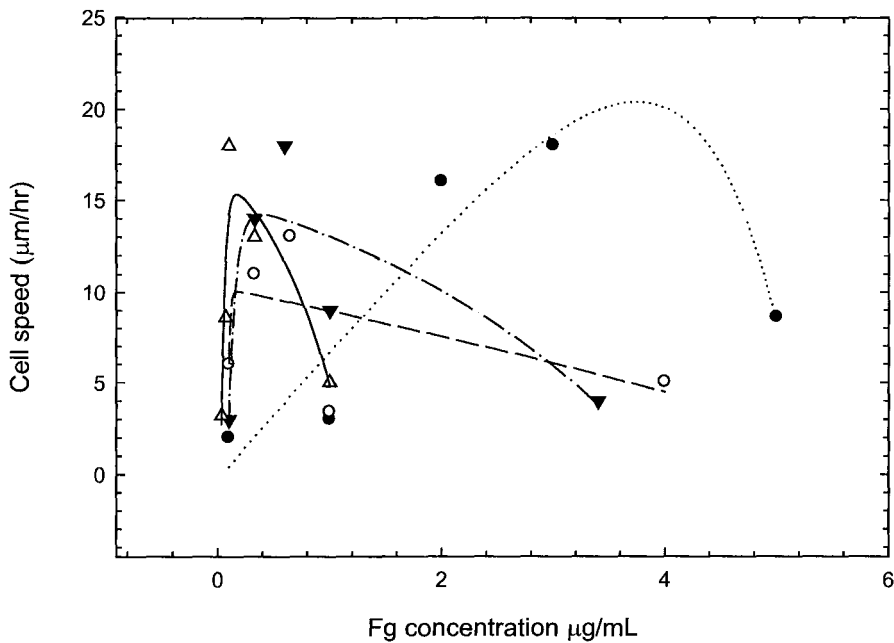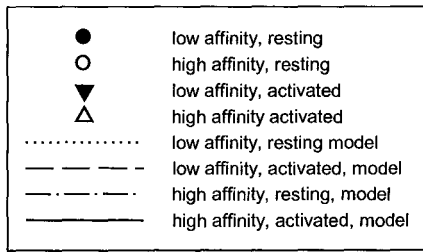
Figure 11a: Cell speed on different FG surface densities at different integrin activation and affinity states: low affinity, resting (LAR) (filled circles), high affinity resting (HAR) (open circles), low affinity activated (LAA) (filled triangles), high affinity activated (HAA) (open triangles). The solid lines represents the model using the high affinity activated integrin, the dash dot line represents the model using the high affinity resting integrin, the dashed line represents the model using the low affinity activated integrin and the dotted line represents the model using the low affinity resting integrin. $\beta_o$ was set as a constant of 19 for all integrin concentrations. This was a guess between the highest values of each integrin concentration (from the data). All other values were determined from SigmaPlot. Shifts in the graph of $x_{oi}$, $x_{ooi}$, $\tau_{oi}$, $\tau_{ooi}$ were then determined with respect to the high affinity, activated integrin states. Data taken with permission from Palecek 1997, Figure 1b
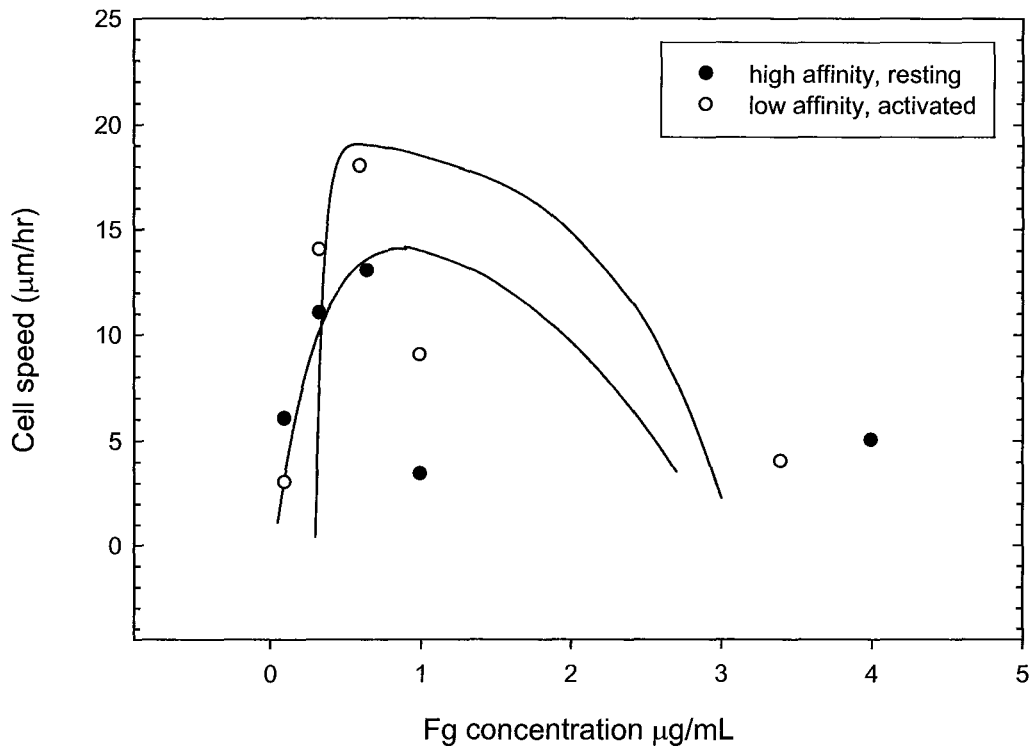
Figure 11b: Cell speed on different FG surface densities at different integrin activation and affinity states: high affinity resting (HAR) (filled circles), low affinity activated (LAA) (open circles). The solid lines represent the model with hand selected parameters. For this model, the parameters in Figure 11a were instead hand selected as the Marquardt-Levenburg algorithm did not do an accurate job at capturing the model with this set of data. For the parameters found in Table 2, HAR integrin affinity, activity and concentration parameters were taken with respect to LAA. Data taken with permission from Palecek 1997, Figure 1b.

Figure 12 demonstrates cell movement on acrylic surfaces at a low, medium and high

values of surface tackiness (Kayatama 2007). Adhesive force is measured with a

tackiness tester in grams of force (gf). This adhesive force can be defined by the amount

of force exerted in order to separate the acrylic material from the probe of the tackiness

tester. The procedure for measuring tackiness is described in detail by Kayatama and

colleagues. (Kayatama 2007) The trend observed in Figure 12 is monophasic with an $R^2$

of 1.0, again based on the fact the number of data points is limited. However, it is clear

from the results that cells travel with greater speed on surfaces with high tackiness

compared to those with low tackiness.
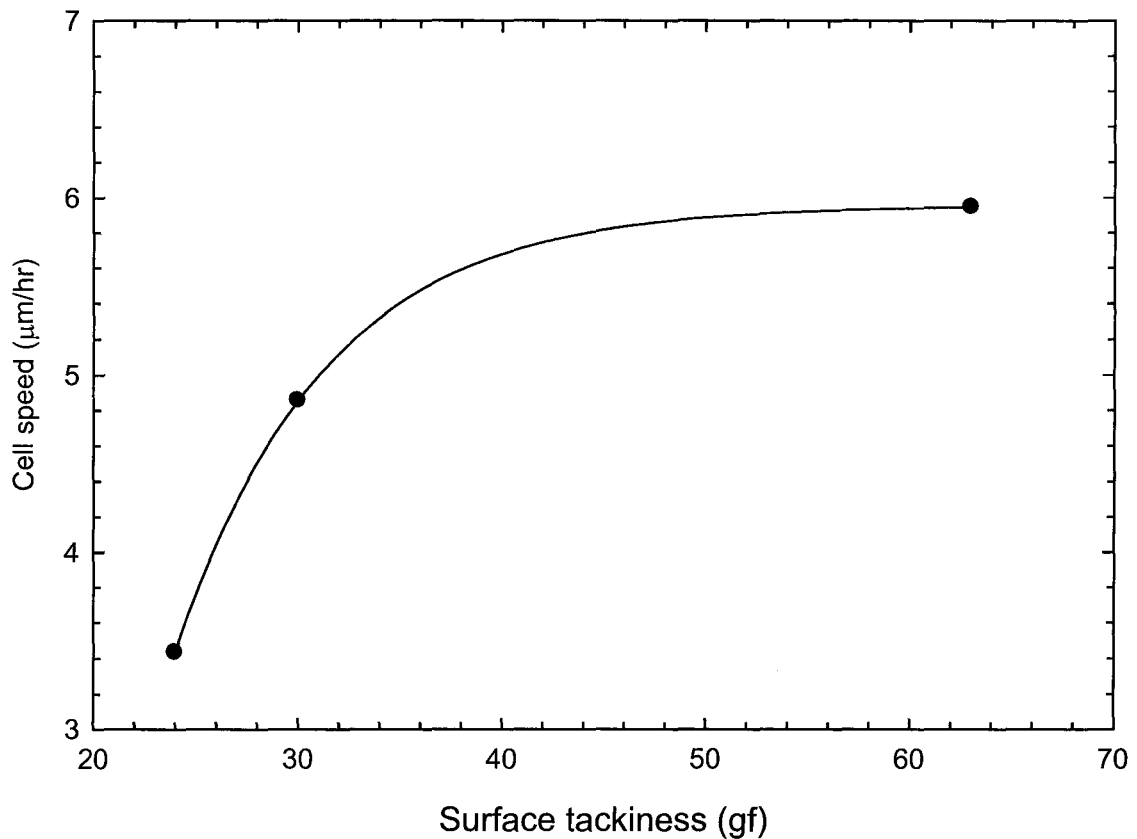


Figure 12: Cell speed on an acrylic surface of low, medium and high adhesivity. The
filled circles represent the data and the solid line represents the model. Data taken with
permission from: Kayatama 2007, Figure 5. Adhesive force is measured with a tackiness
tester in grams of force (gf).

Figures 13, 14 and 15 show the relationship between various factors and the time it would

be expected to take lens epithelial cells to breach the posterior based on a travel distance

of 1500 μm. In Figure 13, it can be seen that both FN and LN of intermediate surface

density results in the cells breaching the capsule posterior within 24hr to 48hr. However,

with increasing density of both proteins, the time increases to approximately 10 days for

the cells to breach the posterior. In Figure 14, it can be seen that on the high end of

adhesivity of FN based on higher affinity receptors, cells can take up to 63 days to breach

the posterior while on CN IV, it can take up to 30 days. While it is necessary to

determine that the differences between the two figures are due to differences in the nature

of the interactions between the cells and the proteins on the surfaces and are not purely

due to differences in the cells, these results are quite significant and demonstrate that with

surface modification of IOL materials, it may be possible to alter significantly the speed

of cell migration and therefore increase the time it takes for lens epithelial cells to

migrate from the anterior surface of an IOL to the posterior. For acrylic surfaces in

Figure 15, shortest time predicted for cells to breach the capsule posterior is

approximately 5 days which is on the high end of adhesivity for the given data. At the

lowest recorded value of adhesivity, the model predicts that the cells will take

approximately 9.5 days to breach the posterior capsule. This result suggests that the

material alone will not be sufficient to minimize migration and that some additional

modification will be necessary to ensure that PCO does not occur.
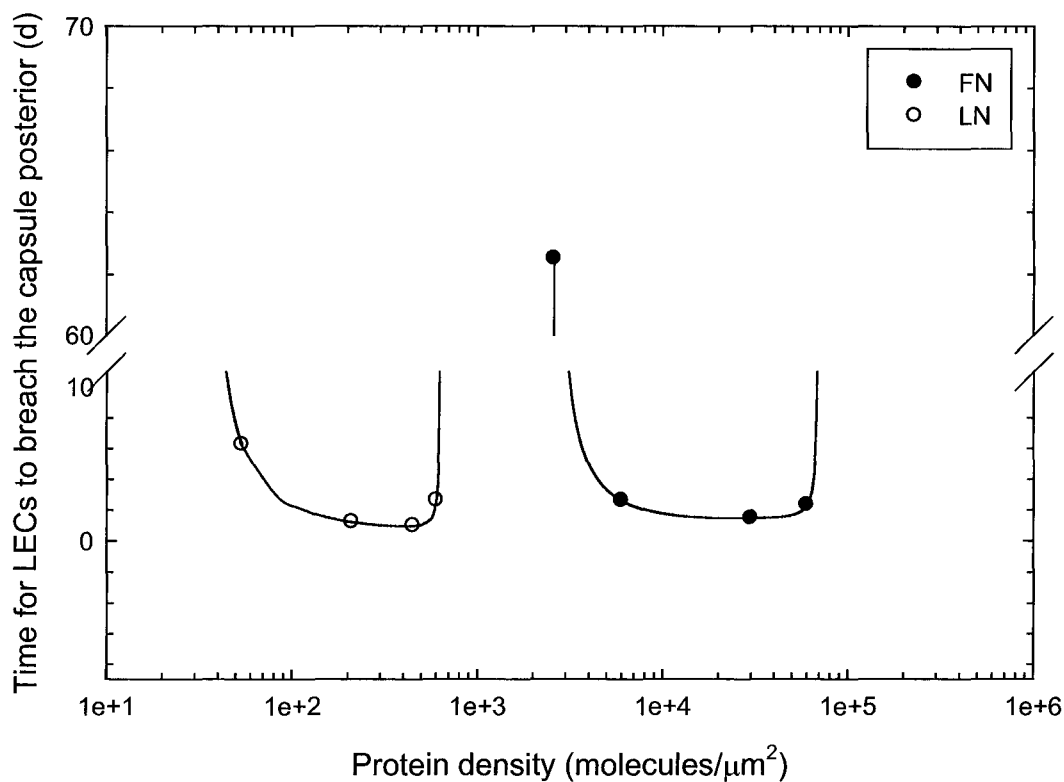
Figure 13: Time for LECs to breach the capsule posterior on different FN densities (filled circles) and LN densities (open circles) The solid line represents the model where the model parameters were taken from Figure 6 for FN and Figure 7 for LN. Data taken with permission from Maheshwari 2000, Figure 3a and Goodman 1989, Figure 5a.
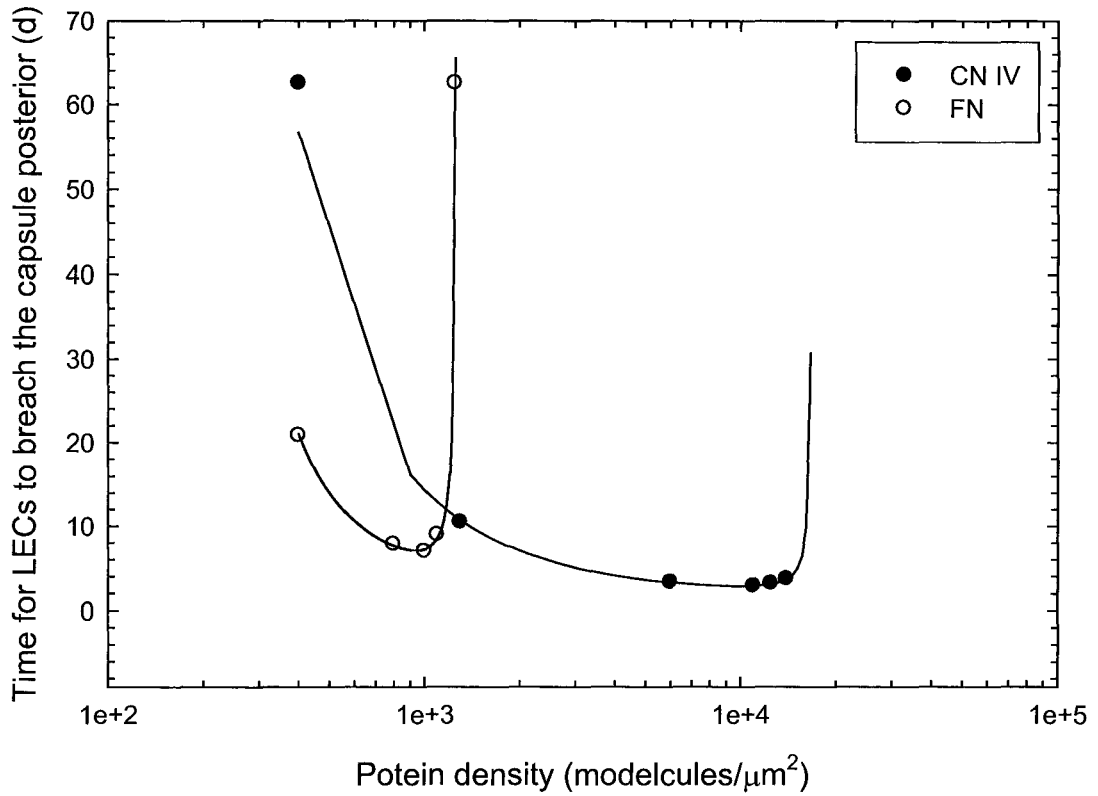
Figure 14: Time for LECs to breach the capsule posterior on different CN densities (filled circles) and FN densities (open circles) The solid line represents the model where the model parameters were taken from Figure 8. Data taken with permission from DiMilla *et al.* 1993 Figure 3b.
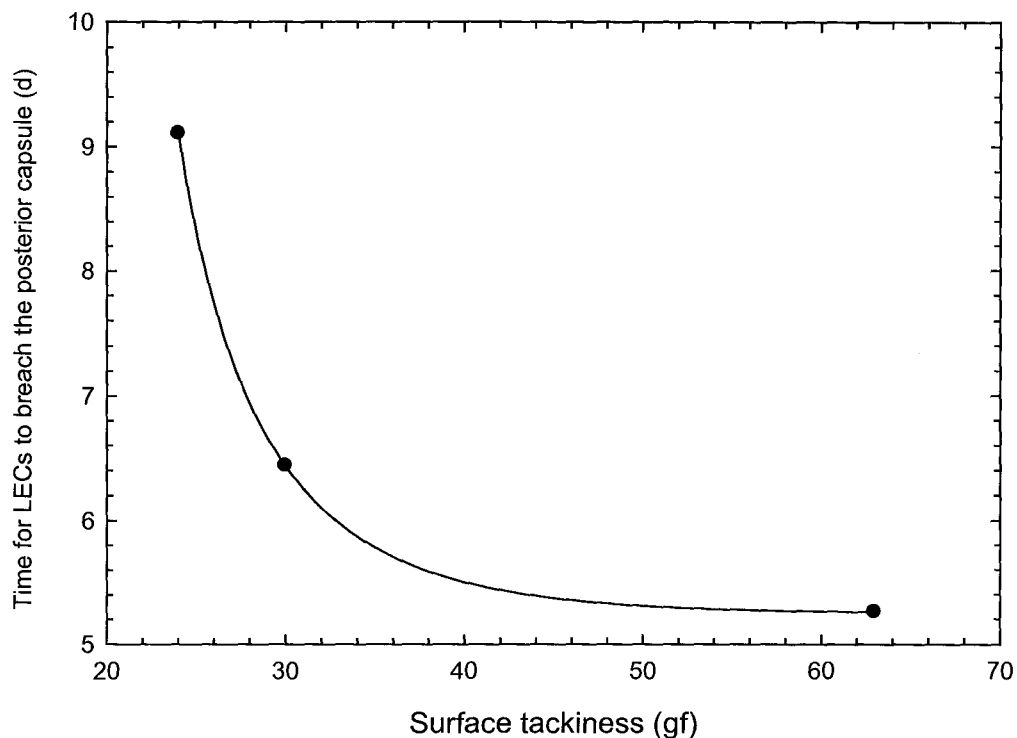
Figure 15: Time for LECs to breach the capsule posterior on an acrylic surface of low, medium and high adhesivity. The filled circles represent the data and the solid line represents the model. Data taken with permission from: Kayatama 2007, Figure 5

## 4.2 MODEL DISCUSSION

The goal of developing the LEC migrational model was to better understand the motility of cells during PCO. The model was first tested using data found in the literature, although since ultimately, the goal in developing this model was to use it in the development of better IOL materials and surfaces, it will be necessary to perform migration studies with lens epithelial cells on various surfaces to develop the model

parameters.

In general, despite the limited data available, the model was able to predict the effect of cell speed and therefore, the time taken by LECs to breach the posterior capsule as a function of adhesivity of natural proteins surfaces and acrylic biomaterial surfaces. The data were found to be normally distributed. However, presumably due to the limited data points available for fitting, the $R^2$, Durbin-Watson and constant variance tests were inadequate. The model seems to fit the triphasic and the monophasic data most accurately but was less effective at fitting curves of a more narrow and irregular shape such as those found in Figure 10 in HAR and LAA integrin states. As such, it was necessary to plot the data using hand selected parameters as shown in Figure 10b. Furthermore, it can be seen in Figure 10, both HAR and LAA data exhibit more of an "s"-shaped or tetraphasic curve which is an indication of either outliers or a trend not captured by the model. A terphasic relationship is quite possible as Garcia and colleagues found that the $\alpha_5\beta_1$ integrin has three different conformational or activity states which can cause different affinities to different binding domains such as RGD and PHSRN at different times which therefore dictate different binding strengths to FN. (Garcia *et al.* 2002) This particular integrin binds cooperatively to RGD, PHSRN and other external synergy sites. It was determined that a weaker integrin state was responsible for short term binding and has an affinity for RGD while higher affinity ligands are responsible for long-term binding. It was demonstrated that the shift from short term to long term binding involved a reduction in binding affinity for RGD and an

increase in affinity for FN sites outside of the two main synergy sites. (Garcia 2002). In all, the work of Garcia and colleagues demonstrates that there exists many possible cell speeds at a given protein density and time and depending on the synergistic effect of the environmental, cell and substrate conditions, the cell may be able to exhibit "s"-shaped behaviour in the cell speed curve. Clearly, the process of integrin adhesion is quite complex and therefore, numerous different shapes for the cell speed curve could be possible. It may be useful in future studies to examine these effects with lens epithelial cells given the fact that cell migration is known to be the major contributing factor to PCO.

A non-linear regression model assumes that the errors are uncorrelated random variables with a mean of zero and a constant variance. (Montgomery 2003) All of the models tested were normally distributed. However, with the exception of Figure 9 (in the presence of EGF) and Figure 8, all of the data failed the Durbin-Watson test indicating that the there exists serial correlation between the residuals. Nine out of sixteen of the cases in Table 2b failed the constant variance test indicating that in the majority of cases the model may not be capturing all of the trends present in the data. All of these tests however are dependent on the quality of the data and the fit of the data to the model. Moreover, as there are minimal data in the literature, more accurate statistical results could possibly be obtained by performing additional experimental studies.

However, the generation of more in vitro data, while improving the $R^2$ value and giving more accurate parameters, may not lead to improved statistics. *In vivo*, all of the

factors described by the model will interact. Growth factors and integrins have many common elements in their pathways. (Schwartz 2002) For example, *in vitro*, TGFβ2 was shown to have a profound effect on the dispersion of the α5β1integrin. Moreover, association with actin filaments in TGFβ-treated cells was extremely disperse compared to healthy cells which formed focal contacts at the ends of the actin stress fibres. (Marcantonio 2004) It is also well known that different growth factors can significantly influence on each other. Intracellular cross-talk(s) between the TGFβ-Smad and the FGF2-matrix associated protein kinase (MAPK) signaling pathways occur which will ultimately influence LEC proliferation. (Tanaka 2004) Finally, the integrin expression and activation state are known to influence how the cell binds to its native substrata. Integrin expression therefore, will dictate the strength of the ligand-receptor bond or the adhesiveness to a surface. Additionally, integrins will have different affinities for different substrates. For example the $\alpha_5\beta_1$ integrin has the highest affinity towards FN and a lower affinity for LN as it binds solely to the RGD adhesion domains. (Marcantonio 2004) Moreover, integrins will have an influence on the strength of the bond and therefore dictate surface adhesivity and vice versa. Therefore, all of the factors in this model will potentially be correlated and may influence others. The data sets collected from the literature proved to be normally distributed, however the majority of the data sets do not have constant variance or serial correlation of their residuals when evaluated with the non-linear regression. Ultimately, the model should be reevaluated with additional data for a more accurate prediction of the ability of the model to predict

cell speed with influences on surface adhesivity, in the presence and absence of growth

factors, and under different integrin concentrations, states and conformations.

Model parameters are summarized in Table 2. The parameter $x_{oo}$ for Figure 10a

has a slightly negative value of -0.84 molecules/$\mu m^2$ which is physically impossible. In

this case however, this value was the best selection of parameter to fit the data. Since it is

close to zero and given the error in biological data, it is likely that a zero value for this

parameter is not unreasonable. However, additional data will provide more information

on the nature of this value. Other negative parameters exist in Figures 9 and 10, namely,

$x_o$, $x_{oo}$, $\tau_{oi}$, and $\tau_{ooi}$. A negative x value indicates a shift to the left in the cell speed curve,

while a negative $\tau$ value increases the overall $\tau$ value and makes the speed of the cellular

migrational response slow down. All other parameters were as expected.

LEC migration on the capsule is critical to consider because *in vivo,* it will

compete with the IOL to govern cell speed. As such a capsular cut-off density of 307.5

molecules /$\mu m^2$was determined. Densities above this value must be selected for the cells

to prefer to adhere to the IOL and therefore for the IOL surface to control cell speed.

Results shown for FN in Figures 6,8, 9, 13 and 15 give densities much higher than this

cutoff. Similarly, the results shown in Figures 8 and 14 for CN IV are relevant as the

densities are even higher for this molecule. However the results shown in Figures 7 and

13 (for LN) may be affected by the cutoff density. LECs travelling on the low range of

adhesivity, below approximately 48$\mu m$/hr, may be governed by the capsule. Figures 10

and 11 are expressed in terms of concentration. However, it can be assumed that the

cutoff density for Figure 10 will not apply because the substrate is FN. It was assumed

that FG will act similarly to FN as is not a native part of the lens capsule and therefore

the cutoff value can also be ignored for Figure 11.

The results shown in Figures 12 and 14 for acrylic lenses, with units of gf, are

difficult to directly compare to a protein. Furthermore, it is not known how this

"tackiness" impacts protein adsorption which is the factor governing cell adhesion

although it is presumed that since the cell studies in this work were performed under

serum containing conditions, the results are relevant. Regardless, the results suggest that

the lens materials alone are not sufficiently adhesive to allow for sufficient decreases in

cell migration. It would to be interesting to examine cell migration on FN adsorbed lens

materials and to examine FN production as a function of lens tackiness.

It is clear that manipulation of the interactions between the cell surface integrins

and the ECM can be used to alter the rate of cell migration. In Figure 11a, it can be seen

that as the integrin is activated or if the integrin is raised to a higher affinity, the cell

speed curve characteristically shifts left and narrows. This is due to receptors forming

bonds with the ligands more quickly at higher activities and affinities. The overall

maximum speed should not be affected by a change in concentration. (Hersel 2003,

Palecek 1997) Thus, the $\beta_o$s were held constant at 17 $\mu$m/hr and 19 $\mu$m/hr respectively.

In both Figures 10 and 11 however, the data suggest that different maximum speeds are

attained. It is difficult to determine if an actual trend is present or if this is attributed to

error within the limited data.

Figure 9 predicts a shift in the cell speed curve with the addition of a growth

factor. Essentially, the presence of a growth factor causes the cell to become less

adhesive. Therefore, the cell speed curve shifts up, which is reflected in Figure 8 by the

increase in height of $\beta_{GF}$. This is increase in cell migration is also supported by Hersel

and colleagues. (Hersel *et al* 2003) The presence of growth factor can additionally cause

the cell speed curve to shift to the right; however $x_o$ in the presence and absence of EGF

was 803.88 molecules/$\mu m^2$ and 824.03 molecules/$\mu m^2$ which is an insignificant

difference. In Figure 9 therefore, $\tau_o$ for the graph in the absence of EGF may be too

small. Moreover, the $\tau_o$ in the presence of EGF could be too large. Although EGF was

used to test the model in the lens environment, *in vivo*, TGF$\beta$ and FGF2 are the

predominant growth factors and therefore, response to these growth factors should be

examined. While the model and the literature predicts that the same trend will be

observed with any growth factor (Hersel 2003), this fact would require validation. An

increase in cell speed would be expected however with TGF$\beta$ as this growth factor has

been shown to induce synthesis of matrix metalloproteinase (MMP) 2 and 9 when added

to both rat lenses and chicken lens annular pad (CLAP) cells in a serum free medium *in

vitro*. (Dwivedi 2006, Tamiya 2000) Similarly, FGF2 has been shown to induce

synthesis of MMP2 in bovine choroidal endothelial cells. (Wang 2005) MMPs are a

class of proteolytic enzymes which aid in numerous remodeling functions including

cellular migration. (George 2004) These enzymes are known to be expressed in the lens

and upregulated during wound healing and cataract formation. (George 2004, West-Mays 2006) MMPs can cleave ECM proteins as well as cell-cell adhesion junctions known as cadherins. (George 2004, West-Mays) Both FGF and TGFβ have a strong affinity for the ECM, and upon ECM cleavage, these growth factors are released and can be activated by MMPs. (Jenkins 2008, McCawley 2001, Whitelock 1996 Yu 2000) Specifically, MMP 2 releases FGF2 from the lens capsule while MMP 2and 9 release and activate TGFβ. (Jerkins 2008, Tholozan 2007, Yu 2000) This also induces a TGFβ positive feedback loop. Additionally, TGFβ is known to be activated primarily by αvβ6 integrin, an integrin known to be expressed in LECs. (Jerkins 2008, Sponer 2005) Moreover, DiMilla and colleagues have demonstrated that the strength of the cell substratum attachment and ECM surface density can be related to each other and are directly related to the speed, both possessing a biphasic relationship (DiMilla 1993). Assuming that these cells are on the high end of the cell adhesion and strength of cell-substratum adhesion curves (which they should be if they are adherent to the point of immotility on their substratum), removing cell-substratum integrin bonds will increase the cell speed. In summary, the addition of growth factors TGFβ and FGF2 will cause the production of MMPs which may cleave the cells from each other or their substrate, ultimately causing the cells to be less adherent and more migratory. Moreover, mouse LEC speed was found to be increased in the presence of TGFβ compared to that of the control. (Gotoh 2007)

The model predicts in order of slowest migration and therefore greatest time cells

will take on a given surface to breach the posterior capsule is as follows: FN>LN>CN

IV> acrylic where LN and CN IV can switch places depending on which cell type is

used. Figure 13 reveals that FN surfaces have higher adhesive capabilities than LN as the

cell speed curve is two orders of magnitude lower on FN than on LN and reaches a

maximum at 43 μm/hr compared with 67 μm/hr. Although the same cell type is not used

for these comparisons, this conclusion is also supported by Sondermann and colleagues

who compared cell migration on LN and FN surfaces and assessed the microstructures

within their focal adhesions. Both substrates demonstrated clustering and aggregation of

integrins, talin, vinculin and, paxillin which demonstrates a tight association between

these proteins and the ECM. (Sondermann 1999) The concentration of these proteins in

LN however was much lower than that of FN indicating a stronger adhesion of FN.

Additionally, as predicted by this model, cell speeds were much higher in LN than in FN

all of which indicate stronger adhesion of FN. Goodman and colleagues also confirm this

result with migration assays where the cell speed curve of FN is found to the left of LN.

(Goodman 1989)

Figure 8 confirms that FN is more adhesive than CN IV as the curve for cell speed

on FN is narrower and to the left of the CN IV curve, and the speeds are lower. The FN

and CN IV cell speed curves initiate at the same surface adhesivity of 400

molecules/μm$^2$. However, CN IV spans a density approximately three times that of FN.

LECs on CN IV demonstrate that much greater cell speeds are possible on this surface

with a maximum of 22 μm/hr compared to 9 μm/hr for FN. The greater affinity of the FN

for the cells suggests that the cell speed curve will be saturated much more quickly than that of CN IV likely because integrins possess higher affinity for FN than CN IV. Likely, LEC receptors will bond with the substrate ligands of FN more quickly and with more strength than with those of CN IV. Moreover, human smooth muscle cells adhere approximately 70 times more tightly per molecule of FN than CN IV (DiMilla 1993), impeding cellular migration at higher rates. In Figure 8, deceleration of the cells on CN IV at high protein concentrations was not diminished as much as on FN likely because CN IV is considerably less cell adhesive even at high protein concentrations. This is reflected in Figure 14 by the fact that at the highest protein densities cells migrating on CN IV will take 30 d to breach the posterior while on FN they will not breach the posterior as 60d is well beyond the time of capsular bend formation.

The same cell type with LN was not used, and therefore the result cannot be compared directly to those shown in Figure 8. Although cell speed is dictated by the type of integrin, its state and expression rather than by cell type (Hirano 1993), it can clearly be seen from Figures 6 and 8 that the cell speed on FN shows a maximum at very different speeds. Clearly, different cells express different integrin types and, therefore, the speed of different cells on the same surface will be different. Intuitively, it would seem that LN however would fall between FN and CN IV as FN and LN are known to be adhesive proteins while CN IV is a basement membrane protein with lower adhesive properties. (LeBleu 2007,Boateng 2004,Aota 1999) There seems to be some ambiguity in the literature however, presumably due to the different cell types with different integrin

expressions and therefore different surface affinities. Olivero and colleagues

demonstrated that the order of rabbit LEC adhesivity and speeds in descending order is as

follows: FN>CN IV>LN and LN>CN IV>FN respectively. Likely the particular density

selected for the cell migration experiments would be as seen in Figure 16, where the

protein represented by the thin line would be FN which is in the middle upper range of

adhesivity so cell speed is relatively high. The medium thickness line would represent

CN IV in this case where it falls in the lower middle portion of its cell speed curve and

would therefore have an intermediate cell speed. LN would be represented by the thick

line as it would be on the lowest end of its cell speed curve and thus have a relatively low

speed.
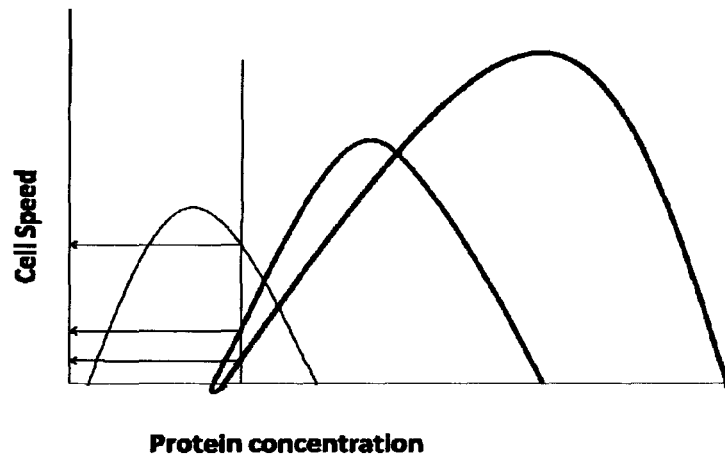


Figure 16: Schematic representation of a high affinity and adhesivity lower speed protein
(thin line), a medium affinity and adhesivity medium speed protein (medium thick line)
and a low affinity adhesivity high speed protein (thick line). At the protein concentration
indicated in pink, the cell speeds would be high for the blue protein, medium for the
orange protein and low for the purple protein as they will be on different spots in there
cell-speed curves.

When Strobel and colleagues assessed the migration of hematopoietic progenitor

cells on FN, LN, and CN IV surfaces, the trends however were different.  Cell speed in

descending order was as follows: FN>LN>CN IV. (Strobel 1997)  Moreover, Oharazawa

and colleagues discovered that the speed of attachment to these surfaces with rabbit LECs

in vitro is FN>LV>CN IV.  (Oharazawa 1999)  Finally, acrylic IOLs will be on the

lowest end of cellular adhesion for reasons previously stated.

As the time it takes LECs to breach the posterior is inversely related to cell speed,

the lowest time to reach the posterior would be on the acrylic surfaces followed by CN IV

followed by LN and the greatest time would be observed on FN.  Moreover, on the high

end of its cell speed curve, FN is presumably the best material for preventing cells from

migrating onto the posterior and acrylic IOLs are the least desirable.  The model

predicted that at a FN density of 1250 molecules/$\mu m^2$ the time for LECs to breach the

posterior capsule would be 63 days.  Since the capsular seal is complete within 4 weeks

(Hayashi 2002, Nishi 2002, Sacu 2005), this gives sufficient time for this wound healing

response to occur before the cells will escape to the posterior. The main issue to the use

FN as an IOL material is that it can induce an immune response.  Therefore, to overcome

these limitations, it would be more appropriate to use adhesion peptides.  Clearly, this

model may be a critical tool for predicting which surfaces will suppress or eliminate

PCO.

# CHAPTER 5: ADHESION PEPTIDE-MODIFIED SURFACES TO MAINTAIN LEC PHENOTYPE AND SUPRESS OR INHIBIT LEC MIGRATION

## 5.0 Rational for Adhesion Peptide-Modified Surfaces

The potential of using adhesion peptide-modified surfaces as IOL surfaces was investigated with goal of promoting cellular adhesion and ultimately decreasing or eliminating migration while maintaining cellular phenotype. Preventing cell migration would presumably allow the cells to maintain their position on the anterior side of the capsule during the formation of the capsular bend and sealing the capsule prior to LEC migration to the posterior side. The purpose of preserving cell phenotype is to allow the LECs to exhibit their normal behaviour where they tend to form a translucent monolayer of cells. (Wormstone 2002) Natural LEC behaviour will not cause wrinkling or light distortion. (Wormstone 2003) Thus, even if the LECs cross the visual axis, they should not cause visual impairment compared to myofibroblasts which deposit a thick irregular ECM which is opaque and can further cause capsular wrinkling. (Wormstone 2002a) Presumably maintaining the phenotype should eliminate the concerns over the location of the cells within the capsule. Reducing migration and maintaining the phenotype of the cells will ultimately help reduce or eliminate PCO.

## 5.1 MATERIALS

Appendix I summarizes the materials and reagents used for the PDMS-modified

surfaces and cell studies.

## 5.2 METHODS

### 5.2.1 Surface modifications

#### 5.2.1.1 Adhesion peptide-modified poly(dimethylsiloxane) PDMS surfaces

Figure 17 depicts the adhesion peptide-modified PDMS surfaces. PDMS is a

polymer used as a model lens material. It is quite hydrophobic on its own and attracts

and denatures proteins at its surface. PDMS surfaces therefore require modifications for

use in the lens environment. (Chen 2006) PEO is a hydrophilic polymer which can be

attached to PDMS using methods developed in the Sheardown lab and which can be

subsequently modified with various biological functional groups including adhesion

peptides. This is thought to eliminate non-specific protein adsorption while facilitating

attachment of the cells to the surface. (Chen 2006) GYRGDS and YIGSR were selected

for attachment to the surface as they are known to promote cell adhesion, reduce

migration and promote the LEC phenotype. (Hersel 2003, Oharazawa 2005, Sasabe

1996, Yoshiko 2003) The modified surfaces were characterized using sessile drop water

contact angles, Attenuated total reflection Fourier transform infrared spectroscopy (ATR-

FTIR) and X-ray photoelectron spectroscopy (XPS). Cell studies were undertaken to

determine the effect of the modification of performance of the materials in the lens

environment.
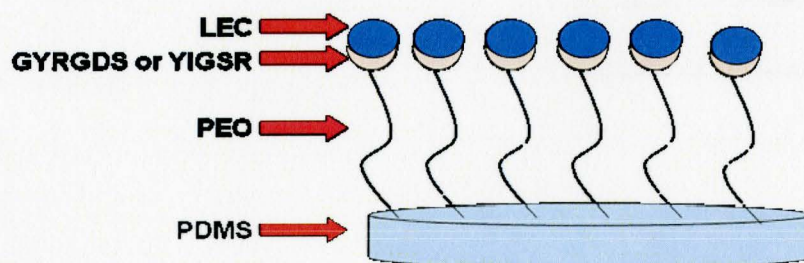


Figure 17: RGD-modified PDMS disk

## 5.2.1.2 Preparation of PDMS discs

Sylgard 184 was prepared as described by the manufacturer by combining the

prepolymer and curing agent in a 10:1 ratio (w/w%) ratio in a polystyrene dish.  The

solution was then degassed for 2 hrs and allowed to cure for of 3 days at ambient

conditions.  The cured elastomer was punched into disks 8 mm in diameter and 0.5mm in

thickness.

## 5.2.1.3 PDMS functionalization with DC1107

Thirty PDMS disks were immersed in a mixture of a 5:3 (v/v) ratio of methanol

and DC1107. The triflic acid catalyst was then added in a 2% (v/v) ratio to methanol.

This solution was placed on a shaker for 30 minutes at 300 rpm at ambient conditions.

The disks were then rinsed with anhydrous methanol (3x5mL), hexane (1x5mL), and

finally with anhydrous methanol (1x5mL). The disks were dried under $N_2$ and placed in

a vacuum oven at ambient temperature for 24 hrs. Figure 18 depicts the Si-H group

functionalization of the PDMS.
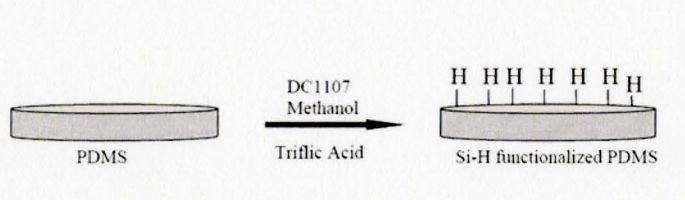


Figure 18: Si-H functional groups are created by reacting DC1107, methanol and a
triflic acid catalyst at the PDMS surface. Taken wither permission from Mikhail
2006, 39.

### 5.2.1.4 Teathering allyl-PEO-OH spacer to the PDMS disk via hydrosilylation

Thirty Si-H-modified disks were separated into 3 separate 20mL glass vials. To

each vial, a solution was added containing 3mL of 2-methoxyethyl ether, 0.3mL

poly(ethylene glycol) monoallylether, (allyl-PEO-OH) with a molecular weight of 550

Da. 15 µL of Pt-catalyst was subsequently added and the mixture was left on a shaker at

300 rpm for 2 hr at ambient conditions. The disks were subsequently washed with

acetone (3x5mL) dried under $N_2$, and placed in a vacuum oven at ambient temperature

for 24 hrs. This surface modification step along with a structural diagram can be seen in

Figure 19.
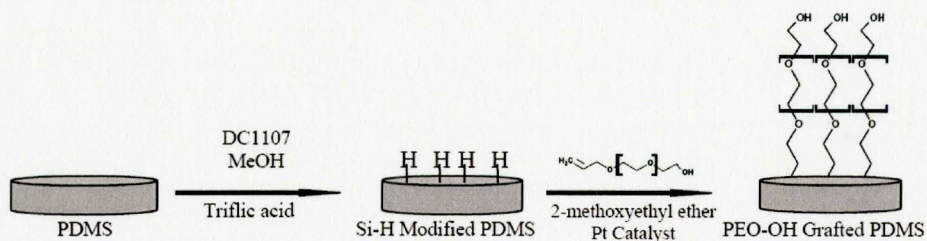


Figure 19:  Steps of chemical modifications to the PDMS surface in order to attach allyl
PEO-OH 550Da to the surface. Taken wither permission from Mikhail 2006, 43.

## 5.2.1.5 Functionalization of allyl-PEO-OH spacer with *N,N'*-disuccinimidyl

## carbonate (NHS) ester

Thirty allyl PEO-OH-modified disks were separated into 3 separate 20 mL glass

vials.  To each vial, a solution of 1mL of acetonitrile, 0.1mL of triethylamine, and 0.2g of

*N,N'*-disuccinimidyl carbonate was added. The vials were purged with $N_2$ and the discs

were allowed to react on a shaker for 6 hrs at 200 rpm.  The discs were then washed with

acetonitrile (2x5mL), 2-methoxy ethyl ether (1x5mL), and finally with acetonitrile

(1x5mL).  The discs were then dried under $N_2$ and put into a vacuum oven at ambient

temperature for 24hrs. The process to surface modification via hydrosilylation and the

final product of this modification step can be seen in Figure 20.
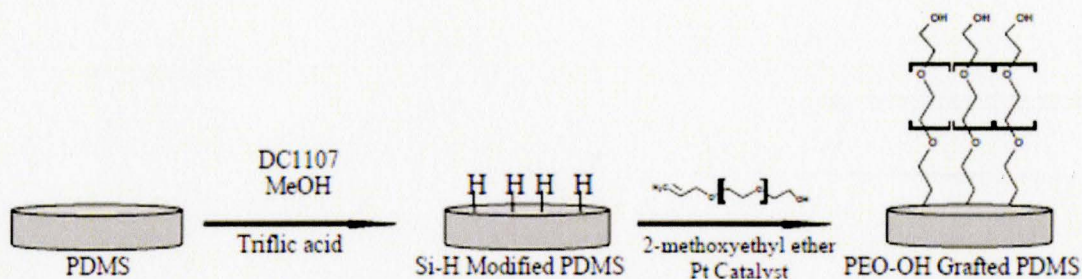
Figure 20: Grafting the allyl-PEO to the PDMS surface via a hydrosilylation reaction.
Taken wither permission from Mikhail 2006, 42.

### 5.2.1.6 Conjugation of adhesion peptides

Cell adhesion peptides, GYRGDS and YIGSR were dissolved in PBS buffer at a

concentration of 25μg/mL and 250μL (per disk) of this solution was then placed into a 96

tissue culture well plate. One PEO-NHS-modified PDMS disc was placed in each well.

The discs were allowed to react for 1hrs and 3hrs followed by a 3x10 minute rinses in

PBS. The discs were then dried under $N_2$ and placed in a vacuum at ambient temperature

for 24 hrs. Adhesion peptide attachment occurs via aminolysis of the amino terminus end

of the peptide with the NHS ester tethered to the end of the PEO spacer. The result of this

reaction produces an amide linkage where the final surface-modified product can be seen

in Figure 21.
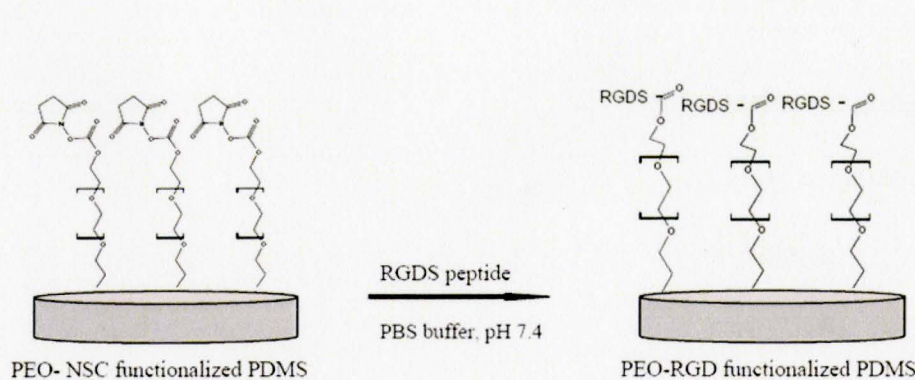
Figure 21: RGDS and YIGSR covalent tethering to PEO spacer on the PDMS disks. Taken wither permission from Mikhail 2006, 45.

## 5.2.2 Surface characterization

### 5.2.2.1 Sessile drop contact angles

In order to assess successful modification of the discs, sessile drop water contact angles were measured in order to determine surface hydrophilicity. PDMS, allyl-PEO-OH-modified PDMS, and peptide-modified PDMS surfaces were measured. Surfaces were placed on a glass slide and an 8μL water droplet was placed on top of each surface. The advancing contact angles were taken in three different places on a disc and three replicate disks per sample were taken with a Rame-Hart NRL 100-00 goniometer. Receding angles were also taken; 3μL of the water droplet was drawn back into the instrument and the receding angle was measured with the same cases measured as that of

the advancing angles. These are performed to assess the hysteresis of a sample which will give an estimation of the roughness or purity of a sample.

## 5.2.2.2 Attenuated Total Reflection Fourier Transform Infrared Spectroscopy (ATR-FTIR)

Attenuated total reflection Fourier transform infrared spectroscopy can determine the chemical composition of a surface (of depths between 1μm to 5μm). This is achieved through the analysis of a specific functional group bond vibrational and/or stretch frequency upon surface exposure to infrared (IR) radiation. ATR-FTIR was done on 2 surfaces per batch at each surface modification step with a TENSOR, Fourier transform infrared spectrometer in order to confirm that the surface had been successfully modified.

## 5.2.2.3 X-ray photoelectron spectroscopy (XPS)

The quantitative elemental composition of the surfaces can be determined by the use of XPS. XPS was performed at Surface Interface Ontario at the University of Toronto using a Leybold Max200 X-ray photoelectron spectrometer. Low and high resolution XPS measurements were performed at takeoff angles of $90^{\circ}$, $30^{\circ}$ and $20^{\circ}$ which allowed analysis of the elemental composition of the surfaces at different depths. Specslab software was used to perform material analysis.

## 5.2.3 Cell studies

### 5.2.3.1 Culturing of lens epithelial cells

The human LEC lines B3 and FHL were grown in MEM:F15 media, with 1% L-glutamine, 0.8% sodium bicarbonate, 20% FBS, 1% sodium pyruvate and 1% antibiotic solution (penicillin-streptomycin). Cells were seeded at a density of 30,000 cells per well into 24 well plates. Medium was replaced every three days. Cells were monitored daily with microscopy.

Once the plate reached confluency (covering more than 70% of the dish surface), the medium was aspirated and 5mL of phosphate buffered saline (pH 7.4) PBS was added followed by gentle swirling for 2 minutes. The PBS was then aspirated and 1mL of trypsin (or triple express) was added and swirled a few times. The dish was then placed in an incubator for 2.5 minutes at 37°C. 8mL of medium was then added to the dish to neutralize the trypsin. The medium and cells were then aspirated and added to a 15mL falcon tube and centrifuged at 1000 rpm for 5 minutes in a Beckman centrifuge. The pellet was then re-suspended in 8mL of media and cells were split equally between 3-5 new containers.

### 5.2.3.2 Cell seeding

Cells were transferred to surfaces of interest to observe behaviour and cell
response.  Surfaces of interest were placed into a 48 well plate.  A 38μL drop of cell-
media suspension containing 10,000 cells was pipetted onto each 0.8 mm diameter disk.
The disks were then put into the incubator for 20 min to allow the cells to adhere to the
surfaces.  0.5 mL media was then added to each well containing a disk and incubated
until analysis was performed, making sure to refresh medium every three days.

### 5.2.3.3 Cell staining for CN

CN I and III are positive markers for the myofibroblast cell phenotype and
therefore serve as positive markers of PCO.  The B3 LECs were cultured on the surface
of interest for 72 hrs and were transferred to a 48 well plate.  To each well, Sirus red
(0.2% solution in MQ water) was added.  The 48 well plate was covered with aluminum
foil and put onto a rotametric shaker at a low setting for 24 hrs.  200μL of supernatant
was transferred to a 96 well plate.  The plate was then read with a Biorad plate reader at
630 nm using a reading of 540 as a blank to determine the CN I and III content.  CN
measurements were normalized with respect to the PDMS surfaces and the FHL LEC
population at 72hrs. The measurement is reported as relative CN/cell with respect to the
PDMS control.  For all surfaces, a positive control for PCO was created by exposing

cultured cells grown on each specific surface to TGFβ at a concentration of 2ng/ml for

24hrs.

**5.2.3.4 Cell Staining for α-SMA**

α-SMA is another positive marker for myofibroblast type cells and therefore

serves as a second marker for PCO. Both B3 and FHL LECs were cultured on the

surface of interest for 96 hrs and then transferred to a 48 well plate. 150 μL of 10%

phosphate buffered formalin (4% formalin solution) was added to each well and left at

room temperature for 20 minutes. The formalin solution was then aspirated and the

surfaces were washed with 150 μL of 70% ethanol 2 times. 250μL of goat serum

solution (5% in PBS) was then added to each well and incubated at room temperature for

30 minutes. The goat serum solution was aspirated and 200μL of anti α-SMA antibody

solution (1:900 in PBS) was added to the wells. The 48 well plate was then covered with

aluminum foil and allowed to shake at room temperature for 1-2hrs. 190μL of

supernatant was then transferred to 96 well black plate. The plate was read with a

Victor3 system fluorometer at 257°C by Workout Software (485 excitation wavelength

for a fluorescein isothiocyanate conjugated primary antibody for SMA). SMA

measurements were normalized with respect to the PDMS surfaces and the FHL LEC

population at 72hrs. The measurement was finally reported as relative α-SMA per cell

with respect to the PDMS control. For all surfaces, a positive control for PCO was

created by exposing cultured cells grown on each specific surface to TGFβ at a

concentration of 2ng/ml for 24hrs.

### 5.2.3.5 Population study

FHL LECs were grown on selected surfaces and counted with a Beckmann

Coulter Counter at 24hrs, 48hrs, 72hrs, 96hrs and 120hrs.

### 5.2 Statistics

For contact angle measurements, three replicate sample per surface were tested

and on each of those surfaces, two contact angle measurements were taken on one side,

and one on the other for both advancing and receding angles for a total of 9 replicates for

both advancing and receding angles.  Standard deviation was performed on all smaples.

Single factor ANOVA was performed for all advancing and receding contact angles for

the same surface. ANOVA was also performed on the PDMS control against each other

surface.  A P value smaller than 0.05 indicates that the sample is significantly different

For XPS, SEM was performed for duplicate or triplicate samples.   For all cell

studies, the standard error was computed.  In the CN IV and SMA staining studies,

triplicate samples were used and in the population study triplicates were used and

samples were each read three times with the Coulter counter for a total of 9 replicate

samples per surface. ANOVA was performed with conditions identical to that of the

contact angle measurements on the raw data of both the α-SMA and CN IV staining

results.

## 5.3 RESULTS

### 5.3.0 Results

GRYGDS- and YIGSR-modified surfaces were generated to further validate the

LEC migrational model and to test the hypothesis that by increasing adhesion and

decreasing EMT, a lower incidence of PCO could be expected.  Various methods were

used to characterize chemistry of the modified surfaces.  Cell interactions with the

modified surfaces were also assessed.

### 5.3.1 Surface Characterization

Figure 22 depicts the advancing and receding sessile drop water contact angles

measured on the PDMS control as well as PEO-, GYRGDS- and YIGSR-modified

PDMS surfaces.  The PDMS surfaces demonstrated a characteristically high contact

angle of $106°±1$, revealing their hydrophobic nature with very little hysteresis. The receding contact angles of the modified surfaces however showed greater hysteresis presumably due to the homogeneity and smoothness of the control compared to that of the modified surfaces. PEO, a more hydrophilic polymer, when attached to the surfaces, resulted in a decrease in the advancing contact angle to $75°±2$ as expected. However, with modification of the PEO surfaces by the peptides YIGSR and GYRGDS the advancing contact angles increased to $91°±1$ and $93°±1$ respectively. ANOVA was significant for all advancing and receding sets as well as PDMS compared to PEO, YIRSR and GYRGDS surfaces. PEO is also significant compared to all other surfaces. Clearly, form these results, successful surface modification has been achieved.
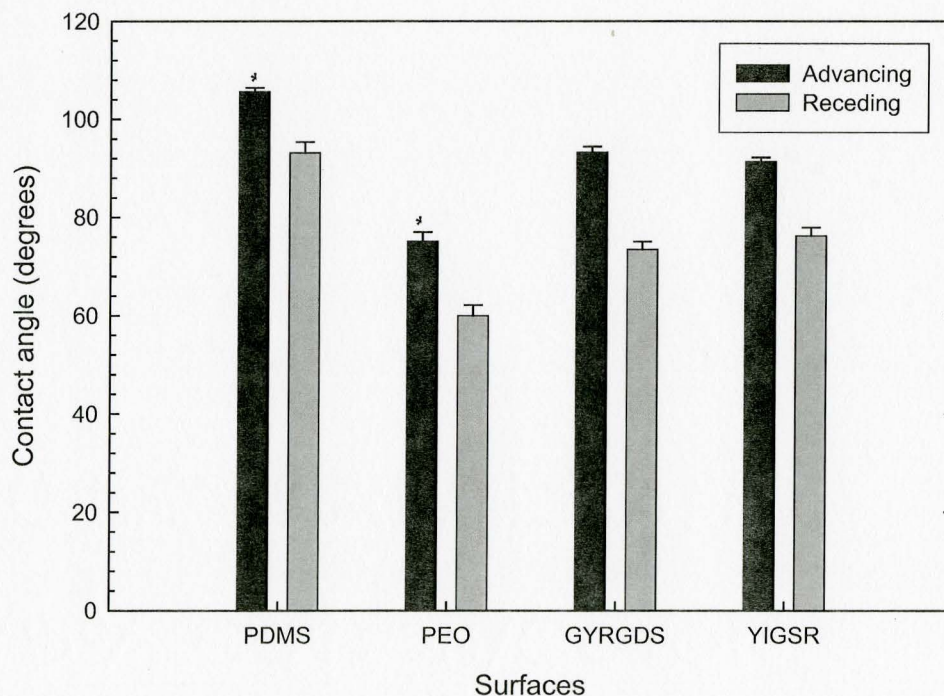
Figure 22: Sessile drop water contact angle measurements on the PDMS control and on
PDMS-modified surfaces including PEO, GYRGDS and YIGSR surfaces. *PDMS and
the PEO are statistically different than all other surfaces as confirmed by a single factor
ANOVA with a P value of 0.05. All advancing and receding pairs are statistically
significant from one another with the same ANOVA specifications.

## 5.3.2 ATR-FTIR

The ATR-FTIR spectra of the PDMS control as well as Si-H-, PEO-, PEO-NSC-

and GYRGDS-modified PDMS are shown in Figure 23. Si-H-modified surfaces reveal a

peak at $2160cm^{-1}$ corresponding to the stretch vibrations of the Si-H bond. On the PEO-

and NCS-modified surfaces, disappearance of the Si-H peak and the appearance of a

predominant peak at $2870cm^{-1}$ representing the glycol $CH_2$ stretch demonstrates

successful modification. On the NSC-modified surfaces, peaks at $1710cm^{-1}$ and at

$1690cm^{-1}$ are present and can be attributed to the C=O stretch of the NSC group. Finally,

on the GYRGDS surfaces, a peak at $1650cm^{-1}$ is present which corresponds to an amide

stretch characteristic of the peptides. The peaks at $1710cm^{-1}$ and $1690cm^{-1}$ have now been

reduced indicating that the NHS group has been successfully modified. The ATR-FTIR

results clearly demonstrate the successful progressive surface modification of the PDMS
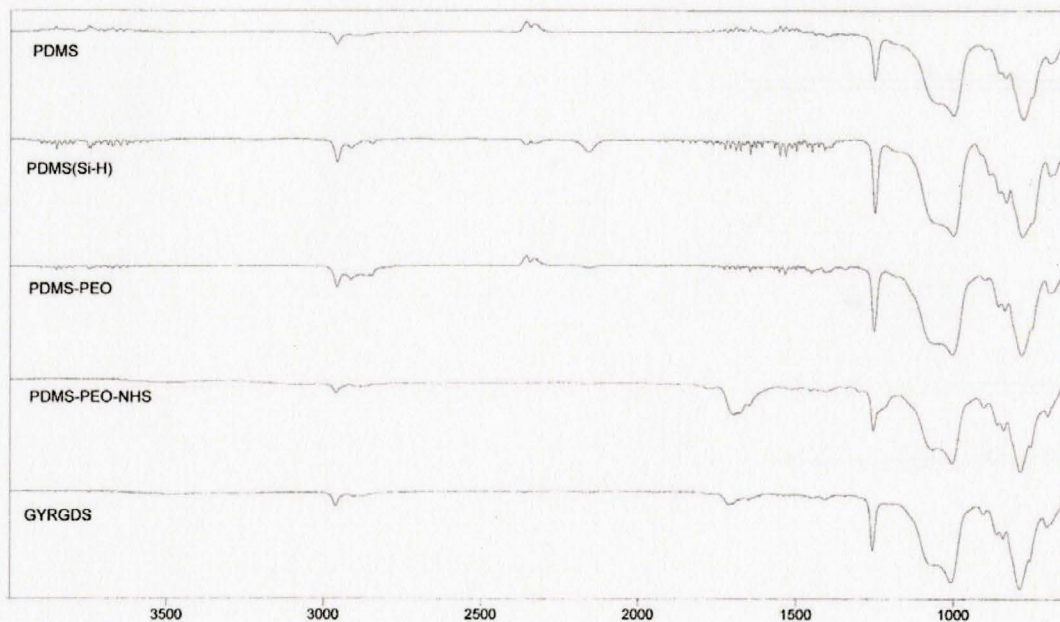
surfaces.

Figure 23:  ATR-FTIR spectra for the PDMS control as well as Si-H-, PEO-, PEO-NSC- and GYRGDS-modified PDMS surfaces.

### 5.3.3 X-Ray Photoelectron Spectroscopy

Elemental composition of the PDMS control and PDMS-modified surfaces was measured by XPS.  The results are summarized in Table 4.  Following modification of the PDMS surfaces with PEO, the amount of C1s increased, while the Si2p content decreased at all take-off angles as expected.  These results are indicative of the attachment of PEO on the PDMS surface.   At a 90$^o$ takeoff angle, an increase in N1s is seen as expected with the addition of the NHS.  This however was not seen with the 30$^o$ or the 20$^o$ takeoff angles, potentially due to the instability of these surfaces to the

presence of moisture in the air. NHS is susceptible to hydrolysis and this is likely the

reason why additional nitrogen was not seen on these samples. Both peptide modified

surfaces exhibited an increase in nitrogen as expected from the amino groups present.

Interestingly, in all samples, there was an increase in nitrogen seen between 1hr and 3hrs

which likely indicates that the extra exposure time allowed for additional peptide

conjugation to the surfaces.

Table 4: X-ray photoelectron spectroscopy of PDMS-modified surfaces of 90°, 30° and
20°. Note that the GYRGDS-PDMS surface was allowed 1hr to react, while the PDMS-
GYRGDS 3hr surface was allowed to react for 3hrs.

| 90 | C1s | standard error | N1s | standard error | O1s | standard error | Si2p | standard error |
|---|---|---|---|---|---|---|---|---|
| PDMS | 43.82 | 0.13 | | | 26.20 | 0.10 | 29.97 | 0.02 |
| PDMS-PEO | 52.16 | 1.42 | 0.09 | 0.06 | 28.87 | 0.97 | 18.87 | 1.56 |
| PDMS-NHS | 51.59 | 1.37 | 0.31 | 0.12 | 27.49 | 0.15 | 20.61 | 1.63 |
| PDMS-GYRGDS | 49.55 | | 0.38 | | 26.81 | | 23.26 | |
| PDMS-GYRGDS3hrs* | 50.14 | | 0.51 | | 24.91 | | 24.44 | |
| 30 | C1s | standard error | N1s | standard error | O1s | standard error | Si1s | standard error |
| PDMS | 42.77 | 0.14 | 0.08 | 0.05 | 25.39 | 0.28 | 31.77 | 0.07 |
| PDMS-PEO | 49.79 | 2.73 | 0.62 | 0.41 | 26.62 | 0.68 | 22.97 | 4.58 |
| PDMS-NHS | 46.77 | 0.60 | 0.08 | 0.08 | 24.24 | 0.52 | 28.93 | 0.04 |
| PDMS-GYRGDS | 48.00 | | 0.26 | | 24.84 | | 26.90 | |
| PDMS- | 47.44 | | 0.54 | | 23.49 | | 28.54 | |

| GYRGDS3hrs* | | | | | | | | |
|---|---|---|---|---|---|---|---|---|
| **20** | **C1s** | **standard error** | **N1s** | **standard error** | **O1s** | **standard error** | **Si1s** | **standard error** |
| **PDMS** | 42.75 | 0.15 | 0.08 | 0.05 | 25.39 | 0.23 | 31.77 | 0.07 |
| **PDMS-PEO** | 49.53 | 4.93 | 0.57 | 0.43 | 26.06 | 0.68 | 23.04 | 6.25 |
| **PDMS-NHS** | 46.77 | 13.30 | 0.08 | 0.08 | 24.24 | 0.64 | 28.93 | 0.06 |
| **PDMS-GYRGDS** | 46.87 | | 0.15 | | 24.83 | | 28.15 | |
| **PDMS-GYRGDS3hrs*** | 47.44 | | 0.54 | | 23.49 | | 28.54 | |

*Completed by Renita D'Souza.

High resolution C1s spectra at a takeoff angle of $90°$ are summarized in Figure 24, a through d. Figure 24a shows the PDMS control with the peak at 285eV indicative of a C-C or C-H stretch present in the PDMS. Peaks at 286eV and 288eV are likely contamination present within the polymer or unreacted oligomer. In Figure 24b, a peak at 286 eV is clearly present which corresponds to the C-O bonds of the PEO chains indicating that successful attachment has taken place. In Figure 24c, the PDMS-PEO surface has been modified with NSC which is indicated by the small peak at 288eV corresponding to the C=O stretch and small peak at 290eV corresponding to the carboxylic acid terminal group both present on the NSC molecule. In Figure 24d, the C=O stretch can be seen at 288eV and the carboxylic acid can be seen at 289eV both of which are present in amino acids. Finally, at 287eV a C-O or C-N bond is present indicating more evidence of the presence of amino acids which indicated the successful attachment of the GYRGDS group to the PDMS surface.
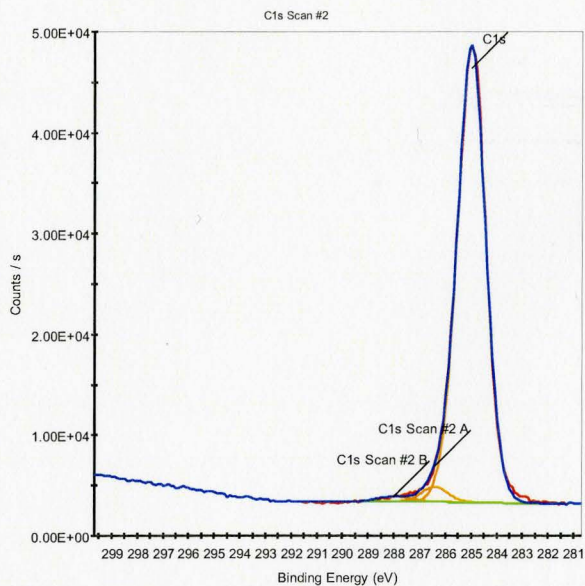
Figure 24a: High resolution C1s spectra at a takeoff angle of 90° of the PDMS surface
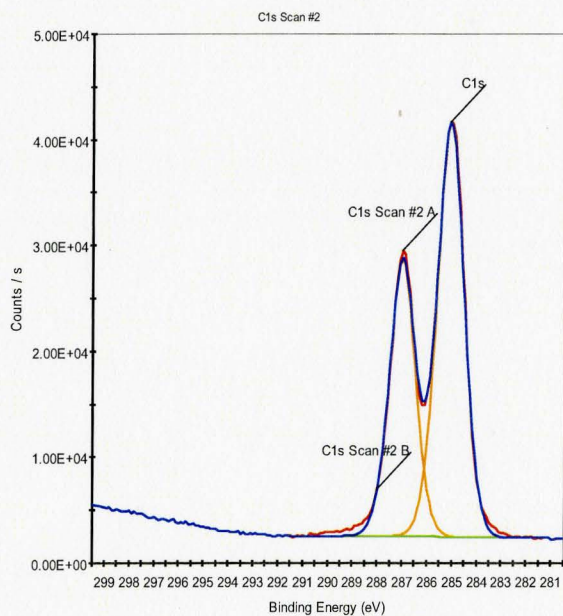


Figure 24b: High resolution C1s spectra at a takeoff angle of 90° of the PDMS-PEO-OH-modified surface
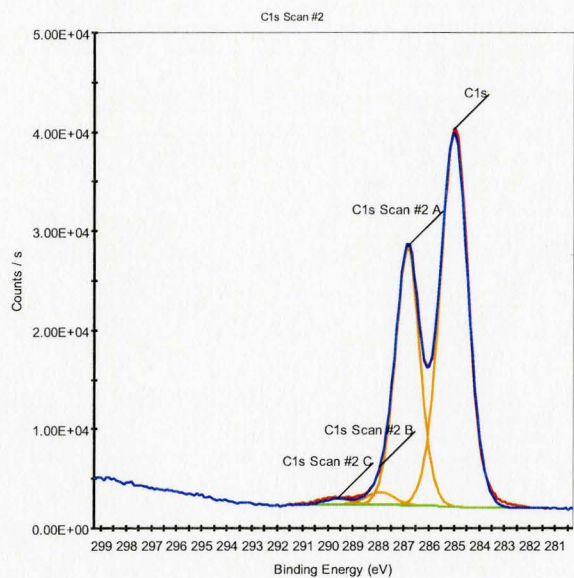
Figure 24c: High resolution C1s spectra at a takeoff angle of 90° of the PDMS-NSC-modified surfaces.
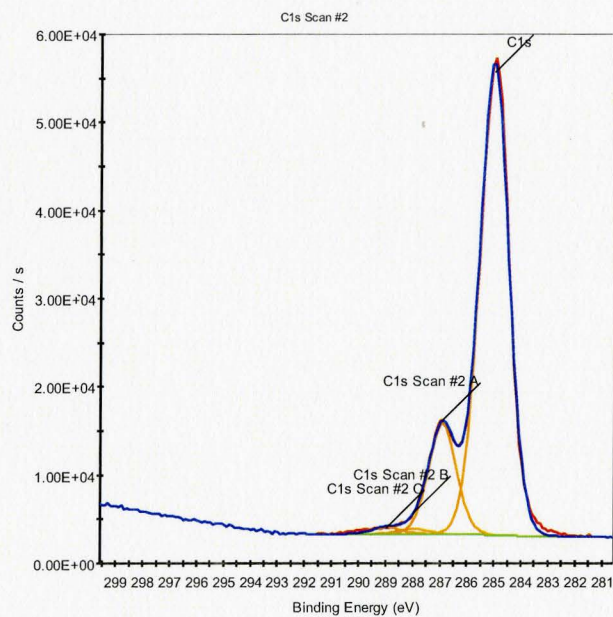


Figure 24d: High resolution C1s spectra at a takeoff angle of 90° for the PDMS-GYRGDS-modified surfaces.

### 5.3.4 Cell Interactions with Modified Surfaces

Figures 25 and 26 reveal α-SMA and CN IV staining of two human LEC cell lines on the modified surfaces. PDMS was used as the control surface while TGF-β treated surfaces served as positive controls as TGFβ is known to induce EMT. (Wormstome 2003) For the α-SMA results, in Figure 25a, B3 LECs showed that the PDMS control was higher for SMA than the positive controls of GYRGDS and YIGSR treated with TGF-β. In addition, the YIGSR and GYRGDS surfaces were equivalent to the positive controls which was not as expected. ANOVA however, confirmed than none of these results were significant. In Figure 25b, the YIGSR modified surface had lower α-SMA production all other surfaces as confirmed by significant ANOVA tests. Positive controls and the PDMS control were similar. Surprisingly, the cells grown on the GYRGDS surfaces produced extensive amounts of SMA compared to all other surfaces confirmed by ANOVA which was unexpected. Since α-SMA changes are only visible after a minimum of 144hrs (Mansfeild 2004, Wormstone 2002, Wormstone 2006), it is likely that the LECs were not given sufficient time for its production for both B3 and FHL LEC lines.
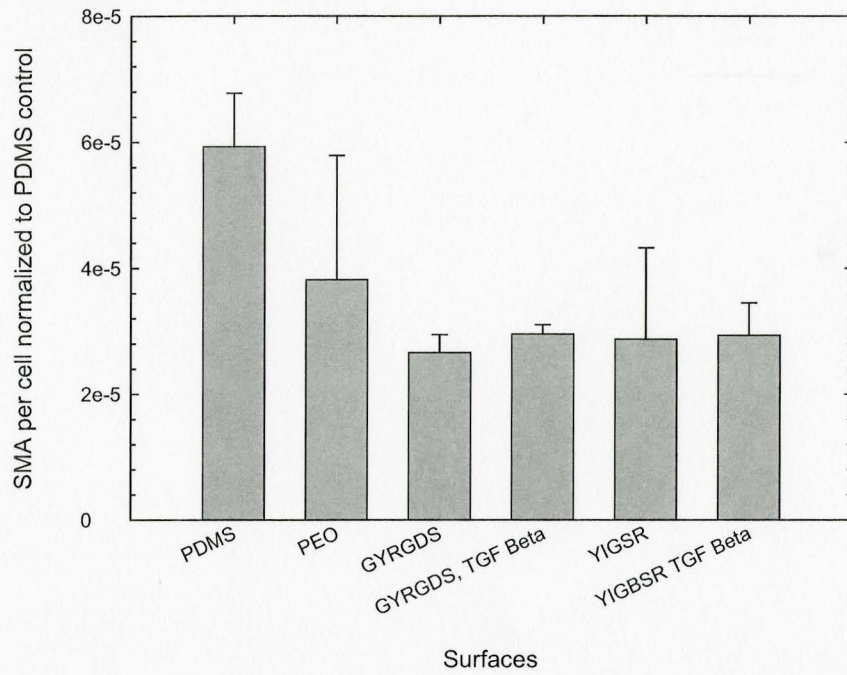
Figure 25a: Smooth Muscle Actin (SMA) production on B3 lens epithelial cells after 98
hours. PDMS is the control while the TGF-β treated surfaces are positive controls.

Figure 25b: Smooth Muscle Actin (SMA) production on FHL lens epithelial cells after 98 hours. PDMS is the control while the TGF-$\beta$ treated surfaces are positive controls. *GYRGDS and YIGSR are significantly higher and lower respectfully compared to the rest of the surfaces as confirmed by a single factor ANOVA with P value of 0.05.

Figure 26 shows the non-specific production of CN I and III on selected surfaces. Cells grown on GYRGDS surfaces produced less CN than the positive control and than the PDMS and PEO surfaces. The positive controls were however higher than that of the PDMS control and the cells grown on the YIGSR surfaces produced more CN than the positive control. All of these results were statistically insignificant however as confirmed by ANOVA.
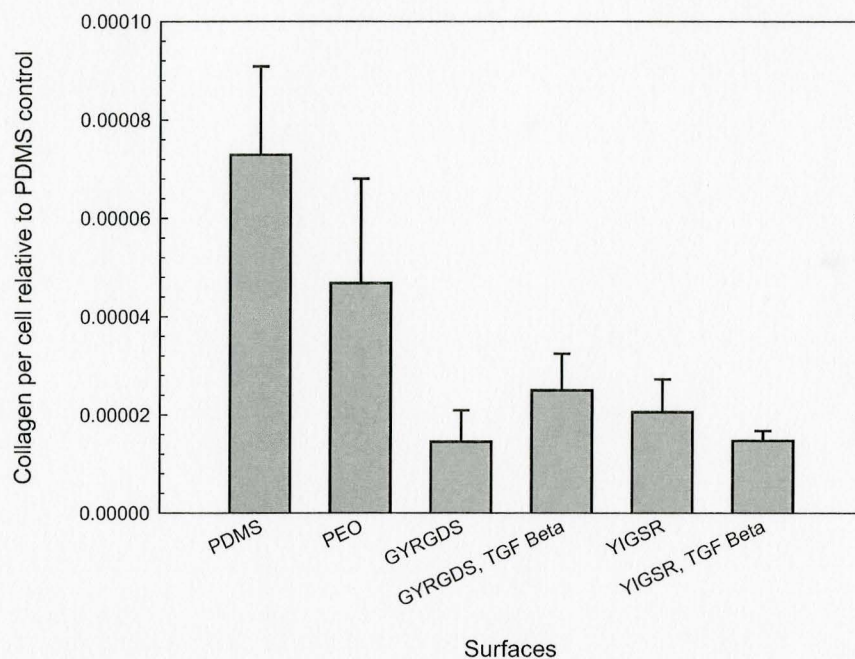
Figure 26: CN I and III production on FHL lens epithelial cells after 98 hours. PDMS is the control while the TGF-β treated surfaces are positive controls.

Figure 27 shows FHL LEC growth every 24 hrs over 120hrs. Each surface shows cellular growth over 120 hrs as expected indicating successful cellular division over 120 hrs. A hemocytometer count was done to assess the LEC viability, however, the cell counts were too low to get an accurate measurement (data not shown). An MTT (3-(4,5-Dimethylthiazol-2-yl)-2,5-diphenyltetrazolium bromide, a tetrazole) assay should be used to assess cell viability. Cell growth on PDMS and PEO surfaces was similar and both positive controls experienced more growth compared to these surfaces. Cells experience more growth on the treated compared to the untreated surfaces and the most growth of all the surfaces.
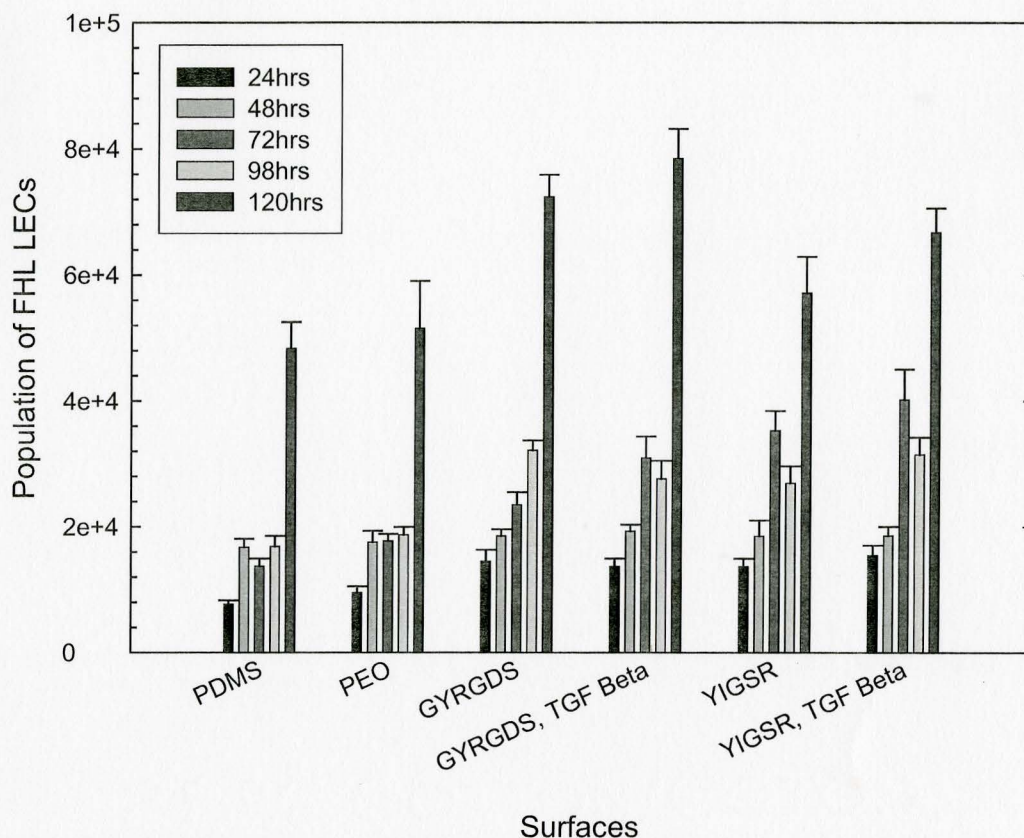
Figure 27: Population growth of FHL LECs over 120 hrs

## 5.4 DISCUSSION

Adhesion peptide-modified surfaces were created to further validate the LEC

migrational model and to test the hypothesis that adhering the cells to a surface which

was similar to the normal extracellular membrane of the lens would alter cellular EMT.

Therefore, goal of using these surfaces was to minimize PCO by preserving the LEC

phenotype, increasing cell adhesion to the IOL material and ultimately decreasing cell migration. Maintaining the LEC phenotype should presumably decrease the amount of fibrous ECM deposition and cell migration - both of which normally occur in EMT. (Ishibashi 1994, Kalluri 2003, Linnola 2000a, Linnola 2000b) Additionally, maintaining the LEC phenotype may result in the formation of an ordered translucent monolayer similar to what exists in vivo. (Tanaka 2004) Based on the model results and the results in the literature, encouraging adhesion should reduce migration, allowing the capsular bend to seal before the cells can escape from the anterior to the posterior side of the capsule - a process with is thought to be the main contributor to PCO. (Nishi 2007)

PDMS was used as a model substrate for these studies. The surface was first modified with PEO which serves to minimize the non-specific adsorption of proteins and which acts as a flexible tether for the biological molecule of interest. Modification with two cell adhesion peptides was performed YIGSR derived from laminin which is known to comprise a significant fraction of the lens epithelial basement membrane and GYRGDS, derived from many cell adhesion proteins include FN which was shown to have promise in the model.

Evidence of successful surface modification was reflected in the results of the sessile water contact angle, ATR-FTIR, and XPS measurements. The hydrophobic PDMS surface showed increased hydrophilicity when modified with PEO and a subsequent change in water contact angle was observed with peptide modification. ATR-FTIR, while not particularly surface sensitive, showed peaks characteristic of

modification with the various compounds of interest. Finally, both high and low

resolution XPS results demonstrated that the surfaces had been successfully modified

with the peptides. Ultimately however, radiolabeling studies should be performed in

order to quantify peptide densities on the surface for better correlation with the model.

Similar results have also been demonstrated for all modification steps reviewed for

sessile water contact angle measurements, XPS and ATR-FTIR results. (Chen 2006,

Mikhail 2006) Therefore, peptide densities on the surface can be assumed to be on the

order of 10 to 55 pmol/cm$^2$. (Mikhail 2006)

Preliminary cell studies were conducted to determine if the LEC phenotype could

be maintained on these surfaces. Cells were stained for positive markers of EMT, namely

α-SMA and CN and cell growth was assessed. As shown in Figure 25, α-SMA staining

results for the two lens epithelial cell lines examined were dramatically different. These

differences were thought to be due to changes in the cells with immortalization as well as

the fact that simply culturing the cells induces some degrees of EMT. The expectation

was that the TGFβ-treated surfaces would produce more α-SMA and CN than the

untreated controls and that the lowest levels of EMT markers would be observed on the

adhesion peptide modified surfaces. While the YIGSR modified surfaces produced

significantly less SMA than the corresponding positive controls, modification with the

FN based peptide, hypothesized based on the model to lead to decreased migration,

resulted in significantly larger amounts of the EMT markers. While there are several

possible reasons for this, it may be that a combination of factors must be considered when

designing a surface for minimizing PCO.   It is known that cells grown in the presence of

TGFβ require at least 6 days in order to stimulate a response.  In the human capsular bag,

expression of α-SMA occurs 7days to 1 month following treatment with TGFβ.

(Mansfeild 2004,Wormstone 2002, Wormstone 2006) Eyes of Wistar rats exposed to

alkali burns which is known to induce TGFβ production showed the presence of SMA at

20 days. (Shirai 2006)

Figure 27 depicts the population growth over 120 hrs of the PDMS control, the

PEO, the YIGSR and the GYRGDS and their positive control surfaces.  In general, the

cell populations increased over the 120 hours.  At 72 hours on PDMS and at 92 hours on

YIGSR and on both positive control surfaces, the population slightly decreases which is

likely attributable to error in both growing and counting the LECs. TGFβ-treated surface

populations are either equivalent or greater than the corresponding YIGSR or GYRGDS

surfaces demonstrating that at the concentrations examined, TGFβ is not particularly

stimulatory or inhibitory for LEC growth. Paradoxically, TGFβ is known to inhibit

cellular migration and induce cell apoptosis.  (Mansfeild 2004)  TGFβ may be inducing

the autocrine production of other mitogens such as FGF2.  FGF2 is a known autocrine

regulator recognized for its role in counteracting the loss of cells which have been

exposed to TGFβ and inducing cellular proliferation. (Mansfeild 2002, Wormstone 2001)

FGF2 is known to be the key growth factor for the maintenance of the long-term survival

of LECs in PCO. (Thlozan 2007)  Gotoh and colleagues also demonstrated higher cell

populations with TGFβ treated cells compared to that of the control which corresponds

well with results in Figure 30. (Gotoh 2007)

Attaching adhesion peptides to silicone biomaterials poses a very promising

solution to suppress or inhibit cellular migration and to preserve the LEC phenotype. The

construction and testing of these surfaces is an ongoing work. Although cell

differentiation does occur on these surfaces, it is possible that by maintaining phenotype

and inhibiting migration through for example the use of combinations of cell adhesion

peptides may lead to improved results. Testing using a lens explant model would also

likely be more representative of the actual situation due to the presence of the capsule and

therefore should be examined in future work. Cell migration assays should also be

performed in order to validate the results. Finally, *in vivo* studies need to be conducted in

order to assess the reduction or elimination of PCO.

There are a number of issues surrounding the successful design of this surface.

The density of the peptide on the surface should ideally be at the high end of the adhesion

curve based on the results obtained using the model. The capsule is made of several

ECM components; however FN is the most adhesive high-affinity protein. FN will

therefore likely play a key role in determining the overall behaviour and control of the

capsule. Observations of competition between RGDS molecules and a FN surface will

provide a reasonable estimate of which peptide modified surface will have dominant

control over cell response. RGDS and GYRGDS achieved 100% inhibition of the

attachment of rabbit LECs to the culture plate when added at to the culture medium.

(Sasabe 1996) Moreover, migration was significantly inhibited when GYRGDS to the

culture medium of human LECs on FN surfaces. (Oharazawa 2005)  GYRGDS, however, has less effect with LN and no effect with CN IV, likely due to the expression of and effect on different adhesion receptors.  Lack of inhibition with other ECM types is something to consider as the capsule will be partially controlled by ECM components. This is the reason for testing both GYRGDS and YIGSR.  In future work, these adhesion peptides should also be combined and tested in different ratios to determine the best combination for inhibition or should be combined with other synergistic peptides in order to enhance the results.

The results of Garcia and colleagues who observed a decrease over time in the affinity of the $\alpha5\beta1$ integrin for RGDS is of potential concern. (Garcia 2002)  A surface modified with RGD –based adhesion peptides may need additional synergy groups to promote long-term LEC adhesion.  This phenomenon may be overcome by modifying the surfaces with a combination of GYRGDS, synergy peptide PHSRN and YIGSR. Many other peptides combinations can also be evaluated.  On the other hand, this particular integrin is known as the mesenchymal integrin and is upregulated during EMT. As such, other integrins may play a more dominant role in non-differentiating LECs.  Moreover, a reduction in migration will discourage the process of EMT because, by definition part of the process of EMT is increased migration.  It is likely the more adhesive the RGD surface, the more it may prevent transdifferentiaiton of LECs. (Oharazawa 2005)  FHL culture on the GYRGDS surface and staining for CN revealed these results, although because cell culture activates the cells, this is difficult to state with certainty.

## CHAPTER 6: CONCLUSIONS

A mathematical model for LEC migration was developed to enable the prediction of the effects of various factors including surface protein density or adhesivity, the presence of growth factors TGFβ and FGF2 and integrin expression activity and affinity on LEC migration. The migration model was designed from a first order rate of decay model typically used in process control with the addition of an exponential decay term in order to capture shapes from monophasic to triphasic and from wide to narrow functions.

The model parameters were determined and the model was fitted to data found in the literature using the Marquardt-Levenburg algorithm. Statistical analysis revealed that the data are normally distributed. However there exists both serial correlation between the residuals and variance which is not constant, although both of these factors can be explained with the lack of data points available to fit the model and the fact that all factors assessed in the model are presumably correlated in some manner. The model is therefore unable to account for some of these trends.

The model was well suited to determining the effects of ECM proteins on cell migration both in the presence and absence of a growth factor. It fit less well however to situations where there were variations in integrin concentration affinity and activity, likely, due to the narrow, irregular shapes in the data. By hand –selecting parameters however, fits of these data were possible. The model predicts the range of cell speeds over a variety of protein densities and surface adhesivities and demonstrates that cells move slowest on FN surfaces with CN IV and LN showing variable results depending on

the cell type examined. Therefore, it is reasonable to predict that modification of lens surfaces with FN or with FN based peptides should limit cell migration and minimize PCO as the time to breach the capsule posterior with these surfaces was considerably greater than the time required in theory to seal the capsule. Specifically, the model predicted that it would take 63 days for the LECs to breach the posterior capsule at a FN density of $1250$molecules/$\mu m^2$.

In order to further validate the model, adhesion peptide-modified surfaces were created with the goal of reducing LEC migration by increasing adhesion as well as by maintaining cell phenotype in order to suppress or eliminating PCO. Surfaces were modified with the FN based peptide GYRGDS and with YIGSR derived from LN. Modification was demonstrated using various techniques. The response of two LEC lines to the modified surfaces was examined. The results demonstrated that cells grown on YIGSR modified surfaces showed significantly production of the fibroblast marker $\alpha$-SMA production than the positive control which suggests that EMT is occurring to a lesser extent with these surfaces. Surprisingly, the level of $\alpha$-SMA on the GYRGDS modified surfaces was significantly greater than other surfaces. Migration studies were not performed on these materials. However, these results suggest that both inhibition of migration and inhibition of EMT may be optimal and that this may be possible through modification with combinations of cell adhesion peptides. Additional studies with lens explants may be useful in generating surfaces with appropriate properties.

# BILIOGRAPHY

Abela-Formanek C, Amon M, Schauersberer J, Kruger A, Nepp J, Schild G.  Results of hydrophilic acrylic, hydrophobic acrylic, and silicone intraocular lenses in uveitic eyes with cataract.  J Cataract Refract Surg.  2002;28:1141-1152.

Aota S, Yamada K.  Fibronectin and cell adhesion: specificity of integrin-ligand interaction.  Adv. Enzymol. Relat. Areas Mol. Biol.  1995;70:1-21

Apple D, Solomond K, Tetz M *et al.*  Posterior Capsule Opacification.  Surv Ophthalmol.  1992;37:73-116

Banerjee P, Irvine D, Mayes A, Griffith L. Polymer latexes for cell-resistant and cell-interactive surfaces.  J Biomed Mater Res.  2000;50:331-339

Bassnett S, Beebe D.  Coincident loss of mitochondria and nuclei during lens fiber cell differentiation.  Dev Dyn 1992;194:85-93

Beck R, Nebe B, Guthoff R, Rychly J.  Inhibition of lens epithelial cell adhesion by the calcium antagonist Mibefradil correlates with impaired integrin distribution and organization of the cytoskeleton.  Graefe's Arch. Clin. Exp. Ophthalmol. 2001;239:452-458

Bloemendal H.  Lens proteins as markers for terminal differentiation. Ophthalmic Res. 1979;11:243-253

Boateng S, Lateef S, Mosley W, Hartman , Hanley L, Russell B.  RGD and YIGSR synthetic peptides facilitate cellular adhesion identical to that of laminin and fibronectin but alter the physiology of neonatal cardiac myocytes.  Am J Physiol Cell Physiol. 2005;288:C30-8.

Boukamp P, Fusenig, N.  "Trans-differentiation" from epidermal to mesenchymal/myogenic phenotype is associated with a drastic change in cell-cell and cell-matrix adhesion molecules. J Cell Biol.  1993;120:981-993.

Bullimore MA, Bailey IL.  Foreward: Clarifying Cataract. *Optometry and Vision Science,* 1993;70:867-868

Cammarata P, Cantu-Crouch D, Oakford L, Morrill A.  Macromolecular organization of bovine lens capsule. Tissue & cell.  1986;18:83-97

Chen H, Brook M, Sheardown H, Chen Y, Klenkler B.  Generic bioaffinity silicone surfaces. Bioconjugate Chem. 2006;17:21-28.

Clark R, An J., Greling D, Khan A, Schwarzbauer J. fibroblast migration on fibronectin requires three distinct functional domains. J. Invest Ophthalmol. 2003; 121: 695-705

Coller B. Activation affects access to the platelet receptor for adhesive glycoproteins. J. Cell Bio. 1986;103:451-456

Colognato H, Yurchenco PD. Form and function: the laminin family of heterotrimers. Dev Dyn 2000;218:213–234

Cook G, Wilkinson D, Crossno Jr. J, Raghow R, Jennings L. The tetraspanin CD9 influences the adhesion, spreading, and pericellular fibronectin matrix assembly of Chinese hamster ovary cells on human plasma fibronectin. Exp Cell Res. 1999;251:356-371

Davidson M, Morgan D, McGahan M. Effect of surgical technique on *in vitro* posterior capsule opacification. J Cataract Refract Surg 2000; 26:1550-1554

Delforge D, Gillon B, Art M, Dewelle J, Taes M, Remacle J. Design of a synthetic adhesion protein by grafting RGD tailed cyclic peptides on bovine serum albumin. Lett Pept Sci. 1998;5:87-91

DiMilla P, Barbee, K, Lauffenburger, D. Mathematical model for the effects of adhesion and mechanisms on cell migration speed. J. Biophys. 1991;60:15-37

DiMilla P, Stone J, Quin J, Albelda S, Lauffenburger D. Maximal migration of human smooth muscle cells on fibronectin and type IV collagen occurs at an intermediate attachment strength. J Cell Biol. 1993;122:729-737

Duband J, Nuckolls G, Ishihara I, Hasegawa T, Yamanda K, Thiery J, Jacobson K. Fibronectin receptor exhibits high lateral mobility in embryonic locomoting cells but is immobile in focal contacts and fibrillar streaks in stationary cells. Cell Biol. 1988;107:1385-1396

Dwivedi D, Pino G, Banh A, Nathu Z, Howchin D, Margetts P, Sivak J, West-Mays J. Matrix metalloproteinase inhibitors suppress transforming growth factor-β-induced subcapsular cataract formation. Am J pathol. 2006;168:69-79

Findl O, Buehl W, Menapace R, Sacu S, Georgopoulos M, Rainer G. Long-term effect of sharp optic edges of a polymethyl methacrylate intraocular lens on posterior capsule opacification: a randomized trial. Ophthalmology. 2005;112:2004-8

Fine I. Cortical cleaving hydrodissection. J cataract refract surg. 1992;18: 508-512

Garcia A, Schwarzauer J, Boettiger, D.  Distinct activation states of alpha 5 beta 1 integrin
      show differential binding to RGD and synergy domains of fibronectin.  Biochemistry.
      2002;41:9063-9069

George S, Dwivedi A.  MMPs, cadherins, and cell proliferation. 2004.  Trends Cardiovasc
      Med 2004;14:100–105

Goodman S, Riesse G, von der Mark K.  The E8 subfragment of laminin promotes
      locomotion of myblasts over extracellular matrix.  J Cell Biol.  1989;109:799-809

Gotoh N, Perdue N, Matsushima H, Sage E, Yan O, Clark J.  An *in vitro* model of posterior
      capsular opacity: SPARC and TGF-β2 minimize epithelial-to-mesenchymal transition
      in lens epithelium.  Invest Ophthalmol Vis Sci. 2007;48:4679–4687

Graf J, J., Y. Iwamoto Y, M. Sasaki M, G. R. Martin , H. K. Kleinman, F. A. Robey, Y.
      Yamada.Identification of an amino acid sequence in laminin mediating cell
      attachment, chemotaxis, and receptor binding. Cell. 1987;48:989-996

Hawse J, DeAmieis-Tress C, Cowell T, Kantorow M.  Identification of global gene
      expression differences between human lens epithelial and cortical fiber cells reveals
      specific genes and their associated pathways important for specialized lens functions.
      Mol Vis.  2005;11:274-283

Hayashi H, Hayashi K,  Nakao F, Hayashi F.  Elapsed time for capsular apposition to
      intraocular lens after cataract surgery

Hersel U, Dahmen C, Kessler H.  RGD modified polymers; biomaterials for stimulated cell
      adhesion and beyond.  Biomaterials.  2003;24:4385-4415

Hirano Y, Ohuno M, Hayashi T, Goto K, Nakajima A.  Cell-attachment activities of surface
      immobilized oligopeptides RGD, RGDS, RGDV, RGDT, and YIGSR towards five
      cell lines.  J Biomater Sci Polymer Edn.  1993;4:235-243

Hollik E, Spalton D, Ursell P, Pande M.  Lens epithelial cell regression on the posterior
      capsule with different intraocular lens materials.  Br J Ophthalmol.  1998;82:1182-
      1188

Hynes R. Integrins: versatility, modulation and signaling in cell adhesion. Cell. 1992;69:11-
      25

Hynes R.  Integrins: bidirectional, allosteric signaling machines.  Cell.  2002;110:673-687

Huttenlocker A, Ginsberg M, Horowitz A.  Modulation of cell migration by integrin-

mediated cytoskeletal linkages and ligand-binding affinity. J Cell Biol. 1996;134:1551-1562

Ido H, Nakamura A, Kobayashi R, Ito S, Li S, Futaki S, Sekiguchi K. The requirement of the glutamic acid residue at the third position from the carboxyl termini of the laminin gamma chains in integrin binding by laminins. J Biol Chem 2007;282:11144–11154

Imoto Y, Ohguro N, Yoshida A, Tsujikawa M, Inoue Y, Tano Y. Effects of RGD peptides on cells derived from the human eye. Jpn J Ophthalmol. 2003;47:444-453

Ingber D, Folkman J. Mechanochemical switching between growth and differentiation during fibroblast growth factor-stimulated angiogenesis *in vitro*: role of extracellular matrix. J Cell Bio. 1989;109:317-330

Ishibashi T, Hatae T, Inomata H. Collagen types in human posterior capsule opacification. J cateract refract surg. 1994;20:643-646

Jenkins G. The role of proteases in transforming growth factor-β activation. Int J BiochemCell Biol. 2008;40:1068-1078

Jong-Hesse Y, Lang K, Kampmeier J, Lang G. Effect of growth factors on the differentiation of porcine lens epithelial cells. Klin Monatsbl Augenheilkd. 2004 Mar;221(3):175-9

Kalluri R, Neilson E. Epithelial to mesenchymal transition and its implications for fibrosis. J Clin Inv. 2003;112:1776-1784

Kappelhof JP, Pameyer JH, De Jong PTVM, *et al.* The proteinaceous coating and cytology of implant lenses in rabbits. Am J Ophthalmol 1986; 102:750-758

Kayatama Y, Kobayakawa S, Yanagawa H. The relationship between the adhesion characteristics of acrylic intraocular lens materials and posterior capsule opacification. Ophthalmic Res. 2007;39:276-281

Kojetinsky C, Baatz H, Pleyer U, Hartmann C, Rieck P. *In vitro* bovine and human lens epithelial cell culture studies on inhibition of posterior capsule opacification using a cyclic RGD peptide. Ophthalmology. 2001;98:731-735

Koo L, Irvine D, Mayes A, Lauffenburger D, Griffith L. Co-regulation of cell adhesion by nanoscale RGD prganization and mechanical stimulous. J Cell Sci. 2002;115:1423-1433

Kuo S, Lauffenburger D.  Relationship between receptor-ligand binding affinity and adhesion strength.  Biophys J.  1993;65:2191-2200

Lauffenburger D, Horowitz A.  Cell migration: a physically integrated molecular process.  Cell.  1996:84:359-369

Lee E, Joo C.  Role oftransforming growth factor-beta intransdifferentiation and fibrosis of lensepithelial cells. Invest Ophthalmol Vis Sci.  1999;40:2025–2032

Lens A, Nemeth S, Ledford J.  Ocular anatomy and physiology, second edition. SLACK Inc. 2008. Pp 72-81

LeBleu VS, Macdonald B, Kalluri R. Structure and function of basement membranes.  Exp Biol Med (Maywood).  2007 Oct;232:1121-9.

Linnola R.  Sandwich theory: bioactivity-based explanation for the posterior capsule opacification. J Cataract Refract Surg.  1997;23:1539-1542

Linnola R, Werner L, Pandey SK, *et al.* Adhesion of fibronectin, vitronectin, laminin, and collagen type IV to intraocular lens materials in pseudophakic human autopsy eyes. Part 2: explanted intraocular lenses. J Cataract Refract Surg.  2000; 26:1807–1818

Linnola R, Sund M, Ylo¨nen R, Pihlajaniemi T. Adhesion of soluble fibronectin, vitronectin, and collagen typeIV to intraocular lens materials. J Cataract Refract Surg.  2003; 29:146–152

Liu C, Wormstone M, Duncan G, Marcantonio J.  A study of human lens cell growth *in vitro*. Invest Ophthalmol Vis Sci.  1996;37:906-914

Lois N, Taylor J, McKinnon A, Smith G, van't Hof R, Forrester J.  Effect of TGF-β2 and anti-TGF-β2 antibody in a new *in vivo* rodent model of posterior capsule opacification.  Invest Ophthamol Vis Sci.  2005;46:4260-4266

Maheshwari G, Brown G, Lauffenburger D, Wells A, Griffith L.  Cell adhesion and motility depend on nanoscale RGD clustering.  J Cell Sci.  2000;113:1677-1686

Melinda K, Kleinman H.  The laminins.  Int J Biochem Cell Biol.  1996;28:957-959

Mann B, West J.  Cell adhesion peptides alter smooth muscle cell adhesion, proliferation, migration and matrix protein synthesis on modified surfaces and polymer scaffolds.  J Biomed Mater Res.  2002 60:86-93

Mansfield K, Cerra A, Chamberlain C.  FGF-2 counteracts loss of TGFβ affected cells from rat lens explants: implications for PCO (after cataract).  Molecular Vision. 2003;10:521-532

Marcantonio J, Rakic J, Vrensen G, Duncan G.  Lens cell populations studied in human
donor capsular bags with implanted intraocular lenses. Ophthalmol Vis Sci.
2000;41:1130-1141

Marcantonio J, Reddan J.  TGFbeta2 influences alpha5-beta1 integrin distribution in human
lens cells.  Experimental Eye Research. 2004;79:437-442

Marlin T.  Process control, designing processes and control systems for dynamic
performance. 2000. McGraw Hill Inc.  pp 59-60, 136-158

Maruno K, Lovicu F, Chamberlain C, McAvoy J.  Apoptosis is a feature of TGF beta-
induced cataract. Clin Exp Optom.  2002;85:76-82

McCawley L, Matrisian L.  Matrix metalloproteinases: they're not just for matrix anymore!
Current Opinion in Cell Biology.  2001;13:534–540

Mikhail Andrew.  Peptide modified PDMS: Surface modification for improved vascular
cellular interactions. (MASc thesis, McMaster University, 2006), 39-45

Montgomery D, Runger G.  Applied statistic and probablility for engineers, 3$^{rd}$ Ed.  2003.
John Wiley & Sons, Inc.  pp395, 396.

Nagamoto T, Fujiwara T.  Inhibition of lens epithelialcell migration at the intraocular lens
optic edge; role of capsule bending and contact pressure. Jcateract refract surg.
2003;29:1605-1612

Nagata T, Minakata A, Watanabe I. Adhesiveness of AcrySof to a collagen film.  J Cataract
Refract Surge.  1998;24:367-370

Nishi O, Nishi K, Akaishi T, Shirasawa E.  Detection of cell adhesion molecules in lens
epithelial cells of human cataracts. Invest Ophthalmol Vis Sci.  1997a;38:579-585

Nishi O, Nishi K, Mano C. Ichihara M, Honda T, Saitoh I.  Inhibition of migrating lens
epithelial cells by blocking the adhesion molecule integrin: A preliminary report. J
Cataract Refract Surg  1997b;23:860-865

Nishi O, Nishi K, Wickstrom K.  Preventing lens epithelial cell migration using intraocular
lenses with sharp rectangular edges. J Cataract Refract Surg 2000;26:1543-1549

Nishi O, Nishi K,  Akura J.  Speed of capsular bend formation at the optic edge of acrylic,
silicone,and poly(methyl methacrylate) lenses. *J Cataract Refract Surg 2002;
28:431–437*

Nishi O, Nishi K, Osakabe Y.  Effect of intraocular lenses on preventing posterior capsule opacification:  design versus material.  J Cataract Refract Surg 2004;30:2170-2176

Nishi O, Yamamoto N, Nishi K, Nishi Y.  Contact inhibition of migrating lens epithelialcells at the capsular bend created by a sharp-edged intraocular lens after cataract surgery.  J Cataract Refract Surg.  2007; 33:1065–1070

Nixon D.  *In vivo* digital imaging of the square-edged barrier effect of a silicone intraocular lens. J Cataract Refract Surg 2004; 30:2574–2584

Oharazawa H, Ibaraki N, Lin LR, Reddy VN. The effects of extracellular matrix on cell attachment, proliferation and migration in a human lens epithelial cell line. Exp Eye Res. 1999; 69:603–610

Oharazawa H, Ibaraki N, Ohara K, Reddy V.  Inhibitory effects of Arg-Gly-Asp (RGD) peptide on cell attachment and migration in a human lens epithelial cell line. Ophthalmic Res.  2005;37:191-196

Oshika T, Nagata T, Ishii Y.  Adhesion of lens capsule to intraocular lenses of polymethylmethacrylate, silicone and acrylic foldable materials: an experimental study.  Br J Ophthalmol 1998;82:549-553

Olivero D, Furcht L.  Type IV collagen, laminin, and fibronectin promote adhesion and migration of rabbit lens epithelial cells *in vitro*.  Invest Ophthalmol vis sci. 1993;34:2825-2834

Páez M, González M, Serrano N, Shoenfeld Y, Anaya J.  Physiological and pathological implications of laminins: from the gene to the protein. Autoimmunity. 2007;40:83-94

Palecek S, Loftus J, Ginsberg M, Lauffenburger D, Horwitz A.Integrin-ligand binding properties govern cell migration through cell-substratum adhesiveness.  Nature. 1997;385:37-540

Palmade F, Sechoy-Chambon O, Regnouf de Vains J, Coquelet C, Bonne C. Inhibition of cell adhesion to lens capsule by LCM 1910, an RGD-derived peptide.  J Ocular Pharmacology.  1994; 10:623-632

Pandey S, Apple D, Werner L, Maloof A, Milverton E.  Posterior capsule opacification: A review of aetiopathogenesis, experimental and clinical studies and factors for prevention.  Curr Ophthalmology.  2004;52:99-112

Parmigiani C, McAvoy J. The roles of laminin and Fibronectin in the development of the lens capsule. *Curr. Eye Res.* 1991;10:501-511

Pierschbacher MD, Hayman E, Ruoslahti E.  Location of the cell-attachment site in fibronectin with monoclonal antibodies and proteolytic fragments of the molecule. Cell. 1981;26:259-267

Pierschbacher M, Ruoslahti E.  Cell attachment activity of fibronectin can be duplicated by small synthetic fragments of the molecule.  Nature. 1984;309:30-33

Pierschbacher MD, Ruoslahti E.  Influence of stereochemistry of the sequence Arg-Gly Asp-Xaa on binding specificity in cell adhesion.  J Biol Chem 1987:262:1794-8

Prockop DJ, Kivirikko KI. Collagens: molecular biology,diseases, and potentials for therapy. Annu Rev Biochem 1995; 64:403–434

Pytela R, Pierschbacher MD, Ruoslahti E.  Identification and isolation of a 140 kd cell surface glycoprotein with properties expected of a fibronectin receptor.  Cell. 1985 Jan;40(1):191-8

Ruoslahti E, Pierschbacher M. New perspectives in cell adhesion: RGD and integrins. Science 1987;238:491–7.

Ruoslahti E. Integrin signaling and matrix assembly. Tumour Biol. 17:117-124, 1996

Sacu S, Findl O, Linnola R.  Optical coherence tomography assessment of capsule closure after cataract surgery.  Cataract Refract Surg 2005; 31:330–336

Saika S, Kawashima Y, Miyamoto T, Okada Y *et al.*  Immunolocalization of Prolyl 4-Hydroxylase Subunits,$\alpha$-Smooth Muscle Actin, and Extracellular Matrix Components in Human Lens Capsules with Lens Implants. 1998

Saika S, Miyamoto Y, Kawashima Y, Okada Y, Yamanaka O, Ohnishi Y, Ooshima A. Immunolocalization of TGF-$\beta$1, - $\beta$2 and $\beta$3, and TGF-$\beta$ receptors in human lens capsules with lens implants.  Arch Clin Exp Ophthalmol.  2000;238:283-294

Saika S, Miyamoto T, Ishida I, Okada Y, Ohnishi Y, Ooshima A.  Lens epithelial cell regeneration of a capsule–like structure during postoperative healing in rabbits.  J Cataract Refract Surg.  2001a;27:1076-1078

Saika S, Okada Y, Miyamoto T, Ohnishi Y, Ooshima A, McAvoy J.  Smad translocation and growth suppression in lens epithelial cells by endogenous TGFbeta2 during would repair.  Exp Eye Res.  2001b;72:679-686

Saika S, Miyamoto T, Tanaka S, Tanaka T, Ishida I, Ohnishi Y, Ooshima A, Ishiwata T, Asano G, Chikama T, Shiraishi A, Liu CY, Kao CW, Kao W. Response of lens

epithelial cells to injury: role of lumican in epithelial to mesenchymal transition. Invest Ophthalmol vis sci. 2003;44:2094-2102

Saika S. Relationship between posterior capsule opacification and intraocular lens biocompatibility. Progress in Retinal and Eye Research. 2004;23:283-305

Sasabe T, Suwa Y, Kiritoshi A, Doi M, Yuasa T, Kishida K. Differential effects of fibronectin-derived oligopeptides on the attachment of rabbit lens epithelial cells *in vitro*. Ophthalmic Res. 1996; 28:201-208

Schwarz M, Ginsberg M. Networks and crosstalk: integrin signaling spreads. Nature Cell Biology. 2002;4:E65-E68

Shimaoka M, Lu C, Palframan R, von Andrian U, McCormack A, Takagi J, Springer T. Reversibly locking a protein fold in an active conformation with a disulfide bond: integrin alphaL I domains with high affinity and antagonist activity *in vivo*. Proc. Natl. Acad. Sci. USA 2001;98:6009-6014

Shimaoka M, Takagi J, Springer T. Conformational regulation of integrin structure and function. Ann rev biophyys biol. 2002;31:485-516

Shirai K, Saika S, Tanaka T, Okada Y, Flanders K, Ooshima A, Ohnishi Y. A new model of anterior subcapsular cataract: involvement of TGFβ/Smad signaling. Molecular Vision. 2006;12:681-691

Sondermann H, Dogic D, Pesch M, Aumailley M. Targeting of cytoskeletal linker proteins to focal adhesion complexes is reduced in fibroblasts adhering to laminin-1 when compared to fibronectin. Cell Adhes Commun. 1999;7(1):43-56

*Sponer* U, Pieh S, Soleiman A, Skorpik C. Upregulation of alphavbeta6 integrin, a potent TGF-beta1 activator, and posterior capsule opacification. J Cataract Refract Surg. 2005;31:595-606

Steinert R, Puliafito C, Kumar S, Dudak S, Patel S. Cystoid macular edema, retinal detachment, and glaucoma after Nd:YAG laser posterior capsulotomy. Am J Ophthalmol. 199;112:373-80

Strobel E, Mobest D, von Kleist S, Dangel M, Ries S, Mertelsmann R, Henschler R. Adhesion and migration are differentially regulated in hematopoietic progenitor cells by cytokines and extracellular matrix. Blood. 1997;90:3524-3532

Symonds J, Lovicu F, Chamberlain C.  Posterior capsule opacification-like changes in rat lens explants cultured with TGFb and FGF: Effects of cell coverage and regional differences.  Exp Eye Res.  2006;82:693–699

Tamiya S, Wormstone M, Marcantonio J, Gavrilovic J, Duncan G.  Induction of matrix metalloproteinases 2 and 9 following stress to the lens.  Ex eye res.  2000;71:591-597.

Tanaka T, Saika S, Ohnishi Y, Ooshima A, McAvoy J, Liu C, Azhar M, Doetschman T, Whei-Yang Kao.  Fibroblast growth factor 2: roles of regulation of lens cell proliferation an epithelial-mesenchymal transition in response to injury.  Mol Vis. 2004;10:462-7

Tarone G, Hirsch E, Brancaccio M, De Acetis M, Barberis L, Balzac F, Retta SF, Botta C, Altruda F, Silengo L. Integrin function and regulation in development. Int J Dev Biol 2000;44:725–731

Terranova VP, Aumailley M, Sultan LH, Martin GR, Kleinman HK.  Regulation of cell attachment and cell number by fibronectin and laminin.  J Cell Physiol. 1986 Jun;127:473-9

Tholozan F, Gribbon C, Li Z, Goldberg M, Prescott A, McKie N, Quinlan R.FGF-2 release from the lens capsule by MMP-2 maintains lens epithelial cell viability.  Mol Biol Cell. 2007;18:4222-31

Tzu J,  Marinkovich P.  Bridging structure and function: structural regulatory, and developmental role of laminins.  Int J Biochem Cell Biol. 2008 ;40: 199–214

Van Obberghen-Schilling E, Roche NS, Flanders KC, *et al.* Transforming growth factor b1 positively regulates its own expression in normal and transformed cells. J Biol Chem. 1988; 263:7741–7746

Vyas A, Narendran R, Bacon P, Apple D Three-hundred-sixty degree barrier effectof a square-edged and an enhanced-edgeintraocular lens on centripetal lensepithelial cell migration: Two-year results. J Cataract Refract Surg 2007; 33:81–87

Wallentin N, Wickstrom K, Lundberg C.  Effect of cataract surgery onaqueous TGF-beta and lens epithelialcell proliferation. Invest Ophthalmol Vis Sci.  1998;39:1410–1418

Weisel J. Nagaswami C, Vilaire G and Bennett J.  Examination of the platelet membrane glycoprotein IIb-IIIa complex and its interaction with fibrinogen and other ligands by electron microscopy. J. Bio.Chem. 1992;267:16637-16643

Werblin T.  Another view of neodymium:YAG capsulotomy.  J cateract refract surge. 2006;32:373-374

Whitelock JM, Murdoch AD, Iozzo RV, Underwood PA: Thedegradation of human endothelial cell-derived perlecan and release of bound basic fibroblast growth factor by stromelysin,collagenase, plasmin, and heparanases. *J Biol Chem* 1996, 271:10079-10086.

WHO. Ageing: a public health challenge. In: *Fact sheet N°135.* (Ed.^(Eds) (1998)

WHO. Blindness: Vision 2020 - The Global Initiative for the Elimination of Avoidable Blindness. In: *Fact sheet N°213.* (Ed.^(Eds) (2000)

Wormstone M, Liu C, Rakic J-M, *et al.* Human lens epithelial cell proliferation in a protein-free medium. Invest Ophthalmol Vis Sci. 1997; 38:396–404

Wormstone M, Rio-Tsonis K, McMahon G, Tamiya S, Davies P, Marcantonio J, Duncan G. FGF: An autocrine regulator of Human lens cell growth independent of added stimuli. Invest Ophthalmol Vis Sci. 2001:42;1305-1311

Wormstone M. Posterior capsule opacification: A biological perspective. Exp Eye Res. 2002a;74:337-347

Wormstone M, Tamiya S, Anderson I, Duncan G. TGF-β2-induced matrix modification and cell transdifferentiation in the human lens capsular bag. Invest Ophthamol Vis Sci. 2002b;43:2301-2308

Wormstone M, Tamiya S, Eldred J, Lazaridis K, Chantry A, Reddan J, Anderson I, Duncan G. Characterisation of TGF-β2 signalling and function in a human lens cell line. Exp Eye Res. 2004;78:705-714.

Wormstone M, Anderson I, Eldred J, Dawes L, Duncan G. Short-term exposure to transforming growth factor β induces long-term fibrotic responses. Exp Eye Res. 2006;83:1238-1245

Yoneda A, Ogawa H, Kojima K, Matsumoto I. characterization of the ligand binding activities of vitronectin: interaction of veteran actin with lipids and identification of the binding domains various ligands using recombinant domains. Biochemistry. 1997; 37: 6351-6360

Yoshino M, Kurosaka D, Obazawa M, Takayama F. Presence of alpha 5 beta 1 Integrin and Fibronectin in the Anterior Subcapsular Cataract. Japanese J of Ophthalmol. 2001;45:429-429

Yu Q, Stamenkovic I.  Cell surface-localized matrix metalloproteinase-9 proteolytically
    activates TGF-beta and promotes tumor invasion and angiogenesis. Genes Dev.
    2000;14:63–176

Yuen C, Williams R, Batterbury M, Grierson I.  Modification of the surface properties of
    lens material to influence posterior capsule opacification.  Clin Exp Ophthalmol.
    2006;34:568-574

Zavadil J, Bottinger E.  TGE-β and epithelial-to-mesenchymal transitions.  Oncogene.
    2005;24:5764-5774

Zelenka P.  Regulation of cell adhesion and migration in lens development.  Int J Dev Biol.
    2004;48:857-865

Zelenka P, Arpitha P.  Coordinating cell proliferation and migration in the lens and cornea.
    Sem Cell Dev Biol.  2008;19:113-24

## APPENDIX I
Appendix Table 1: Materials and reagents

| | |
|---|---|
| Poly(ethylene glycol) monoallylether 550Da | Clariant Corp. (Markham ON) |
| N,N'-disuccinimidyl carbonate | Sigma Aldrich®, Oakville, ON. CA |
| triethylamine (99%) | Sigma Aldrich®, Oakville, ON. CA |
| acetonitrile (99%, anhydrous) | Sigma Aldrich®, Oakville, ON. CA |
| Karstedt's Pt catalyst (2-3 wt% in xylene, platinum-divinyltetramethyldisiloxane, [(Pt)2(H2C=CH-SiMe2OSiMe2CH=CH2)3]) | Sigma Aldrich®, Oakville, ON. CA |
| Trifluoromethanesulfonic acid, (triflic acid), ≥99% | Sigma Aldrich®, Oakville, ON. CA |
| Diethylene glycol dimethyl ether, (2-methoxyethyl ether) | Sigma Aldrich®, Oakville, ON. CA |
| Silicone Elastomer Kit (Sylgard 184 curing agent and silicone elastomer base). | Dow Corning®, Midland, MI. U.S.A. |
| Poly(methylhydrogen siloxane), (MeHSiO)n, (DC1107). | Dow Corning®, Midland, MI. U.S.A. |
| Gly-Tyr-Arg-Gly-Asp-Ser (GYRGDS) peptide, >99% purity. | American Peptide®, Sunnyvale, CA. U.S.A. |
| Arg-Gly-Asp-Ser (RGDS) peptide, >95% purity. | Sigma Aldrich®, Oakville, ON. CA |
| Tyr-Ile-Gly- Ser-Arg (YIGSR) | Sigma Aldrich®, Oakville, ON. CA |
| Arg-Asp-Gly-Ser (RDGS) peptide, >95% purity. | Sigma Aldrich®, Genosys, Oakville,ON. CA |
| Methanol (anhydrous) | Sigma Aldrich®, Oakville, ON. CA |
| Hexane | Sigma Aldrich®, Oakville, ON. CA |
| Trifluoroacetic acid | Sigma Aldrich®, Oakville, ON. CA |
| Fetal bovine serum | Invitrogen®, Burlington, ON, CA |
| B3 lens epithelial cells | American Type Culture Collection (ATCC), Manassas, VA. |
| FHL lens epithelial cells | American Type Culture Collection (ATCC), Manassas, VA. |
| Eagle's minimal essential medium F15 | Invitrogen®, Burlington, ON, CA |
| Sodium pyruvate | Invitrogen®, Burlington, ON, CA |
| Sodium bicarbonate | Invitrogen®, Burlington, ON, CA |
| L-glutamine | Invitrogen®, Burlington, ON, CA |
| Transforming growth factor TGFβ | Peprotech, Rocky Hill, NJ, US |
| Penicillin-streptomycin | Gibco, Burlington ON, CA |
| Dimethyl sulphoxide | Invitrogen®, Burlington, ON, CA |
| Tryple express® or trypsin | Invitrogen®, Burlington, ON, CA |
| Direct Red80 | Sigma Aldrich®, Burlington, ON. CA |
| FITC-conjugated anti-alphaSMA primary antibody raised in mouse | Sigma Aldrich®, Burlington, ON. CA |
| Phosphate buffered saline, pH 7.4 | Invitrogen®, Burlington, ON, CA |
| Tissue culture materials | Invitrogen®, Burlington, ON, CA |
| Fluorescein isothiocyanate conjugated primary antibody for SMA | Sigma Aldrich®, Burlington, ON. CA |